Technische Universität Braunschweig

GEOMAR
Helmholtz Centre for Ocean Research Kiel

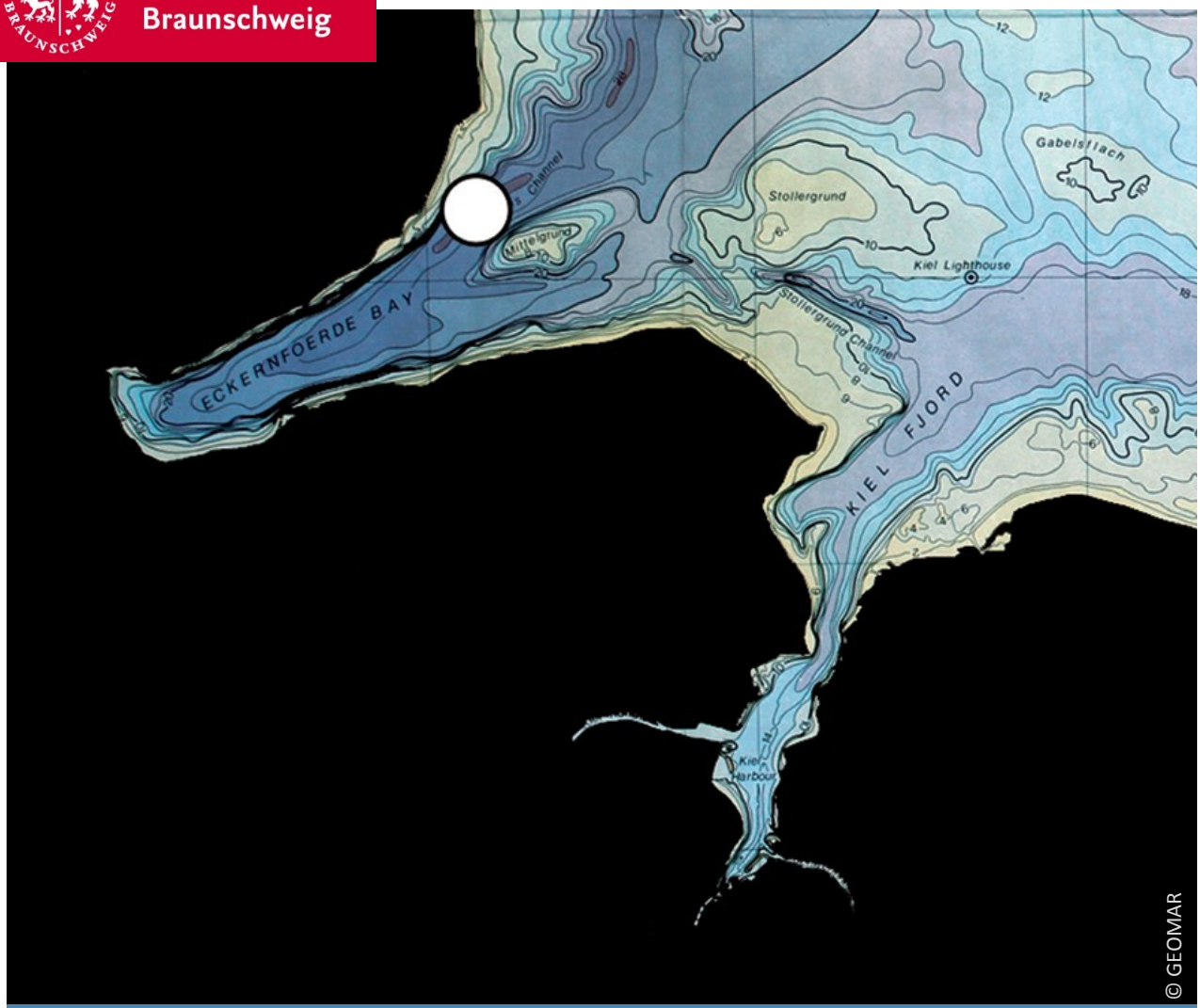

Masterthesis

Time Series Analysis and Development of a 1D Box Model to Simulate Trace Gas Concentrations at the Time Series Station Boknis Eck, Baltic Sea

Sinikka Lennartz

1st Examiner: Prof. Harald Biester
2nd Examiner: Prof. Hermann Bange

Masterthesis

submitted by

Sinikka Lennartz
Mat.-Nr. 4202316
TU Braunschweig

1st Examiner:

Prof. Harald Biester
TU Braunschweig
Institut für Geoökologie
Braunschweig

2nd Examiner:

Prof. Hermann Bange
GEOMAR
Helmholtz Centre for Ocean Research
Marine Biogeochemistry
Kiel

November 2013

Eidesstattliche Erklärung

Hiermit erkläre ich, Sinikka Lennartz, dass ich die Masterarbeit

'Time Series Analysis and Development of a 1D Box Model to simulate Trace Gas Concentrations at the Time Series Station Boknis Eck, Baltic Sea'

selbstständig verfasst sowie alle inhaltlichen und wörtlichen Zitate als solche gekennzeichnet habe. Diese Arbeit hat in gleicher oder ähnlicher Form noch keiner Prüfungsbehörde vorgelegen.

Statutory Declaration

I, Sinikka Lennartz, affirm that I have authored the master thesis

'Time Series Analysis and Development of a 1D Box Model to simulate Trace Gas Concentrations at the Time Series Station Boknis Eck, Baltic Sea'

independently and that I have explicitly marked all material which has been quoted either literally or by content. The thesis in this or any other form has not been submitted to an examination body before.

.....

Sinikka Lennartz

Contents

List of Figures

List of Tables

Acknowledgements

This study would not have been possible without the help and involvement of several people to whom I would like to express my gratitude.
I would like to thank my supervisors: Prof. Harald Biester, for making my master thesis at GEOMAR possible and for his great support during my studies; Prof. Hermann Bange, for providing the very interesting topic (and data!), for the perfect balance between letting me work independently and giving advice as well as for his good humor while answering my numerous questions.
I could always adress Dr. Annette Kock, Tina Baustian, Frank Malien and Henry Bittig for questions, thanks to them for helping in many ways. Thanks also to the captain and crew of the RV Littorina, ship cruises always were a highlight. I would further like to acknowledge the help of Dr. Christian Franzke for providing his MatLab scripts and for discussing results. Thanks to the Heinrich-Böll-Foundation for the financial support during my studies.
Furthermore, I would like to thank everybody in the Marine Chemistry group for the great working atmosphere, the cakes and the music (the latter to Alex and Dennis in particular). It was a pleasure to work with all of you. Moreover, thanks to Lena, Mascha, Britta, Alex, Sebastian, Jan, Tillman and Leonie for the great time in Braunschweig.
Finally, I am indescribably grateful to my family, for their love, support and belief in me as well as for accepting that I now live at the other end of Germany. Thanks to Jonas for the helpful discussions, for finding the many missing 'R' and 'S' and for everything else.

Zusammenfassung

Ziel dieser Studie war die statistische Auswertung der Langzeittrends an der Zeitserienstation Boknis Eck (südwestliche Ostsee) im Zeitraum 1957-2013 sowie das Entwickeln eines einfachen 1D Box Modells zur Simulation der Spurengaskonzentrationen von Methan und Lachgas im Oberflächenwasser.

Mit Hilfe des saisonalen Mann-Kendall-Tests und Wavelet-Analysen wurden zeitliche Veränderungen im Mittelwert und in der Saisonalität neun physikalischer und biogeochemischer Parameter untersucht. Signifikante Veränderungen in allen Parametern lassen darauf schließen, dass sich die Ostsee in einem umgreifenden Veränderungsprozess befindet. Die Trends zunehmender Sauerstoffverarmung bei gleichzeitig rückgängigem Nährstoffeintrag und schwächeren Planktonblüten, die Temperaturzunahme sowie eine verstärkte Stratifizierung stehen in Übereinstimmung mit Trends in weiten Teilen des Ostseeraumes. Die Ergebnisse deuten darauf hin, dass sich verändernde Klimafaktoren dem Rückgang der Eutrophierung entgegen wirken und zur Sauerstoffverarmung im Tiefenwasser beitragen.

Weiterhin konnten 1D Box Modelle entwickelt werden, die die Konzentrationen von Methan und Lachgas im Oberflächenwasser bei Boknis Eck in Abhängigkeit von unter anderem Temperatur, Salinität, Windgeschwindigkeit, Sauerstoff und Chlorophyllkonzentration simulieren. Die simulierten Konzentrationen lagen im Mittel im Bereich der Standardabweichungen der jährlichen gemessenen Konzentrationen und bildeten die Saisonalität zufriedenstellend ab. Für die Oberflächenkonzentrationen beider Gase waren Produktionsprozesse unterhalb der Mischungsschicht sowie anschließender Transport in diese entscheidend. Für die Methankonzentration war das Sediment von großer Bedeutung, da hier anoxische Bedingungen zur Bildung von Methan beitragen. Für Lachgaskonzentrationen war der Transport von unterhalb der Mischungsschicht produziertem Lachgas entscheidend, dessen Intensität wiederum stark von der Sauerstoffkonzentration im Tiefenwasser abhing. Als einzig relevante Senke fungierte für beide Spurengase die Emission in die Atmosphäre. Eine Abschätzung der Entwicklung der für die Konzentrationen der Spurengase wichtigen Prozesse unter einem Szenario anhaltender Langzeittrends deutet darauf hin, dass die Spurengase Methan und Lachgas verstärkt emittiert werden könnten. Für eine genaue Beobachtung der zukünftigen Entwicklung der Spurengasemissionen sowie dem allgemeinen Zustand des Ökosystems bei Boknis Eck ist das Fortführen des monatlichen Monitorings unbedingt notwendig.

Abstract

The goal of the study was to statistically evaluate the long-term trends at Time Series Station Boknis Eck (Southwestern Baltic Sea) in the period of 1957 to 2013 as well as to develop a simple 1D box model to simulate concentrations of methane and nitrous oxide in the mixed layer.

The seasonal Mann-Kendall-test and wavelet analysis were used to detect changes in mean and seasonality of nine physical and biogeochemical parameters. Significant changes were present in all analysed parameters and allow the conclusion that the Baltic Sea is subjected to extensive changes. The trends of increasing oxygen depletion with simultaneously decreasing nutrient and chlorophyll a concentrations, the increase of spring temperatures and the intensified stratification are in agreement with previously found trends in large parts of the Baltic Sea. The results indicate that changing climatic factors may counteract the decline in eutrophication and contribute to oxygen depletion in the bottom water.

Furthermore, two 1D box models were developed that simulated the concentrations of methane and nitrous oxide in the mixed layer in dependance of temperature, salinity, wind speed, oxygen and chlorophyll a concentration. The simulated concentrations were in average in the range of the standard deviation of the measured concentrations and reflected the seasonality well. For the concentration of both gases, production processes below the mixed layer boundary with susequent transport to the mixed layer determined the concentration there. For methane concentrations at the surface, the sediment played the major role as anoxic conditions there enabled the formation of methane that was then transported to the surface. Nitrous oxide was mainly produced in the water column below the mixed layer, the production being highly dependent on the oxygen concentration in the bottom water. For both trace gases, the emission to the atmosphere acted as the main sink.

The development of the concentration of the trace gases under a scenario of continuing long-term trends is estimated to result in a stronger emission of methane and nitrous oxide. To determine the future development of trace gas emissions as well as the general state of the ecosystem at Boknis Eck, it is crucial to continue the monthly monitoring at Boknis Eck.

1 Introduction

1.1. The Need for oceanographic long-term Observations

Long-term observations in oceanography are crucial when it comes to improve the understanding of the state of ecosystems and to monitor their long-term developments. This is the reason why long-term observations have been a core strategy in the last decades and are still considered to have highest priority [Ducklow et al., 2009].

The analysis of time series already proved the ability to change the view on environmental processes in the past. One of the first long-term oceanographic observations that are still operated today started in 1931, when the Continuous Plankton Recorder Survey was initiated [Ducklow et al., 2009] in Plymouth, UK. In 1955, the hydrostation 'S' off Bermuda followed, where observation has continued until today. In the course of the Joint Global Ocean Flux Study, the Hawaii Ocean Time Series (HOT) and Bermuda Atlantic Time Series Station (BATS) were established in 1988 [Ducklow et al., 2009]. Time series such as the atmospheric CO_2 measurements at Mauna Loa in Hawaii became well-known, demonstrating the alarming rise of CO_2 concentration in the atmosphere and fueling the debate on global warming. Ducklow et al. [2009] analysed the achievements of the mentioned time series and concluded that they contributed enormly to the improved understanding of oceanic processes, foodweb dynamics and climate feedbacks.

There is still growing need for long-term observations in oceanography to improve our knowledge on past, present and future processes. First of all, observations over a long period of time reveal trends in the present development of environmental systems. Environmental systems are known to change between stable states, termed regime shifts. These shifts are defined as the abrupt change from one stable state to another [deYoung et al., 2004]. Such regimes often last a decade or more, and to successfully characterise them, observations over several decades are needed.

Second, time series of recent processes can be used to improve our knowledge of the past. Following the principle of uniformitarianism, contemporary processes can be transferred to the past using proxies [Grotzinger et al., 2008]. Time series of observational data can be used to calibrate these proxies, by relating direct and unaltered signals from measurements to the recent development of proxies.

Third, time series are crucial to develop and evaluate accurate models, that are in turn important to forecast and predict future developments. A high level of understanding of environmental systems is needed to successfully parametrise processes in a model, which can be achieved through the

analysis of oceanographic time series. Furthermore, model output can only be evaluated accurately against large observational data sets. Therefore, modelers are drawn to observational data for the iterative process of improving models [Evans, 1999].
However, most of the ocean remains undersampled. The need for long-term observations is still highly topical [Ducklow et al., 2009], as oceanographic time series over several decades are sparse. The time series of Boknis Eck, Baltic Sea, which is analysed in this study, is highly valuable in this context. It covers a time span of 56 years from 1957 on and started earlier than BATS (1988), HOT (1988) or the Helgoland time series (1961) [Wiltshire and Dürselen, 2004]. Against the background of the need for long-term observational data, trends in the temporal development of a variety of oceanographic parameters is evaluated in this study. A time series of trace gases is further used to develop a model on the quantification of processes in the nitrous oxide and methane cycle.

1.2. The ecological Setting of the Baltic Sea

As a nearly enclosed, marginal sea with only a small connection to the North Sea, the Baltic Sea differs in many aspects from the open ocean. Differences are most pronounced in the altered hydrography and the strong human impact on the ecosystem. The Baltic Sea ranges from the Gulf of Bothnia in the Northeast to the Danish straits in the West, where it has a small connection to the North Sea through the Great Belt, Little Belt and Oresund. With a surface area of 415′000 km^2, an average depth of 52 m and a total volume of 21′700 km^2, it is one of the world's largest brackish water seas [Rheinheimer and Nehring, 1995].
In geological time spans, the Baltic Sea is very young as it did not form before the Würm-Weichsel-glacial 12′000 years ago. The basin that is now occupied by the Baltic Sea has been eroded by glaciers and was subsequently filled with water as the glaciers retreated [Rheinheimer and Nehring, 1995]. Since then, conditions have altered between marine, fresh and brackish [Bonsdorff et al., 1997]. During the last major transgression, the Littorina transgression, the present-day's coastlines formed. Simulatenously, the sill of the Danish straits was flooded [Rheinheimer and Nehring, 1995], connecting the Baltic Sea basin to the North Sea.
This small connection defines the frame of the hydrographic setting of the Baltic Sea. The Danish straits are the only location where water with the open sea is exchanged. Inflowing water comes from the West-East directed Jutland current [Dryssen, 1993]. Due to its higher salinity, the inflowing water enters the Baltic Sea as bottom water. At the same time, several major rivers discharge into the Baltic Sea, e.g. the Neva or the Oder. The less saline water forms a fresh surface layer. It is this less saline surface water that forms the outflow at the Danish straits. Thus, saline water at the bottom enters the Baltic Sea in exchange for fresh water flowing out on the surface [Dryssen, 1993].
Besides this regular water exchange, major salt water pulses occur without regularity [Hanninen et al., 2000, Lass and Matthäus, 1996]. As the basin of the Baltic Sea is subdivided by sills that hamper ventilation, major inflows of dense bottom water are important for water exchange. The inflow events are triggered by westerly winds blowing for several tens of days [Lass and Matthäus, 1996].

Hanninen et al. [2000] related the saline inflows to larger scale teleconnections. The North Atlantic Oscillation (NAO) is believed to influence the winds by increasing the westerly winds in a positive phase. Stronger winds would then cause a salt water inflow [Hanninen et al., 2000].
The differences in salinity result in a density gradient throughout the water column, establishing a strong stratification each year [Rheinheimer and Nehring, 1995]. The differences in density hamper the water exchange of the less saline surface water and the saline bottom water. Besides this vertical salinity gradient, there is also a horizontal salinity gradient, as the saline water from the North Sea is more and more diluted towards the Bothnic Gulf [Rheinheimer and Nehring, 1995].
As there is only a small connection to the open sea, the residence time for water in the Baltic Sea is $25 - 35$ years [Feistel et al., 2008]. The reduced exchange of the water masses make the Baltic Sea particularly vulnerable to pollution. Additionally, approximately 85 million people live in the catchment area [HELCOM, 2009]. The consequentially high environmental pressure is expressed by increased pollution with e.g. phosphate and nitrate through various anthropogenic sources. Elevated nutrient inputs lead to eutrophication, which was soon considered as the major threat for the ecosystem of the Baltic Sea in the 1970's [HELCOM, 1974]. Nutrient input by rivers, point sources or diffuse sources like the runoff of fertilizers from agricultural areas as well as atmospheric deposition were listed as the main causes [HELCOM, 2009].
Marine eutrophication is a widespread phenomenon and occurs in many coastal ecosystems [Cloern, 2001]. It has severe primary and secondary effects on the ecosystem. First of all, eutrophication leads to increased productivity, which in turn decreases the transparency of the water [Bonsdorff et al., 1997]. This affects for example sea grass meadows [Karlson et al., 2002] and results in a shift in community composition of submerged aquatic vegetation [HELCOM, 2009]. As a secondary effect, oxygen concentration in the bottom water declines. The sedimentation of organic matter and the subsequent remineralisation is oxygen consuming, so the bottom water becomes undersaturated in oxygen after large plankton blooms [Bonsdorff et al., 1997]. The weak ventilation of the bottom water due to density gradients further aggravates the oxygen decline. Oxygen consuming rates have increased two to three fold between 1960 and 1990 in the Kiel Bight, proportional to the primary production rates [Babenerd, 1991]. Nutrient loads of phosphorous and nitrogen species increased up to 4 to 6 fold [Rosenberg, 1990]. Hypoxia or even anoxia in the bottom water have severe consequences for benthic fauna and flora, whith major implications throughout all trophic levels. Weigelt [1991] found significant short- and long-term alterations in the benthic community after oxygen depletion events. Bonsdorff et al. [1997] proved that zooplankton and fish populations in the Northern Baltic Sea shifted due to eutrophication. Except for some regions in the Bothnian Sea and Bay, all areas of the Baltic Sea are still in a poor to bad state due to eutrophication (fig. 1.1) [HELCOM, 2009].

Since the 1970ies, awareness of the anthropogenic impact through marine eutrophication grew [Bonsdorff et al., 1997]. In 1974, the Helsinki Comission (HELCOM) was set forth by the riparian states. The declared goal of Helcom was to reduce the input of various pollutants into the Baltic Sea and to monitor the future development [HELCOM, 1974, Art. 3]. Widespread measures like the installation of wastewater treatment plants have been undertaken since to reduce the nutrient discharge.

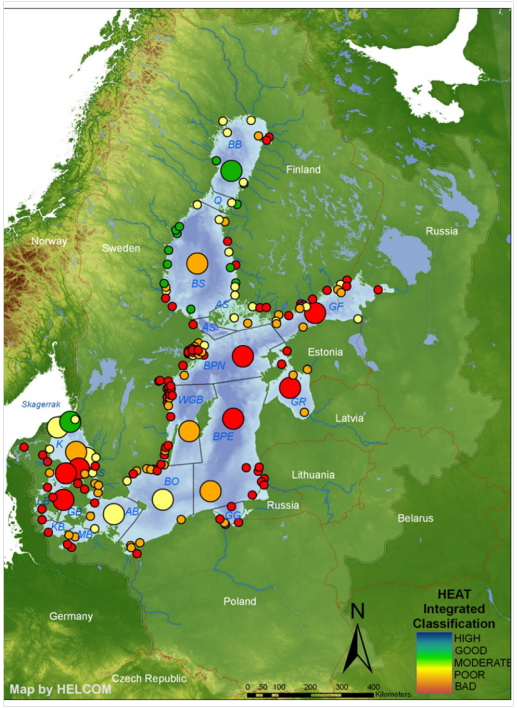

Figure 1.1.: Area-specific state of marine eutrophication in the Baltic Sea. Good status means no effect of eutrophication, large circles indicate open regions, small circles stations or coastal areas [source: HELCOM, 2009].

For example, a Danish case study revealed that phosphorous concentrations decreased by 22 % to 57 % in the Danish straits due to the establishment of waste water treatment plants [Carstensen et al., 2006]. Also, HELCOM denotes a slightly decreasing input of nitrogen and phosphorous, although the target threshold has not yet been reached for both N and P inputs [HELCOM, 2009].
Nevertheless, short- or longterm hypoxia still affected large regions in the Baltic Sea during 2001-2006 [HELCOM, 2009]. The severe impact of human activity on the Baltic Sea throughout all trophic levels has not been stopped and will most likely continue in the future. A monitoring of the future development of the state of the Baltic Sea is still necessary. The time series Boknis Eck provides information on this long-term development over the last 56 years and forms a further tessera in completing the picture of the state and development of ocean and coastal areas.

1.3. Nitrous Oxide and Methane in marine coastal Areas

Nitrous oxide (N_2O) and methane (CH_4) are trace gases which both have an impact on climate [Wang et al., 1976, IPCC, 2007]. Both are known to be produced in marine environments in general, and have been proved to be emitted from the Baltic Sea in particular [e.g. Bange et al., 1998].

N_2O is present in the air in the range of 324.4 $\pm$0.3 ppb (Mace Head, mean 2011). It is known to influence the climate in two ways: First, it acts as a greenhouse gas and enhances global warming [Wang et al., 1976]. Second, it contributes indirectly to ozone depletion, as it can photochemically be converted to NO or NO_2 [Bates and Hays, 1967]. These nitrogen oxides deplete the ozone layer by reacting with oxygen or oxygen radicals [Crutzen, 1970]. Ravishankara et al. [2009] listed N_2O as the dominant contributor to ozone depletion in the 21^{th} century emitted by human activity.

N_2O is emitted from natural sources such as oceans, soils or grasslands as well as anthropogenic activity such as fossil fuel combustion or the application of fertilizers on arable land [Bouwman et al., 1995]. In this context, the oceanic N_2O emissions play an important but not dominant role in the atmospheric budget, as the surface ocean is saturated by 103.5 % by N_2O [Nevison et al., 1995]. Emissions of 3.8 (1.8 – 5.8) Tg N from the open ocean [IPCC, 2007] and 1.7 (0.5 – 2.9) Tg N from coastal areas were reported [Bange et al., 2010b]. Enhanced emissions are usually found in coastal upwelling regions and nitrogen-rich estuaries, where supersaturations of up to 8250 % can be found [Naqvi et al., 2005]. In the Baltic Sea, saturations in the range of 91 – 312 % have been detected in the Bodden waters [Bange et al., 1998] and 123 % in the Bothnian Bay [Rönner, 1983].

The main processes that produce N_2O in the ocean are nitrification and denitrification [Bange et al., 2010b]. Denitrification is the reduction of nitrate to N_2(1.1) by denitrifying bacteria that can use NO_3^- instead of O_2.

$$NO_3 \rightarrow NO_2^- \rightarrow NO \rightarrow N_2O \rightarrow N_2 \tag{1.1}$$

N_2O is an intermediate in this reaction, and its accumulation is highly dependent on the oxygen concentration [Bange et al., 2010b]. This oxygen dependancy results from the redox potential of NO_3^- compared to O_2 and the fact that the involved enzyme, N_2O reductase, is sensitive to O_2 concentrations. Denitrification is thus favoured at suboxic concentrations between 2 – 10 μM, but does not occur under anoxic conditions when nitrate is already consumed [Bange et al., 2010b].

Nitrification is the two-step oxidation of ammonium, where N_2O is a by-product that can be produced from several intermediates of this reaction. Ammonium is first oxidized to nitrite, which is then further oxidized to nitrate (1.2):

$$\begin{aligned} &(I) NH_4^+ \rightarrow NH_2OH* (\rightarrow NO*) \rightarrow NO_2^-* \\ &(II) NO_2^- \rightarrow NO_3^- \end{aligned} \tag{1.2}$$

Compounds marked with an * can serve as a direct precursor to N_2O. Nitrification has long been attributed only to bacteria, e.g. *Nitrosomas* for step I and e.g. *Nitrobacter* for step II [Bange et al., 2010b]. Recently, ammonium-oxidizing genes in archaea have been detected that suggest a major role of archaea as N_2O producers [Löscher et al., 2012].

As N_2O is produced during nitrification and denitrification and both are highly oxygen dependent, the accumulation of N_2O is therefore highly dependent on the oxygen concentration [Bange et al., 2010b]. However, nitrification is believed to be the main production process, with denitrification only contributing 7 % of the oceanic N_2O production [Freing et al., 2011]. If nitrification is the major source for N_2O, a linear relationship between apparent oxygen utilisation and N_2O anomaly exists,

but shows a wide range for different locations [Mengis et al., 1997].
In comparison to N_2O, methane (CH_4) is much more abundant in the atmosphere with a mean concentration of 1873.5 $\pm$10.7 ppb (Mace Head, 2011). Methane acts as a greenhouse gas as well [Wang et al., 1976] and has a global warming potential of 21 in a time span of 100 years [Lelieveld et al., 1998]. Methane undergoes photochemical reactions in the troposphere and therefore also interacts with the ozone layer [Cicerone and Oremland, 1988].
The ocean contributes comparably little to the global methane budget in terms of emissions, as most of the produced methane is already consumed within the water column [Reeburgh, 2007]. The oceans contribute about 2 % [Bange et al., 1994] to 10 % [Grunwald et al., 2009] to the global emissions.
As a source of methane, the sediments play a major role, since most of the methane is produced in anoxic sediments by methanogenesis [Reeburgh, 2007]. Methanogenesis is a microbial process comprising several alternative pathways, the most abundant being CO_2 reduction (I) and the acetate fermentation (II) pathway [Reeburgh, 2007](1.3).

$$\begin{aligned} (I) CO_2 + 4H_2 &\rightarrow CH_4 + 2H_2O \\ (II) CH_3COOH &\rightarrow CH4 + CO_2 \end{aligned} \tag{1.3}$$

Both pathways are thermodynamically favoured only under anoxic conditions.
Estuaries and coastal areas such as the Baltic Sea are believed to play a more important role and may contribute up to 75 % of the oceanic emissions [Bange et al., 1994]. In shallow regions of the Baltic Sea, saturations of $103 - 107$ % were significantly higher compared to deeper regions [Gülzow et al., 2012]. In riverine influenced regions, saturations in the range of $105 - 15500$ % have been detected [Bange et al., 1998]. In general, methanogenesis in the sediments fueled by input of organic matter after plankton blooms is the major source of methane for the Baltic Sea [Thiessen et al., 2006]. However, $87 - 99$ % of the methane is already oxidized within the sediment [Berger and Heyer, 1999]. Methane that is transferred to the water column via diffusion or ebullition is then oxidized in the water column or emitted to the atmosphere [Gülzow et al., 2012]. A further methane input results from pockmark structures in the Eckernförde Bay [Bussmann and Suess, 1998]. These structures are formed by the seeping of groundwater from land-based aquifers [Bussmann et al., 1999]. The groundwater reaching the sediment-water surface in these structures had been enriched in methane by perculating through methane-rich Holocene sediments [Bussmann and Suess, 1998].
In general, both trace gases have common features like their relevance for the global climate, but demonstrate differences in their biogeochemical cycling and sources to the water column.

1.4. Objectives of the Study

As described in section 1.1, the need for evaluating long-term observational data is important for assessing future developments, especially for a highly variable and vulnerable system like the Baltic Sea. This study consists of two main parts which stand on their own, but are linked in a further step. The first goal was to statistically describe the time series of Boknis Eck with regard to long term trends and changes in seasonality. This time series provides one of the longest continuous time

series of oceanographic parameters in the Baltic Sea and is highly valuable to detect changes over decades. Statistical analysis is performed on nine parameters. A focus is set on climatic changes and on eutrophication, the latter being a major problem in the Baltic Sea for many years (section 1.2). Climatic changes are analysed by evaluating the changes in physical parameters such as temperature at the surface and the bottom, salinity at the bottom and the density gradient in the water column as an indicator for stability of stratification. As climate change affects environmental systems worldwide, these parameters are expected to exhibit long-term trends also at Boknis Eck. The second focus addressed is eutrophication. This focus includes analysis of the parameters nutrients and chlorophyll a in the mid water column, Secchi depth and oxygen in the bottom water. As eutrophication is known to decline, nutrients and chlorophyll a are expected to decrease as well. If oxygen concentration is related to eutrophication alone, it is expected to increase in the bottom water as nutrients and primary production decrease. As this is the first statistical evaluation of this time series, a broad statistical approach was chosen. Different statistical tests covering the different components of a time series are applied to gain a first overview on changes in mean and seasonality at Boknis Eck.

The second part stresses the quantification of processes in the nitrogen and methane cycle at Boknis Eck. A 1D box model is developed to simulate trace gas concentrations of nitrous oxide and methane in the surface layer. The goal is to quantificate the processes that influence trace gas concentrations and therefore the air-sea gas exchange of these climatic relevant gases. As relevant processes have not yet been quantified before in this location and precise turnover rates are sparse in literature, optimisation routines with parameter fitting to the measured trace gas concentrations yield first estimations of the turnover rates in this system. The overall question is whether processes are well enough understood to reproduce the seasonal variation in trace gas concentrations. In a further analysis of the model results, the major sources and sinks can be quantified by model output analysis.

The third step links the information of both parts. Part II provides information on which processes influence the trace gas concentrations and therefore the trace gas exchange. These processes are again influenced by other hydrographic parameters. In part I, the trends of these parameters were deciphered. Combining both parts allows a qualitative estimation on the development of the trace gas emissions under the scenario of continuing trends.

2 Material and Methods

2.1. Time Series Station Boknis Eck

The Time Series Station Boknis Eck (BE) is located at the entrance of the Eckernförde Bay (54 °31N, 10 °02 E, 28 m water depth) in the Southwestern Baltic Sea. The monitoring of a variety of physical, chemical and biological parameters was initiated by Prof. Johannes Krey in 1957 [Krey et al., 1980], and has been operated since then on a monthly base with only two major breaks in 1975-1979 and 1983-1985.

As a result of the involvement in different projects, the number of measured parameters varied in time. The time series station BE was supported by DWK Meeresforschung (1957-1975), HELCOM (1979-1995), BMBF (1995-1999), Institut für Meereskunde (1999-2003), IfM-GEOMAR (2003-2012) and GEOMAR (2012-present) [Bange et al., 2011]. Starting with measurements of temperature, salinity and oxygen on April 30^{th}, 1957, the number of parameters has increased almost continuously. Chlorophyll a (since 1960), nutrients (1979) and finally the trace gases nitrous oxide (2005), methane (2006) and DMS (2009) are now part of the monthly routine. A more detailed summary on the parameters and applied methods can be found in table 2.1.

The routine of measurements and analysis has changed little during the observation period. Monthly samples have been taken from research vessels during a half-day trip, the sampling usually starting around 9 to 10 h in the morning. Sea water has been sampled in 6 standard depths (0.5 or 1 m, 5 m, 10 m, 15 m, 20 m, 25 or 26 m) using Niskin Bottles or the like during several casts, prepared on board and cooled until further analysis. Analysis has been carried out mainly in the days following the cruise.

The time series of BE provides a highly valuable dataset due to three main reasons. First, the time span of observation covers 56 years and hence provides continuous information on changes in the time span of decades. Second, there have only been little changes in the methods used for determining the parameters. This consistency strongly enhances the quality of the data, as shifts in the data signals through different methods of analysis can be excluded. Third, the location of Boknis Eck was initially chosen because it reflects the hydrographic setting of the Kiel Bight [Krey et al., 1980]. Being exposed to salt water inflows from the North Sea through Kattegatt and Belt Sea, stratification of the water column occurs during summer. Then, saline water from the North Sea is overlain by fresher water from the Baltic Sea. This stratification is known to occur in other regions of the Southwestern Baltic Sea as well (see section 1.2). As there are no major rivers discharging into the Eckernförde Bay, riverine inputs of e.g. nutrients can be neglected.

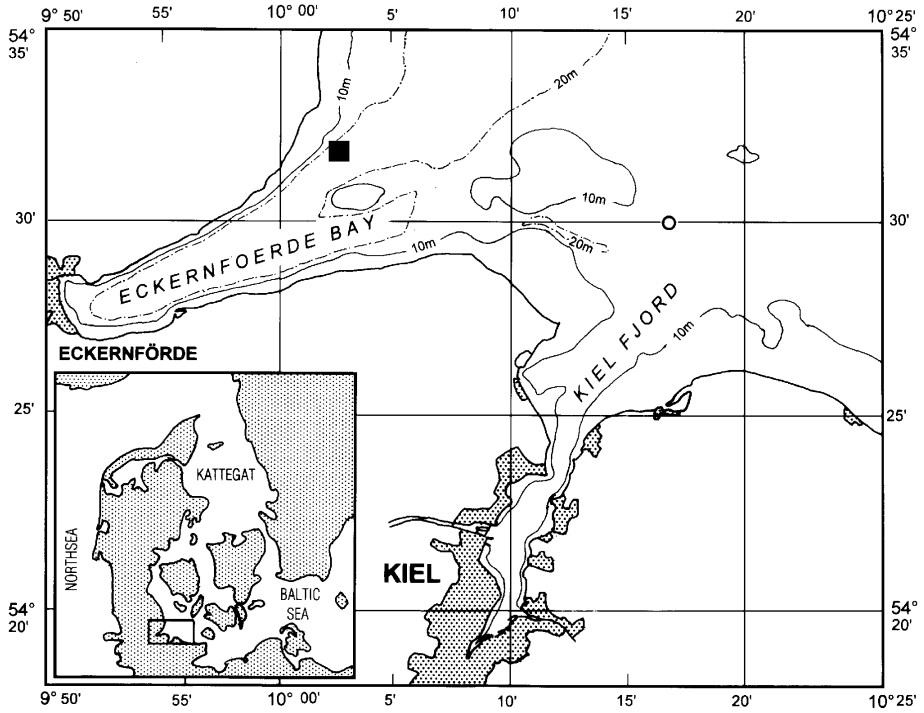

Figure 2.1.: Location of Time Series Station Boknis Eck (black square), at the entrance of Eckernförde Bay, Baltic Sea [from: Hansen et al., 1999].

2.2. Time Series Analysis

2.2.1. Data Preparation prior to Analysis

Depth Categories

The database of the Time Series Station Boknis Eck consists of mainly monthly data from at least 6 standard depths over a time span of the last 56 years. Nevertheless, there are several irregularities in the data that had to be solved before performing the analysis. Some samples were taken in different or additional depths. To obtain constant depth levels, the measurements were averaged over depth intervals, resulting in 6 categories: 0 – 2.5 m, 3 to 7.5 m, 8 to 12.5 m, 13 to 17.5 m, 8 to 22.5 m, 23 to 30 m. The categories are later referred to as 1 m, 5 m, 10 m, 15 m, 20 m and 25 m.

Parameters selected for Time Series Analysis

Temperature, salinity and oxygen concentrations were measured for the longest time. The time series of these parameters starts in April 1957 and lasts until present (here: February 2013). Temperature

Table 2.1.: Synopsis of methods used for determining oceanographic parameters at Time Series Station Boknis Eck since 1957. 1957 to 1979 is described in Krey et al. [1980], during the HELCOM project 1975 to 1995, recommendations of Grasshoff et al. [1999] were given and followed acc. to pers. comm. F. Malien. (n.r. = not reported, CTD = conductivity, temperature, depth, SCFA = Segmented Continuous Flow Analyser, nM=10^{-9}mol/L, μM=10^{-6}mol/L), [1] no time series analysis in this study, listed here for completeness.

Parameter	Unit	Method	Reference	Timespan
Temperature	°C	Reversing thermometer	Krey et al. [1980]	1957 - 1975
	°C	Electrical thermometer, CTD	HELCOM, Grasshoff et al. [1999]	1979 - present
Oxygen	mg/L, μM	Winkler	Krey et al. [1980], Grasshoff et al. [1999]	1957 - present
Salinity	‰	Refractometer	Krey et al. [1980]	1957 - n.r.
	psu	Salinometer, CTD	Krey et al. [1980]	n.r. - present
Total Phosphorous[1]	μg/L	Titration	Kalle [1935]	1957 - June 1970
	μM	Photometer ELKO Zeiss II	Grasshoff et al. [1999]	July 1970 - 1975
	μM	Oxisolv-digestion (Merck), SCFA	Grasshoff et al. [1999]	1979 - present
Phosphate	μg/L	Photometer ELKO Zeiss II	Grasshoff et al. [1999]	1957 - June 1970
	μM	Acidified molybdate reagent, SCFA	Grasshoff et al. [1999]	July 1970 - present
Total Nitrogen[1]	μM	Oxisolv-digestion (Merck), SCFA	Grasshoff et al. [1999]	1979 - present
Nitrate	μM	Reduction to nitrite, SCFA	Grasshoff et al. [1999]	1979 - present
Nitrite	μM	Aromatic amine reagent, SCFA	Grasshoff et al. [1999]	1979 - present
Ammonium	μM	Alcaline hypochlorite solution, SCFA	Grasshoff et al. [1999]	1986 - present
Silicate[1]	μM	Molybdate solution, SCFA	Grasshoff et al. [1999]	1997 - present
Chlorophyll a	μg/L	Methanol-extraction, photometer	Krey [1939]	1975 - 2009
	μg/L	Fluorometer	Welschmeyer [1994]	2009 - present
Secchi depth	m	Secchi disc	Tyler [1968]	1986 - present
N2O	nM	Gas chromatography, headspace	Bange et al. [2001]	2005 - present
CH4	nM	Gas chromatography, headspace	Bange et al. [2010a]	2006 - present

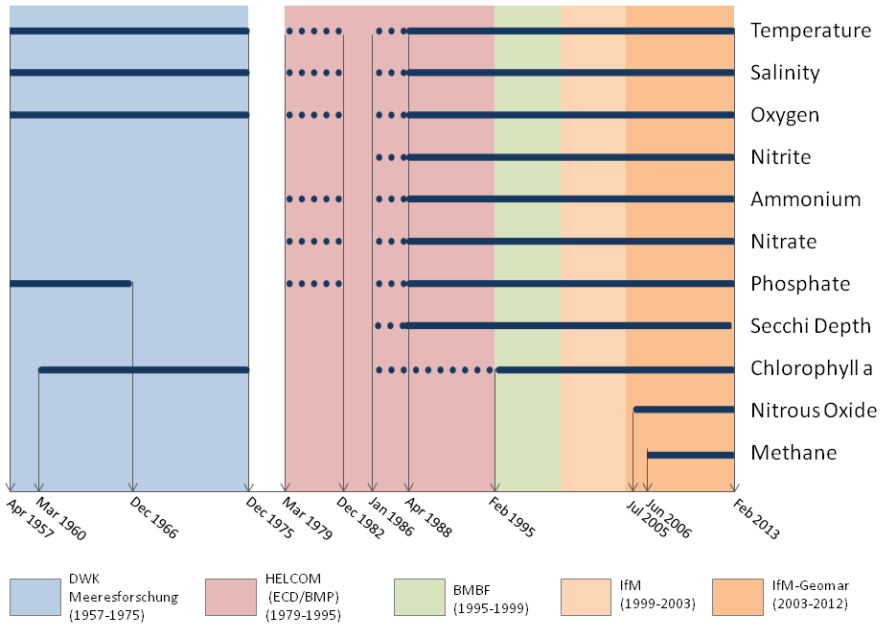

Figure 2.2.: Synopsis of the periods during which the different parameters analysed in this study were measured. Dotted lines indicate a series with many interruptions, a straight line series where only up to 2 months in a row are missing occasionally. Colors indicate under which project the time series measurements were conducted.

changes were analysed at the surface (1 m) and in the bottom water (25 m). Oxygen concentrations were analysed in the bottom water as well, as this is the depth with the largest variation per year. Furthermore, oxygen saturations were caluclated using the time series of oxygen, temperature and salinity according to Garcia and Gordon [1992]. The saturation is the quotient of the actual concentration c_w in the water and the equilibrium concentration c_a under given temperature and salinity conditions (2.1):

$$Sat\,[\%] = 100 \cdot \frac{c_w}{c_a} \tag{2.1}$$

As saturation takes into account the solubility at a specific temperature, changes in saturation provides information on effects other than the purely physical solubility effect. Salinity is analysed in the same depth. As for nutrients, nitrate, nitrite and ammonium and phosphate were examined. Except for phosphate, the measurements started in the early 1980's, but for interpolation, only time series since 1986 were used. Chlorophyll a monitoring already started in the 1960's, but as the two time series differed too much and the gap was larger than 10 years, analysis was carried out seperately for series I (1960-1975) and II (1986-2013). The trace gas observations for methane and nitrous oxide started only recently in 2005 resp. 2006 and were used as a reference in the model simulation. Other parameters measured were total nitrogen, total phosphorous, silicate, DMS, DIC and occasionally more, but these were not included in the time series analysis in this study.

Besides these measured parameters, seawater density was calculated from the salinity and tempera-

ture measurements. The density gradient in the water column is seen here as an indicator of intensity of stratification. The density is calculcated using the equations of UNESCO [1981]. The gradient is then calculated by the difference between surface (1 m) and bottom (25 m) density divided by the distance between the two standard depths (24 m).

Missing Values

Due to cruise cancellations, analysis problems or the like, some data was missing. Most of the analysis could be performed with the raw data including missing values, such as the Mann-Kendall-Test, but for other analyses like wavelet analysis or quantile regression, a continuous, uninterrupted time series was needed. Two different types of missing data appeared: First, in some cases, only data for one or two months in a row were missing. This lack of information was solved by interpolation, as there was sufficient information provided by the surrounding months to estimate the missing values. Here, a linear interpolation was used which is equivalent to a distance-weighted average of the two neighbouring data points. For this purpose, the Matlab function *interp1* with a linear interpolation option was applied. As a consequence, missing maximal or minimal values are under- or overestimated respectively, as this replacement method cuts off peaks. This has to be kept in mind as it renders the estimate for trends in extreme values more conservative.
A more delicate problem are the two missing time periods in 1975-1979 and 1982-1985. Here, two different methods were applied: For temperature, a model output for Boknis Eck, coming from the Baltic sea-ice ocean model (BSIOM) developed by GEOMAR [Lehmann, 1995], was available. Data was compared for the depth of 1 m, and yielded satisfying results with a Pearson's R value of 0.99 (fig. 2.3). Thus, the missing years were replaced by the model outputs. For nutrients and other time series, no model result existed. These missing values were replaced by the median value of the corresponding month, day 15. This replacement method is robust against outliers and ensures that there are no artificial extreme values.

Regular Spacing

Regularly spaced data was needed for testing for significance in quantile regression and for wavelet analysis. If measurements were taken several times a month, they were averaged. Measurements were then shifted to the 15^{th} of each month. This ensures that all measurements taken were considered in their full magnitude, so no extreme values were lost. Gaps for months without measurements were interpolated as described above. The final filled and interpolated time series consists of the 15^{th} day of each month from May 15^{th}, 1957 to Febuary 15^{th}, 2013.
To check whether the gap filling changes the time series significantly, the mean and variance of the time series was compared before and after the refilling as recommended by Trauth [2010]. If they were similar, the refilled time series was used for further analysis.

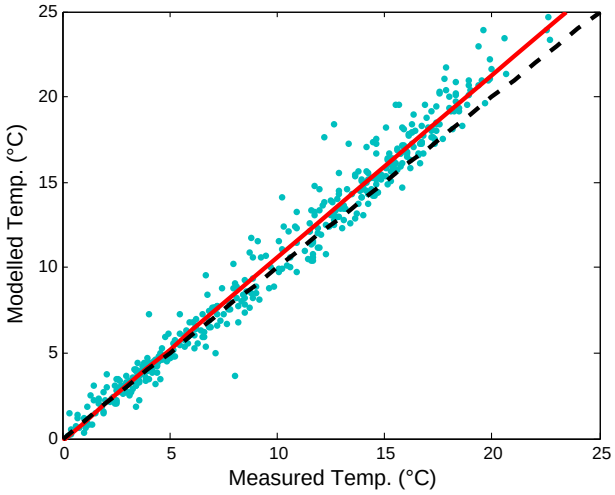

Figure 2.3.: Comparison of modelled (Baltic Sea-Ice Ocean Model, [Lehmann, 1995]) and measured temperatures in a depth of 1m at Boknis Eck (R=0.99), with linear regression (-) and bisectrix (- -).

2.2.2. The classical Component Model of a Time Series

A time series is defined as a number of observations taken sequentially over a certain time span [Box et al., 2008]. The obtained sequence may contain the superposition of several signals from different sources overlaying each other. Separating the superposition of the different components is an essential part of time series analysis [Schlittgen and Streitberg, 2001]. The basic concept of this so called *classical component model* decomposes a time series into at least three main components, termed trend, cyclic and residual component [Schlittgen and Streitberg, 2001].

The trend is mainly seen as the longterm systematic change in the mean of the time series [Schlittgen and Streitberg, 2001]. Trends can be modelled parametrically as linear, polynomic or exponential, the first being most often the case [Woodward and Gray, 1993]. As applied here, a trend can also be tested in a nonparametrical way, i.e. no model is defined beforehand (see section 2.2.4). However, it is important to state that the trend only refers to the observed time span. As the time series were not modelled in this study, it cannot necessarily be assumed that the trend further continues with the same magnitude.

The second component includes one or several periodically repeating cycles [Schlittgen and Streitberg, 2001]. A cyclic component that is present in the majority of environmental time series is for instance an annual cycle Trauth [2010]. Several cycles can be superposed and do not necessarily occur throughout the whole observed time span (see section 2.2.6).

The residual component comprises random noise in the signal and includes all oscillations that cannot be explained [Schlittgen and Streitberg, 2001]. In the time series analysed in this study, this component can occur due to small scale and short term variability of the measured parameters or fluctuations within the measuring inaccuracy.

To accurately describe the trend and the cyclic component of the time series, statistical tests dealing with one of these components were performed. Testing for breakpoints and the Mann-Kendall-Test cover the first component whereas wavelet analysis, including fourier transform, deals with the cyclic component. Further tests regarding extreme values revealed additional information on the long term behavior of the parameter although they are not part of the classical component model.

2.2.3. Identifying Breakpoints in Time Series

Breakpoints in time series were defined here as changes in the magnitude or direction of a long-term trend. Testing for a long-term trend using the Mann-Kendall-Test as described in section 2.2.4 tests the null hypothesis of a monotonic trend [Hirsch and Slack, 1984]. The result might be misleading if a breakpoint and hence a variation in the trend over time occurs. Therefore, breakpoints had to be identified first.

To detect breakpoints in the time series, a simple approach was followed, as the breakpoints were only considered as a precondition for the Mann-Kendall-Test. Basically, the slopes between adjacent data points were computed and cumulatively added. Several positive slopes in a row indicated a longer increasing tendency in the time series, negative slopes the opposite. A breakpoint was defined here as the maximum or minimum between a sequence of positive or negative slopes of the cumulated sum. In contrast to other methods, the method described here did not require a predefined model, which made it suitable for testing the precondition of a nonparametric test as the Mann-Kendall-Test.

2.2.4. Testing for long-term trends: the Mann-Kendall-Test

The Mann-Kendall-Test (MKT) is a statistical test to decipher significant monotonic long-term trends in time series. The test was first proposed by Mann [1945], modified by Kendall [Hirsch and Slack, 1984] and is now an established test for detecting trends in environmental time series. It tests the null hypothesis that all variables are randomly distributed against the alternative hypothesis that a monotonic trend exists in the time series on a given significance level α (here always α=0.05).

The MKT is a rankbased, nonparametric test, meaning that no model is defined beforehand and then fitted to the data like e.g. in a linear regression. The MKT simply states whether there are significantly more data points larger (or smaller) than the previous one in the time series. If this is the case, a significant increase (or decrease) exists. The test statistic of the MKT is summarized in the following according to Hirsch and Slack [1984]. First, each data point X_i of a time series X_1, X_2, ..., X_n is compared to the previous one and ranked according to equation 2.2:

$$\begin{aligned} sgn(x) &= -1 \quad \text{if } x_i < x_{i-1} \\ sgn(x) &= 0 \quad \text{if } x_i = x_{i-1} \\ sgn(x) &= +1 \quad \text{if } x_i > x_{i-1} \end{aligned} \tag{2.2}$$

The test statistic S is the sum of these ranks (2.3):

$$S = \sum_{i=1}^{n-1} sgn(X_i - X_{i-1}) \tag{2.3}$$

The test statistic S has a mean of zero with a variance σ^2=n(n-1)(2n+5)/18 under the null hypothesis of a random distribution [Hirsch and Slack, 1984]. If S differs significantly from zero, e.g. lies outside the quantile of the variance that is defined by the level of significance, a trend exists. A level of significance of $\alpha = 0.05$ requires that S lies within the range of $1 - \frac{1}{2}\ \alpha$ (two-sided) of the variance for accepting the null hypothesis of no homogeneous trend.
The MKT is advantageous when the data contains missing values, violates the assumption of normal distribution or includes censored values [Hirsch and Slack, 1984]. These are problems often encountered in environmental time series, which makes the MKT a widely used test in hydrology and climatology. Furthermore, it can be modified to decipher trends in seasonal data, e.g. monthly data like the BE time series. Then, a MKT for each season is performed with the alternative hypothesis of a monotonic trend in one or more seasons against the null hypothesis of randomly distributed data [Hirsch and Slack, 1984]. This might be misleading if the seasons show opposite trends, so a test for homogeneity of trend is performed first. The test statistic S' for the seasonal test is the sum of the single test statistics S_g from seasons 1,2,...,p (2.4):

$$S' = \sum_{g=1}^{p} S_g \tag{2.4}$$

The S_g are distributed around a mean of zero and a variance of var[S'] (2.5) under the null hypothesis:

$$var[S'] = \sum_{g} \sigma_g^2 + \sum_{g,h(g\neq h)} \sigma_{gh} \tag{2.5}$$

The first term of equation 2.5 is the variance of the single test statistics S_g, the second term is the sum of the covariances. The underlying assumption in the test proposed by Hirsch and Slack [1984] is that the data are independent and therefore the covariance is always zero (see below).
Nevertheless, the MKT also has weaknesses. As a nonparametric test, the MKT has less power than a parametric one. This lower power means that a present trend might not be detected at the given level of significance. However, the advantages that no model has to be defined beforehand outbalance this weakness. Secondly, the MKT is sensitive against serial correlation in the time series. Even small serial correlation might lead to inaccurate results [Kulkarni and Von Storch, 1995]. How to cope best with serial correlation has been widely debated. Kulkarni and Von Storch [1995] advocated for a prewhitening procedure removing the serial correlation. Yue and Wang [2002] stated that this would also lead to a removing of the trends and is therefore not suitable. In this study, a method to overcome this problem was used that was proposed already in 1984 by Hirsch. This method estimated the

serial correlation from the data and adjusted the variance in equation 2.5 accordingly [Hirsch and Slack, 1984]. Nevertheless, if the months are tested individually, it is assumed that there is no residual effect from the same month last year. Hence, there is no accountation for serial correlation in these monthly series.

If a trend is present in the time series according to the MKT, a slope was computed using Sen's method [Sen, 1968]. This slope b is the median of the slope between each pair of points used for the ranking in MKT (2.2).

$$b = median \frac{x_j - x_l}{j - l} \forall l < j \tag{2.6}$$

95 % confidence intervals were computed accordingly. The MKT test was applied to the raw data including missing and tied values, the latter were averaged within the MKT function. For the test, a MatLab function from Burkey [2012] based on the MKT accounting for serial correlation by Hirsch and Slack [1984] and Sen's method [Sen, 1968] was used.

2.2.5. Testing for long-term Trends in extreme Values: Quantile Regression

For some parameters, evidence of a trend in extreme values might be more meaningful than a general trend in the time series. For instance, this is the case for oxygen, where the increase in anoxic events has more severe consequences than a general slight decrease in concentration. The de- or increase of extreme values within the time series was evaluated by quantile regression. This regression technique is a commonly used method to analyse the variation of extreme values over time not only in environmental time series [Yu et al., 2003, Koenker and Hallock, 2001].

Quantile regression is a least-squares optimisation technique similar to linear regression [Yu et al., 2003, Koenker and Hallock, 2001]. In linear regression, a linear model is fit to the data by minimizing the residuals between the data and the model (2.7) [Koenker and Hallock, 2001]:

$$min \sum_{i=1}^{n} (y_i - \mu(x_i, \beta))^2 \tag{2.7}$$

y_i refers to the single data points in the time series, μ (x_i, β) to the fitted model, with the dates x and the estimator β in y=βx. In a linear model, this term is also referred to as the conditional mean. Quantile regression does not minimize the difference to the conditional mean but the conditional quantile by using a weighting function for the residuals ρ (2.8)[Koenker and Hallock, 2001]:

$$min \sum_{i=1}^{n} \rho_t (y_i - \xi(x_i, \beta)) \tag{2.8}$$

ρ is a function that assymmetrically weights the residuals according to the distance from the quantile (fig.2.4a), ξ is the conditional quantile, e.g. the quantile function expressed by an assumend model. Qantile regression can be used in a nonparametric way or with a variety of different models [Koenker and Hallock, 2001, Franzke, 2013], but here, a linear regression line y=βx+n was used. The quantiles

90 % and 10 % were chosen to represent the extreme values.

An estimate of the changes in extreme values of a particular time series alone does not provide information on statistical significance. Franzke [2013] proposed a method to assess the significance in changes in extreme values in time series. This method follows an constrained Monte-Carlo-approach to generate surrogate data. Quantile regression is then applied to each of the surrogate data sets. A statistically significant trend is present if the trend in the original time series lies outside of the 95 % boundaries of the trends for the surrogate data, which equals a level of significance $\alpha = 0.1$ (two-sided).

The surrogate data was generated by following an approach of Schreiber and Schmitz [1996]. The goal was to generate a surrogate time series with the same linear characteristics as the original data, that is, with the same serial correlation and the same distribution of values. Several time series can have the same serial correlation if their power spectrum is the same, e.g. cycles with the same frequencies are present within the data. Schreiber and Schmitz [1996] proposed an iterative algorithm that generates time series with the same power spectrum and the same range of values which is summarized in the following.

1. **Fourier Transform I and shuffeling**
   A Fourier transformation (FT) was performed on the original time series. To each frequency, the power with which it is present in the time series is assigned. This is referred to as the fourier power spectrum [Glover et al., 2011]. The squared amplitudes of the fourier spectrum as well as a sorted list of the values of the original time series was then stored. The values were shuffled randomly without replacement, resulting in a new artificial time series.
2. **Fourier Transform II and replacement**
   The new time series was fourier transformed. Different time series can have the same power spectrum, and if this is the case, they also have the same serial correlation according to the Wiener-Khinchin theorem [Schreiber and Schmitz, 1996]. After the FT of the new time series, the amplitudes were replaced by the amplitudes of the FT of the old time series. Then, the new and replaced time series was transformed back into physical space with inverse FT.
3. **Rank ordering**
   Now the same serial correlation has been produced, but usually the range of values has changed. The new series was then rank ordered according to the original time series. This led to a better fit of the distribution range of the two time series, but alterated the spectrum again.
4. **Iteration**
   Steps 2. and 3. were repeated iteratively until the defined criterium of convergence was reached. In the code used here, the iteration was stopped if no further improvement in the amplitude spectrum could be made, e.g. the distance between the old and the new time series could not be reduced after a further iteration step. The maximum number of iterations was set to 500.

Following this approach, 500 surrogate time series were generated. As the generation of the surrogate data required complete time series, both the quantile regression and the generation of the data

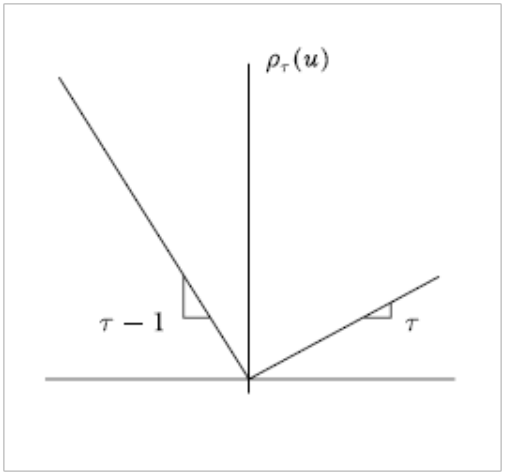

(a) Weighting function ρ for quantile regression [Koenker and Hallock, 2001].

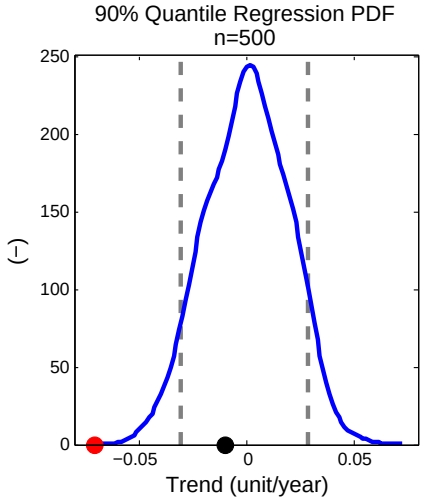

(b) Schematic probability density function (PDF) of the pooled trends of 500 surrogate data sets with a significant trend (red) and a nonsignificant trend (black).

Figure 2.4.: Quantile regression.

sets were performed with the interpolated and gap-filled time series described in subsection 2.2.1. Following Franzke [2013], quantile regression was performed with each of the surrogate time series. The resulting trends were pooled. Franzke [2013] showed that the distribution of the trends in the surrogate time series is centered around zero. Comparing the trend of the original time series with the pool of the newly generated trends provides information whether the trend computed by quantile regression is significant or not. With the level of significance set to $\alpha = 0.1$, a trend detected in the quantiles of the original time series is considered statistically significant if it lies outside the 5-95 % interval of the pooled trends (fig. 2.4b).

A difficulty with this method may arise if not enough surrogate time series are created to assess the significance of the trend. However, the centering around zero for the pooled trends was checked before proceeding with the analysis, and 500 surrogate data sets yielded satisfactory results. On the other hand, one large advantage of this method is that all data could be used and not only data above or below a predefined threshold [Franzke, 2013].

For the analysis performed here, the original MatLab code by Franzke [2013] was used. Quantile regression was computed using a MatLab code by Grinsted [2011], based on the quantile regression algorithm by Koenker and Hallock [2001].

2.2.6. Testing for Changes in seasonal Cycles: Wavelet Analysis

As discussed in section 2.2.2, a time series can be decomposed in a trend, a seasonal component and noise. Wavelet analysis concentrates on separating the superposed cycles present in a time series. The major advantage of wavelet analysis opposite to Fourier transform alone is that the first yields

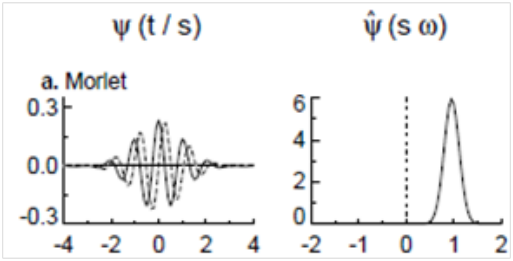

Figure 2.5.: Morlet mother wavelet as used for wavelet transform with a wavenumber of 6 and a real (-) and a complex (- -) part [source: Torrence and Compo, 1998]. Left: Morlet wavelet in time space, Right: Morlet wavelet in frequency space.

results in time as well as in the frequency space [Trauth, 2010]. Wavelet analysis reveals which frequency of a cycle, say a typical annual cycle with a frequency of 1, is present where in the time series, e.g. only during the first half. In this example, Fourier transform would only reveal that a seasonal cycle of the frequency 1 is present somewhere in the time series.

A wavelet is a function that is localized specificly in time and in frequency domain in contrast to sine or cosine waves used for Fourier transform. A sine or cosine wave is localized in frequency space, as it has a particular frequency, but it continues infinitely, hence it is not localized in the time domain. A wavelet also has a specific frequency in the center, but oscillates to zero on the edges, resulting in a localization also in the time space. This difference makes it suitable for detecting frequency and position of seasonal cycles in a time series.

The principle of wavelet analysis is to scale the wavelet to different center frequencies that are each translated along the time series. The convolution of the wavelet with the original time series provides information on how well the wavelet with the particular frequency correlates with the time series at a certain point [Glover et al., 2011]. A high correlation means a high power of the particular frequency. The scaling serves to test different frequencies, that is to find seasonal cycles that differ in length of the period.

One drawback of the method is that wavelet analysis requires a complete and regularly spaced time series [Trauth, 2010]. Thus, the gap-filled and interpolated time series was used. However, as there is no alternative and only modified time series that do not vary too strong in variance and mean were considered, this shortcoming was accepted.

Furthermore, the selection of the right wavelet is not trivial. Following the recommendations of Torrence and Compo [1998], a Morlet mother wavelet Ψ (fig. 2.5) with a wave number of 6 was chosen which is defined as (2.9):

$$\Psi(x) = exp(-0.5x^2) \times cos(5x) \tag{2.9}$$

The Morlet wavelet is nonorthogonal and complex as recommended for the use with time series, has an acceptable band width in both freuency and time space and a shape that reflects the main features of the time series [Torrence and Compo, 1998]. The mother wavelet was then scaled between the frequency of a half-year cycle and the length of the time series with a stepsize of 0.25.

For the wavelet analysis, the MatLab code by Torrence and Compo [2004] was applied. The time

series was padded with zeros at the end as recommended by Torrence and Compo [1998] to the next length of a power of 2 (here 2^{10}) to reduce edge effects and accelerate the FT. It was standardized by subtracting the mean and dividing by the standard deviation before analysis. A continous wavelet transform was performed as it yields smoother results compared to a discrete wavelet transform. Wavelet analysis does not only yield qualitative results but can be tested statistically for significant cycles present in the time series. Torrence and Compo [1998] suggested testing against a series of red or white noise to decipher the major seasonal components. Here, a red noise spectrum was chosen as the autocovariance of the time series did not equal zero as required for a white noise spectrum. There is one other restriction for significant areas in the wavelet power spectrum plot, the so called cone of influence. Edge effects may occur at the beginning and the end of the time series, with extending length at lower frequencies. The cone of influence marks the area where the wavelet analysis shows valid results [Torrence and Compo, 1998].

2.3. Set-up of the 1D Box Model

2.3.1. General Set-up

Trace gas concentrations of nitrous oxide and methane were simulated in the mixed layer of the time series station Boknis Eck (BE) with a simple 1D box model and compared to meaurements in the period of 2005-2012 (N_2O) resp. 2006-2012 (CH_4). The goal was to identify relevant processes that influence the seasonal variability of these gases. The relevant processes for nitrous oxide and methane were different, so the model set up for both gases is similar for the physical but different for the biogeochemical processes. The measured concentration profiles for the trace gases at BE showed an increase with depth for both gases, but the variation for methane was stronger (fig. 2.6). N_2O had a more homogeneous profile. Hence, the concentrations of nitrous oxide were modelled in the surface mixed layer (MLD) whereas the concentrations of methane only account for a depth of 1 m (surface layer), as concentrations were not homogeneously distributed in the mixed layer.

The general model set-up is similar to the model of seasonal variability of methane and nitrous oxide in the Arabian Sea [Bange, 2004]. The temporal variability of the concentrations in the respective depth ($\partial C_w/\partial t$) was simulated as (2.10):

$$\frac{\partial C_w}{\partial t} = (\frac{\partial C_w}{\partial t})_{ase} + (\frac{\partial C_w}{\partial t})_{mix} + \sum(\frac{\partial C_w}{\partial t})_{sp} \tag{2.10}$$

$(\frac{\partial C_w}{\partial t})_{ase}$ stands for the air-sea gas exchange across the ocean-atmosphere interface, $(\frac{\partial C_w}{\partial t})_{mix}$ is the change in concentration through upward mixing from the subsurface layer and the last term $(\frac{\partial C_w}{\partial t})_{sp}$ stands for the sum of specific source and sink processes in the mixed layer.

The air-sea gas exchange is modeled here by the quotient of flux density F divided by the mixed layer depth MLD with (2.11):

$$(\frac{\partial C_w}{\partial t})_{ase} = \frac{F}{MLD} \tag{2.11}$$

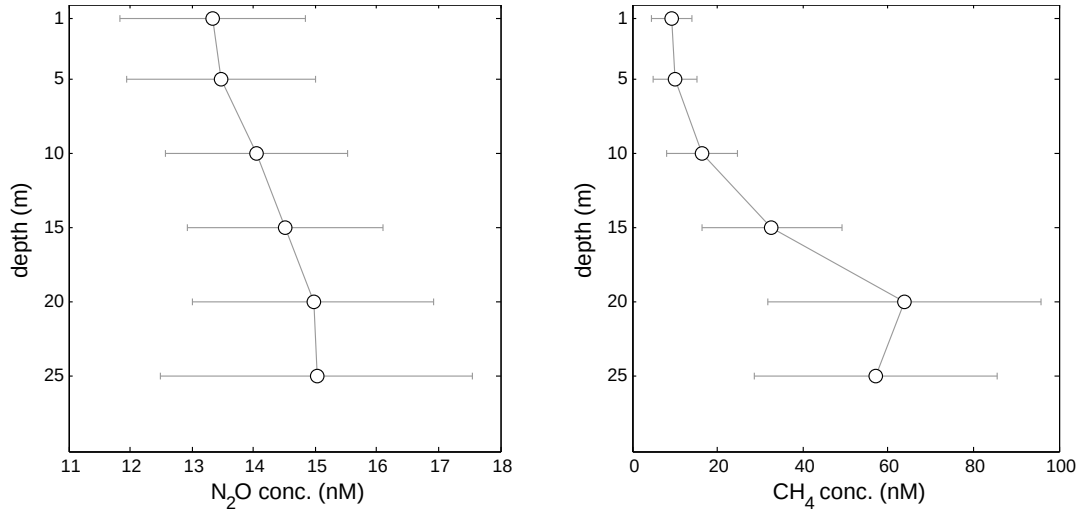

(a) Nitrous oxide **(b)** Methane

Figure 2.6.: Mean profile of measured concentrations at BE during July 2005- September 2012

The flux density is driven by the difference in actual concentration C_w and equilibrium concentration C_a in sea water and is further influenced by the gas transfer coefficient k_w(u) in dependence of wind speed (equ. (2.12)):

$$F = k_w(u) \cdot (C_a - C_w) \tag{2.12}$$

The equilibrium concentration C_a was calculated as the product of Bunsen solubility and dry mole air fraction (2.13).

$$C_a = \beta(T, S) \cdot x' \tag{2.13}$$

The Bunsen solubility is a function of temperature T and salinity S, and was calculated according to Weiss and Price [1980] for nitrous oxide and Wiesenburg and Guinasso [1979] for methane.
The transfer coefficient was used to parametrize the air-sea gas exchange dependent on wind speed. Three different parametrisations were applied. The parametrisation of Liss and Merlivat [1986] is a relationship between wind speed and transfer coefficient which is divided into three linear functions (LM86). The slope of the three functions increases with wind speed, as gas exchange increases from the smooth regime (0-3.6 m/s), to the rough (3.7-13 m/s) and bubble regime (>13 m/s) ((2.14)).

$$\begin{aligned} k_w &= 0.17 \cdot u_{10} \cdot (\frac{Sc}{600})^{\frac{2}{3}} && \text{for u} \leq 3.6 \\ k_w &= (2.85 \cdot u_{10} - 9.65) \cdot (\frac{Sc}{600})^{\frac{1}{2}}) && \text{for 3.6<u} \leq 13 \\ k_w &= (5.9 \cdot u_{10} - 49.3) \cdot (\frac{Sc}{600})^{\frac{1}{2}}) && \text{for 13<u} \end{aligned} \tag{2.14}$$

As the relationship is normalized for CO_2 exchange at a temperature of 20°C, it had to be adapted to the particular gas. This is done by multiplying with the Schmidt number Sc of the particular

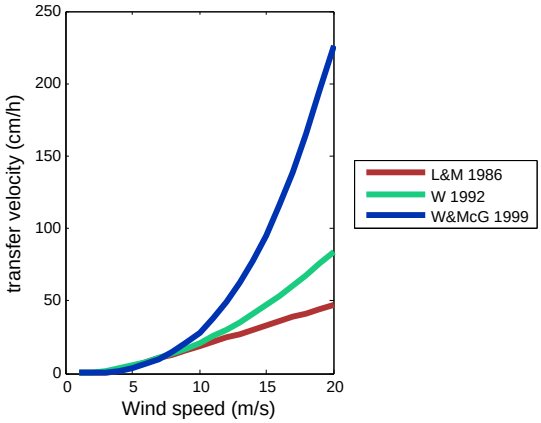

Figure 2.7.: Parametrisations of transfer velocity dependent on wind speed used in the 1D Box Model of Boknis Eck: the tri-linear relationship of Liss and Merlivat [1986], the quadratic relationship of Wanninkhof [1992] and the cubic relationship of Wanninkhof and McGillis [1999].

gas to the power of an empiric exponent. The Schmidt number is calculated as the quotient of the kinematic viscosity of sea water and the diffusion coefficient. The diffusion coefficient of methane was computed according to Jähne et al. [1987], the one for nitrous oxide according to Broecker and Peng [1974].

The second relationship was the cubic relationship of Wanninkhof [1992](W92), derived from wind-wave tank experiments and calibrated with field data (2.15). This relationship referred to steady winds. The relationship is valid for CO_2 exchange at 0°C, and had to be scaled according to the present temperature and gas as above.

$$k'_w = 0.31 \cdot u_{10}^2 \cdot (\frac{Sc}{660})^{\frac{1}{2}} \tag{2.15}$$

The third parametrisation of the transfer coefficient was taken from Wanninkhof and McGillis [1999] (WMcG99), which parametrises air-sea gas exchange for steady and short term winds combined (2.16). Again, the transfer coefficient had to be adjusted as decribed above.

$$k'_w = 0.0283 \cdot u_{10}^3 \cdot (\frac{Sc}{660})^{\frac{1}{2}} \tag{2.16}$$

The second part of equation 2.10, $(\frac{\partial C_w}{\partial t})_{mix}$, is computed as the difference in concentration between the surface C_w and the subsurface layer C_{ssl} scaled to the fraction of the change in mixed layer depth MLD from one time step to the next (2.17).

$$(\frac{\partial C_w}{\partial t})_{mix} = (C_{ssl} - C_w(t)) \cdot \frac{\Delta MLD}{MLD(t) + \Delta MLD} \tag{2.17}$$

The concentration after one time step (Δt=0.5 days) was then calculated as the sum of the previous concentration and the change in concentration during the particular time step (2.18).

$$\begin{aligned} C_w(t+\Delta t) &= C_w(t) + \Delta C_w \\ \text{with } \Delta C_w &= \frac{F}{MLD} \cdot \Delta t + \Delta C_{mix} + \Delta C_{sp} \end{aligned} \tag{2.18}$$

The first measured concentration for each gas in the mixed layer was chosen as initial condition. Therefore, the concentrations across the mixed layer were averaged for nitrous oxide. As for methane, only the concentrations for the surface layer of 1m were simulated, these were chosen as initial conditions.

Results of the simulation are represented as concentrations and as saturations in percent, with C_w as the present concentration in the mixed and surface layer respectively at time step t and C_a the corresponding equilibrium concentration (see eq. 2.1). The concentrations and saturations were compared with actual measurements in that period and saturations computed with measurement data. For N_2O, the whole mixed layer was considered and concentrations used for comparison were averaged over the mixed layer. The methane profiles showed variations independent from the mixed layer depth, so simulations were compared and fitted to surface (1 m) concentration measurements.

2.3.2. Input Data

Mixed layer depth was determined by a specificly developed criterion in the depth profiles at BE during the simulated period. Based on temperature and salinity profiles (CTD, conductivity, temperature, depth), the density was calculated using the UNESCO [1981] international equation of State of Seawater. Derived from the density profiles, a density gradient of 0.8 kg/m^4 was coincident with the location of the pycnokline in the profiles. In few cases (<10%), the mixed layer boundary was not reproduced accurately and was adjusted using the CTD profiles as reference. Mixed layer criteria from Kara et al. [2000] or de Boyer Montegut et al. [2004] did not yield accurate results in agreement with the CTD profiles.

Temperature, salinity, oxygen, ammonium and chlorophyll a data were obtained from the BE time series described above. The concentrations of the subsurface layer were taken from the BE time series as well, but were averaged below mixed layer depth for the N_2O-model.

Air mole fractions of both gases were needed to calculate the equilibrium concentrations. Both were taken from time series measured in Mace Head, Ireland. These data are part of the Advanced Global Atmospheric Gases Experiment and are available online via *http://agage.eas.gatech.edu/data.htm* (retrieved July 2013). Although the station BE and Mace Head are approx. 1600 km distant, air mole fractions were assumed to be comparable. In a study of Bange et al. [1998], mole fraction data of the Southern Baltic Sea were compared with the data from Mace Head and proved agreement in a range of 0.02 ppm for methane and 2 ppb for nitrous oxide.

The wind data was obtained from the German Weather Service (DWD) from the station Kiel Lighthouse. The distance to BE is approximately 20 km, but is assumed to reflect the wind speed over open water at BE. As the measurements were taken at the Kiel Lighthouse station in 34 m above sea

level (until 2007 in 18 m), the wind speed had to be normalized to 10 m as required for the air-sea gas exchange parametrisiation. The logarithmic law of wind speed allows the adaptation of the wind speed u_z in altitude z to 10 m above sea level according to equation 2.19 [Roedel, 2000]:

$$u_{10} = u_z \cdot \frac{\kappa}{\sqrt{cd}} \cdot \frac{1}{\frac{\kappa}{\sqrt{cd}} + ln(\frac{z}{10})} \tag{2.19}$$

κ is the Karman-constant (0.41), cd the drag coefficient $1.3 \cdot 10^{-3}$ [Roedel, 2000], z is the altidute above sea level where windspeed was measured.
All input data were interpolated linearly to a regular grid of a time step of 12 hours before simulation. Figures illustrating the input data are provided in appendix B.

2.3.3. Processes specific for Nitrous Oxide

For the third term in equation 2.10, specific processes to N_2O were implemented. Crucial for implementing processes are turnover rates that allow estimations on the change of concentration over time. If possible, these rates were calculated by actually measured data at BE. However, if that was not possible, parameter estimation for the rates as described in section 2.3.5 was applied.
Two different model set-ups were compared here, that are based on different assumptions. They differ mainly in the location of N_2O production. The first model includes a mean, homogenous production rate that is derived from actual measurements. The second one assumed production only below the mixed layer, with N_2O diffusion upwards.
The first model assumes that N_2O is produced by nitrification and denitrification homogeneously in the water column. This is implemented by a segmented linear relationship between the apparent oxygen utilisation rate (AOU) in the bottom water and the mean N_2O production in the water column.
AOU is calculated as follows (2.20) from measured (meas) and saturation (sat) concentrations:

$$[AOU] = [O_2]^{sat} - [O_2]^{meas} \tag{2.20}$$

For implementing the effect of denitrification and nitrification in the model, AOU is not related to a concentration but to a production rate, as information on the change of concentration over time is needed. This rate is calculated as the difference in concentration between two measurements t_i and t_{i-1} plus the amount of N_2O that is lost by air-sea gas exchange in between. Therefore, a mean flux is calculated as described in section 2.3.1 and added to the concentration difference (2.21).

$$\Delta C_w(t) = \frac{N_2O_{t_i} - N_2O_{t_{i-1}} + N_2O_{flux}}{t_i - t_{i-1}} \tag{2.21}$$

Eight measurements under high oxygen conditions, that are already covered by the ventilation peak implementation (see below) and one very high and two very low production rates were excluded. The

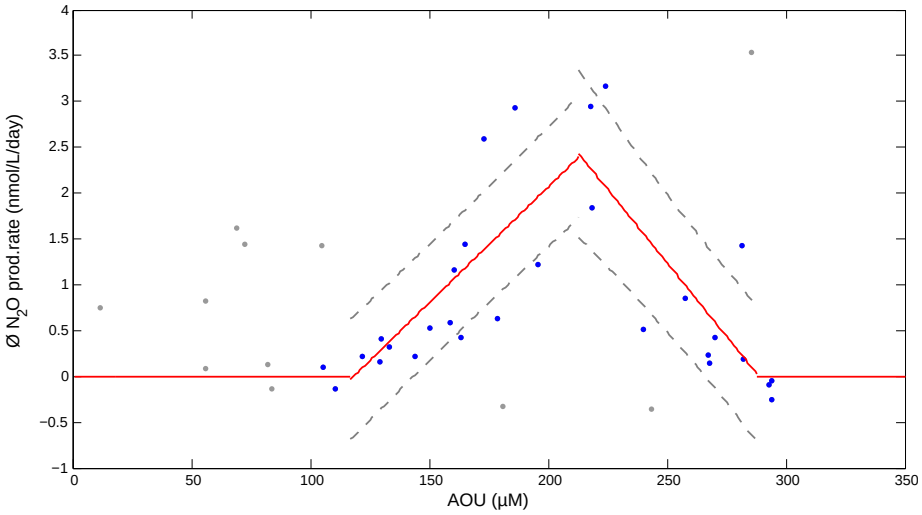

Figure 2.8.: Segmented linear regression to describe mean N_2O production in the water column relative to the bottom water apparent oxygen utilisation (AOU). Measurements marked in grey were excluded either because they are outliers or because AOU was low, indicating a ventilation event.

remaining values were divided into 4 segments (2.22):

$$\begin{aligned} \varnothing N_2O_{prod} &= 0 && \text{for AOU<105}\mu\text{M} \\ \varnothing N_2O_{prod} &= 0.025 \cdot AOU - 2.99 && \text{for 105}\mu\text{M} \leq \text{ AOU<117} \\ \varnothing N_2O_{prod} &= -0.032 \cdot AOU + 9.26 && \text{for 117} \leq \text{ AOU<288}\mu\text{M} \\ \varnothing N_2O_{prod} &= 0 && \text{for 288}\mu\text{M} \leq \text{ AOU} \end{aligned} \tag{2.22}$$

This relationship describes the mean N_2O production $\varnothing N_2O_{prod}$ in the water column per liter per day relative to the bottom water AOU (fig. 2.8).

The second model assumed that the relevent N_2O production takes place below the mixed layer. Thus, no direct production rate is included. However, if the concentration of N_2O below the mixed layer increases, more N_2O is assumed to reach the mixed layer. This process is modelled by a diffusion term dependent on the concentration gradient across the mixed layer boundary and an estimated diffusion coefficient (see section 2.3.5). The diffusion flux density J is simulated by using Fick's first law of diffusion (2.23) with a diffusion coefficient D and the concentration gradient $\frac{\partial c_w}{\partial z}$.

$$J = -D \cdot \frac{\partial c_w}{\partial z} \tag{2.23}$$

A further process that both N_2O models include is enhanced nitrification after the breakdown of summer stratification. Schweiger et al. [2007] analysed hydroxylamine variation during one year at BE and found that a strong pulse of nitrification occurs after the breakdown of the stratification in fall. This enhancement of nitrification is accompanied by an increase in N_2O production [Naqvi et al., 2010]. After this breakdown, the water column becomes aerated again and with increasing

oxygen concentrations, accumulated ammonium is oxidated very suddenly. These ventilation peaks are modelled seperately. Conditions for a ventilation peak are a strong increase in oxygen concentration in the bottom water by 1 μM per day and an ammonium accumulation in the last 30 days. The period of 30 days was chosen as the temporal resolution of the input data was one month.

2.3.4. Processes specific for Methane

For methane, the third term in equation 2.10 is the net flux of methane from the sediment to the surface water and the enhanced methane production after phytoplankton blooms.
The sediment flux cannot be estimated seperately, but rather as the net flux from the sediment already taking into account the methane removed by methane oxidation in the water column. This background flux that the constant methane gradient in the methane profiles suggested (see appendix B) was estimated with parameter estimation. This process is assumed to influence the surface layer only in a completely mixed water column, since this is the only time when the sediment is in contact with the mixed layer.
The second process is based on findings of Bange et al. [2010a], who analysed the methane variation during a year at BE and related it to chlorophyll a. Methane production rises with the sedimentation of organic matter after a plankton bloom and the following remineralisation. The concentration of methane increases with a lag of one month (Bange et al. [2010a]. Hence, the concentration increase in methane at time step t is modeled as a first order kinetic based on the concentration of chlorophyll a 30 days before at a depth of 25 m and the rate constant k_{CH_4} (2.24).

$$\Delta C_w(t) = k_{CH_4} \cdot [Chl.a]_{t-30} \tag{2.24}$$

2.3.5. Parameter Estimation

For some processes, accurate rates of change in concentration over time were missing. Therefore, turnover rates had to be estimated with an optimisation routine. The net flux density from sediment to the surface layer and the rate constant k_{CH_4} (eq. 1.3) for the methane model and the production rate during a ventilation peak for the nitrous oxide model as well as the diffusion coefficient were estimated with the *lsqnonlin* function in MatLab.
The Levenberg-Marquardt method was used as a nonlinear optimisation routine. This method is a least-square method that minimizes the difference between the measured c_{meas} and the modelled concentrations c_{sim} iteratively (2.25).

$$f(t) = c_{meas}(t) - c_{sim}(t) \tag{2.25}$$

The cost function, the squared differences between modelled and measured concentrations, is then minimized (2.26).

$$min_t f(t) = min(f_1(t)^2 + f_2(t)^2 + ... + f_n(t)^2) \tag{2.26}$$

The Levenberg-Marquardt algorithm is an effective method for nonlinear data fitting problems [Glover et al., 2011]. It starts with the method of the steepest descent to approach the minimum in the cost function. Therefore, the gradient, e.g. the first derivation of the cost function in the parameter space, is needed to find the direction of steepest descent. Close to the minimum, the algorithm switches to the Gauss-Newton method. The Gauss-Newton method uses an estimation of the Hessian matrix (the second derivative of the cost function) to find the minimum by iterating until the following iteration does not yield an improvement anymore. The iteration equation is the following (2.27)

$$p_{k+1} = p_k - H^{-1} \cdot \nabla J(p_k) \tag{2.27}$$

with the Hessian-matrix H and the gradient ∇J at the point k to generate the point p_{k+1}. Although this algorithm is a fast way to approach the minimum of the cost function and find the parameter corresponding to that minimum, it can also converge to a local minimum. To prevent such false parameter estimations, a range of starting values is used. However, a local minimum cannot be completely exlcuded.

The opimisation routine refers to the measured concentrations. For nitrous oxide, the concentrations in 2007 and 2008 were considerably lower than in other years and were suspected to be systematicly biased. The reason for this bias is not known. Determination of the concentrations at a different institute yielded higher concentrations, so the concentrations used here were corrected by linear regression between the samples measured at GEOMAR and the samples measured at the University of Göttingen (Institut für Bodenkunde und Waldernährung).

3 Results

3.1. Long-term Trends in Time Series at Boknis Eck

3.1.1. Temperature

The time series of temperature was dominated by a clear seasonal component throughout the depth range. However, the cycles in different depths were not synchronous, thus a thermal gradient and consequently a stratification in the water column occured (fig. 3.4a). During the period 1957 to 2013, the winter months January to April exhibited a homogenously temperated water column. A thermocline develops in April or May which exists until November in a depth of 10 to 15 m. Here, only the temperature sequences in 1 m and in 25 m were analysed.

The overall mean surface temperature (1 m) was 9.8 ± 6.0 °C and had an obvious annual cycle with a mean range of 15.3 °C with the highest temperature usually in August (17.8 ± 2.4 °C) and the lowest in February (2.4 ± 1.3 °C, fig. 3.3a). No major reversing points were detected in the sequence. In general, positive slopes were more frequent except for a short period of decline between 1985 and 1990. Hence, the MKT was conducted on the whole time series and reflects the mean dynamic of the time series, although minor heterogeneties exist. The median slope was 0.18 °C per decade, which is the same increase that a linear regression yielded. However, as there were heterogenous trends for the seasons, the MKT was performed for each month individually in addition. The temperature significantly increased only in January (0.02 °C per year), April (0.07 °C per year) and May (0.06 °C per year). Exact p-values can be found in appendix A. However, the quantiles and hence the extreme values did not vary significantly over time in a homogenous linear way. Testing for trends in the extreme values, e.g. the 90 and 10 % quantile did yield positive tendencies for both quantiles, but they were not significant ($p > 0.05$).

Wavelet analysis further confirmed the clear annual cycle, which was present throughout the whole period. However, the strength of the cycle showed significant variations, as could be seen by the variation in the wavelet power spectrum from 1985 on (see appendix A). These variations did not coincide with the gap filling. The varying strength of the cycles was also manifested in the time series itself, where the annual temperature amplitudes differ in size during this period. The temperature distributions for August, usually the warmest month in a year, revealed that during the second half of the series from 1985 on, both warmer and colder temperature anomalies increased in frequency (fig. 3.1). Anomalies of up to $+2.2$ °C (1997,2003) and -2.3 °C (2012) occurred. As there was more data available from 1985 on (44 opposed to 28 measurements), the histogramm has been normalized to a probability density function to be comparable (kernel smooth, MatLab).

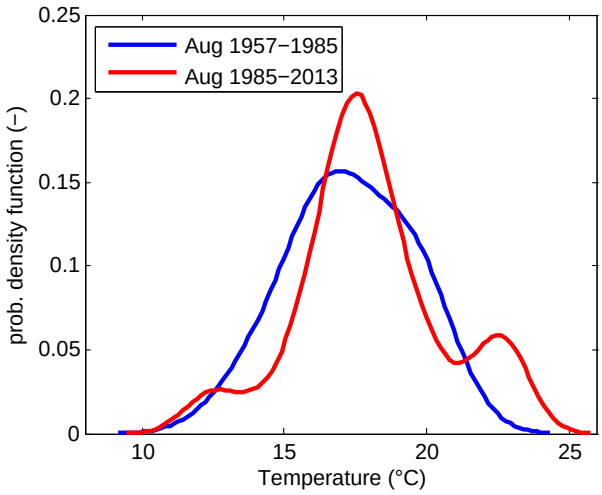

Figure 3.1.: Normalized distribution (kernel smooth) of the temperature distributions in the month of annual maximum (August). Note increasing warmer and colder temperatures in the second half of the time series.

The temperature in 25 m also had a strong annual cycle as the surface, but the warming pattern was different. Highest temperatures usually occurred in October (12.2 ± 1.2 °C), lowest during February (3.0 ± 1.6 °C). Warming tendencies could be detected for all months, with significant warming in the period January to April as well as for June and September. The median slopes were in the range of $0.02 - 0.04$ °C per year, with the highest warming in April ($+0.04$ °C per year) and the lowest in June ($+0.02$ °C per year). Exact p-values can be found in appendix A.

3.1.2. Oxygen

Oxygen concentration in 25 m depth was also dominated by an annual cycle with the highest concentration in March (319.7 ± 52.0 μM) and the lowest in September (38.7 ± 44.7 μM) (fig. 3.3d). Throughout the year, the oxygen concentrations varied in a range of 280.9 μM with a mean concentration of 183.5 ± 116.9 μM.

Negative slopes prevailed during the whole period 1957 to 2013, there were only two minor periods with more frequent positive slopes in 1963-1974 and 1987-1993. But as the mean tenendcy was negative, MKT was performed for the complete series as it still reflected the mean dynamic. Oxygen concentrations were found to be decreasing with a median slope of -0.9 μM per year. To better resolve the trends for the single months, the MKT was conducted for each month individually. A significant decreasing trend could be detected in January and for the summer months from April to September in a range of -0.5 μM per year (July) and -0.8 μM per year (April). Exact p-values can be found in appendix A. The concentrations of the 10 % quantile significantly decreased as well, with a similar intensity of -0.78 μM per year. The decrease in the 90 % quantile was not significant, but had a decreasing tendency.

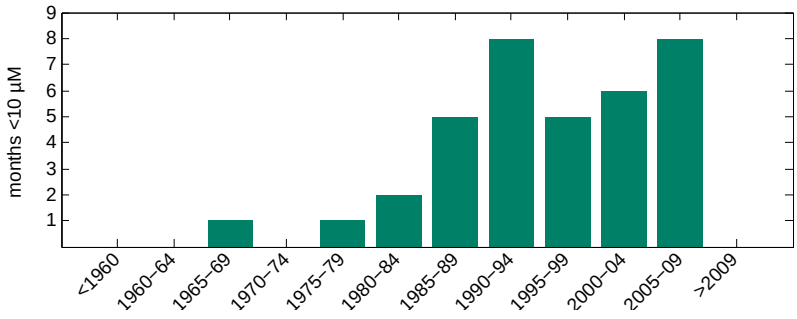

Figure 3.2.: Frequency of months with suboxic events (<10 μM) during five year periods in 25 m depth at BE. Note that gaps were present in 1975-1979 and 1983-1985.

No anoxic event was deteced before August 1989, when anoxic conditions prevailed until October in that same year. During the 1990ies, anoxic events were detected only in October 1992. During the first decade of the 21^{th} century, 4 years showed anoxic events. In September 2003 and October 2007, anoxic events lasted one month, in 2002 and 2005 two months, both September and October. A similar increase in frequency occurs for suboxic (<10 μM) events (fig. 3.2).
Concerning the seasonalities, an annual cycle dominates the variation of oxygen concentrations within one year, as indicated by the the wavelet power spectrum as well as the global power spectrum. Variations in the amplitudes were present throughout the whole period.
Oxygen saturation in 25 m depth also showed strong seasonal variations (time series see appendix A), and the mean decreasing tendency was present in the saturations as well. MKT performed monthly yielded significant decreases in January, April, May, July and September in a range of -0.26 % per year (January) to -0.47 % per year (July).

3.1.3. Salinity

The salinity in 25 m depth displayed strong fluctuations, but did not have a regular annual cycle such as temperature or oxygen. The mean salinity was 26.6 ± 2.0 psu and varied in a mean range of 2.9 psu. In average, the lowest salinity was present in March (20.1 ± 2.0 psu) and the highest in August and September (23.0 ± 1.9 psu and 23.0 ± 1.5 psu), but there was variation in the timing of the maxima and minima. The salinity has rarely been homogenous throughout the water column, with the highest differences between surface and bottom in the summer months from March to October. Consequently, a halocline develops in a depth between 10 and 20 m at that time of the year (fig.3.4c). The slopes did not vary strongly over time, so the time series was analysed completely. No significant trend was detectable with the seasonal MKT for salinity in the period from 1957 to 2012. However, the months March and April showed a small increase in salinity of 0.04 psu (March) and 0.06 psu (April) per year which was significant. Negative tendencies were present in the period between July and October, but these were not significant. All other tendecies were positive but also not significant. Testing for a trend in extreme values revealed a nonsignificant decreasing tendency in the 90 %

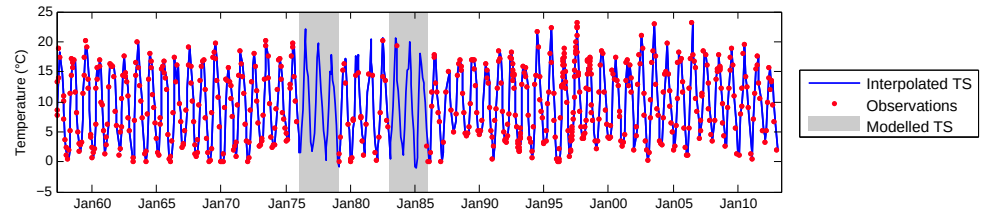

(a) Temperature (1 m)

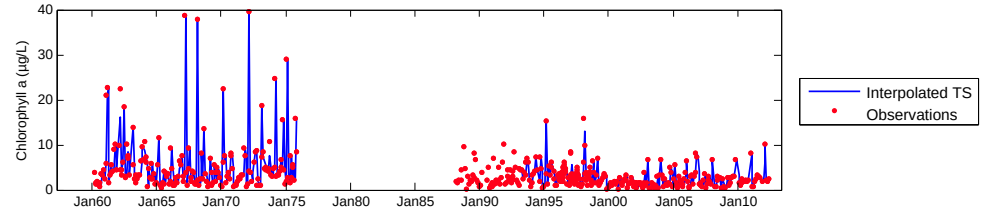

(b) Chlorophyll a (10 m)

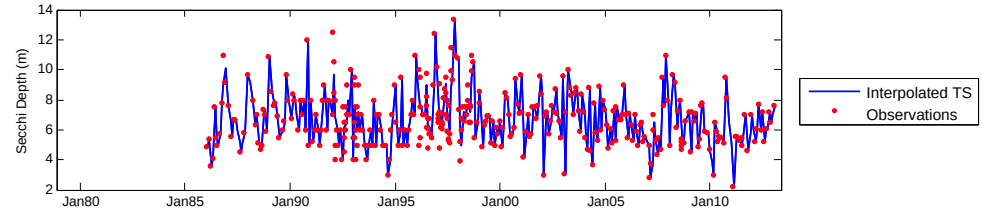

(c) Secchi Depth

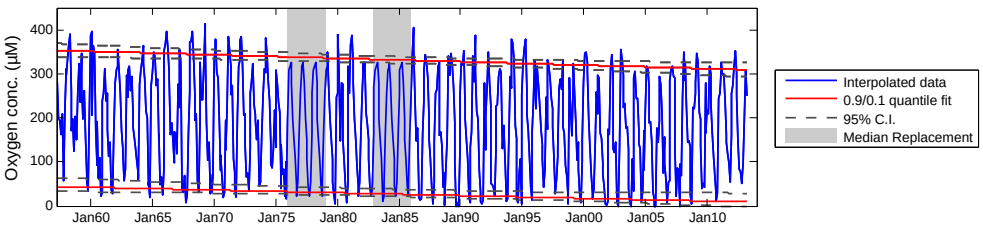

(d) Oxygen (25 m)

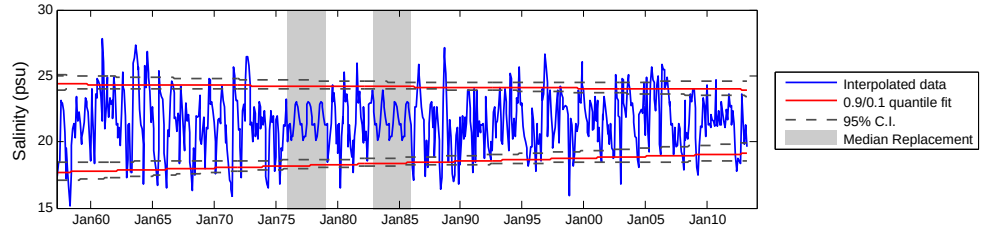

(e) Salinity (25 m)

Figure 3.3.: Time series at Boknis Eck for selected parameters. Oxygen and salinity had significant trends in quantiles, which are shown here. Other parameters did not have significant trends in quantiles. Time series of other parameter discussed in the text can be found in appendix A. Note varying time spans (x-axis) for different time series.

quantile as well as a significant increase in the 10 % quantiles (+0.025 psu per year) (fig. 3.3e).
Striking was also the ceasing of the annual cycle from 1988 on, as indicated by the wavelet power spectrum (fig. 3.8b). The annual cycle appeared with varying strength until 1988 with only a minor break in the late 70ies. After that date, they only reoccured in 2 years in the first decade of the 21^{th} century. In general, the global power spectrum indicated an annual cycle and a less pronounced half-year cycle, which was present occasionally throughout the whole period.

3.1.4. Density Gradient

The density gradient showed clear seasonal variations with minima during winter and maxima during summer months. Significant trends could be found for three months, but not for all 12 seasons together with a seasonal MKT. The highest significant increase was found in April, when the gradient rose by 0.002 kg/m^4 per year (fig. 3.6). Significant negative but weaker trends were detected in July and October (both -0.001 kg/m^4 per year).

3.1.5. Phosphate

The phosphate concentration in 10 m depth displayed a regular seasonal dynamic throughout the whole sequence. During the winter months December to February, the highest concentrations (0.82 ± 0.32 μM) were present. Phosphate concentration declined during the summer months to a mean minimum of 0.08 ± 0.1 μM in May. During the summer months April to July, the mean as well as the variations between years are smaller with 0.12 ± 0.15 μM.
Phosphate was the only series where the standard deviation fluctuated intensively after the gap filling from 1967-1979 and 1983-1986. Hence, for the MKT, only the time series starting on January 7^{th}, 1986, is used. No major trend breaking points occurred in this period. The seasonal MKT did not yield a significant trend for all months. Testing for trends individually revealed negative trends for the winter months December to March as well as in September. The strongest decrease was detected in December (-0.03 μM per year), the weakest in September (-0.007 μM per year). To compare the nutrients among each other, the concentrations during the winter months December, January and February were averaged and linear regression was performed (fig. 3.7a). The slope of the regression line was -0.095 μM per year.
The global power spectrum and the wavelet power spectrum of the period 1986 to 2012 indicated a pronounced annual cycle as the main seasonal compound. However, the amplitudes differed in strength. In 1998 and 2004, the annual cycles were least pronounced, in 1991-1994 they were strongest. This is in accordance with the time series of 10 m, where the highest and lowest peaks were found in the same years, respectively.
The phosphate concentration at 25 m near the sediment also showed a seasonal cycle according to the global power spectrum, but the seasonal variation differed strongly from the one at 10 m depth. The yearly maximum in 25 m depth was in October (4.0 ± 4.1 μM), not in January as in the 10 m

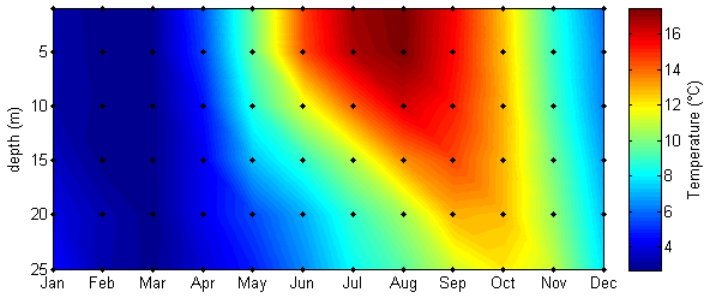

(a) Temperature

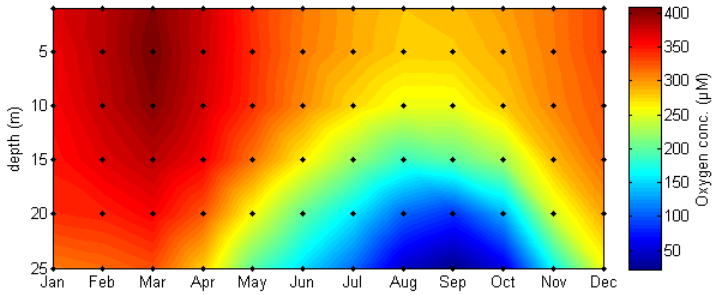

(b) Oxygen

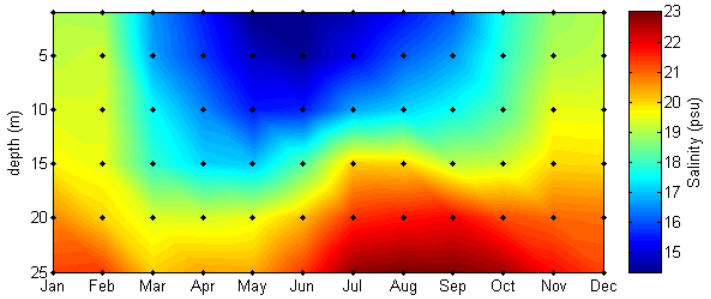

(c) Salinity

Figure 3.4.: Average seasonal cycles at Boknis Eck for selected parameters (1). Monthly means from 6 standard depth (black dots) were interpolated linearly.

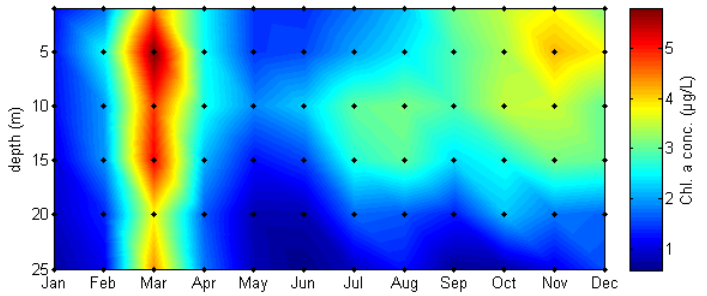

(a) Chlorophyll a

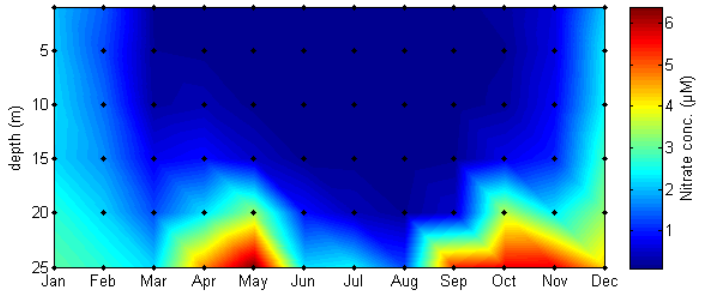

(b) Ammonium

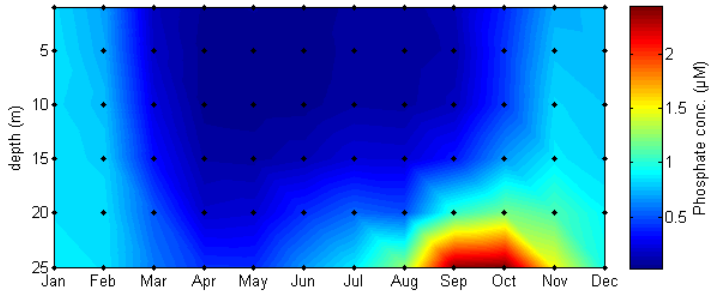

(c) Phosphate

Figure 3.5.: Average seasonal cycles at Boknis Eck for selected parameters (2). Monthly means from 6 standard depth (black dots) were interpolated linearly.

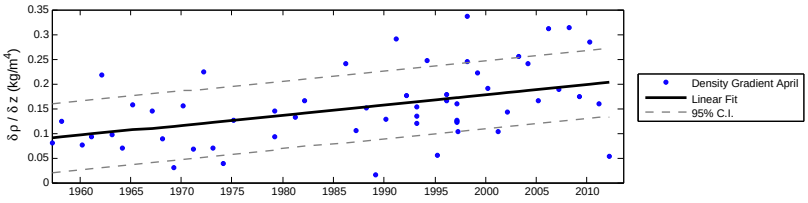

Figure 3.6.: Density gradient between surface and bottom water in April calculated from measurements (·), linear regression (-) and 95 % confidence interval (- -).

time series (fig. 3.5c). Here, the phosphate concentrations were in average 0.95 ± 0.72 μM throughout the year except for the months September and October. During these months, the concentration is elevated to 3.7 ± 3.4 μM, which is considerably higher than the maxima in 10 m depth. The elevated concentration in these months are coincident with the lowest oxygen concentrations during the curse of one year. Negative trends in phosphate concentrations were present in the winter and spring months January to April in a range of -0.01 to -0.03 μM per year for the whole period. A decrease of -0.1 μM per year was present in the September data, which is of one magnitude higher as the other significant trends.

The wavelet spectrum further indicated that the seasonal cycle, although being present the whole time, was only significant in a few shorter periods (fig. 3.8c). These periods were 1986-1994 and 2000-2007. Shorter frequencies in the range of quarter- to half-year-cycles were detected by wavelet analysis in 1993, 2003 and 2006.

3.1.6. Nitrate

The seasonal dynamic of the nitrate concentration at 10 m was similar to the dynamic of phosphate concentration in the same depth. Nitrate concentrations were highest in the winter months December to February with the highest concentrations in February (8.1 ± 3.7 μM). The mean concentration in the winter months throughout the period was 5.6 ± 4.2 μM.

The cumulated slope indicated that the mean dynamic was a decreasing tendency without major breakpoints. MKT was performed for the months individually as the winter months showed higher variances in concentrations than the summer months. Nitrate concentrations decreased significantly between December and April for the period 1992 to 2012. The decrease was strongest in February with a decrease of -0.3 μM per year. For the winter months DJF, linear regression yielded a decrease of -0.16 μM per year (fig. 3.7b)

The global power spectrum further shows a significant half-year and a significant annual cycle. The wavelet power spectrum revealed that the half-year cycle was only present in some years, e.g. 1982, 1986 and 1994. The annual cycle was continuously evident until 2003, then declined and reappeared less intense in 2007 (fig. 3.8d).

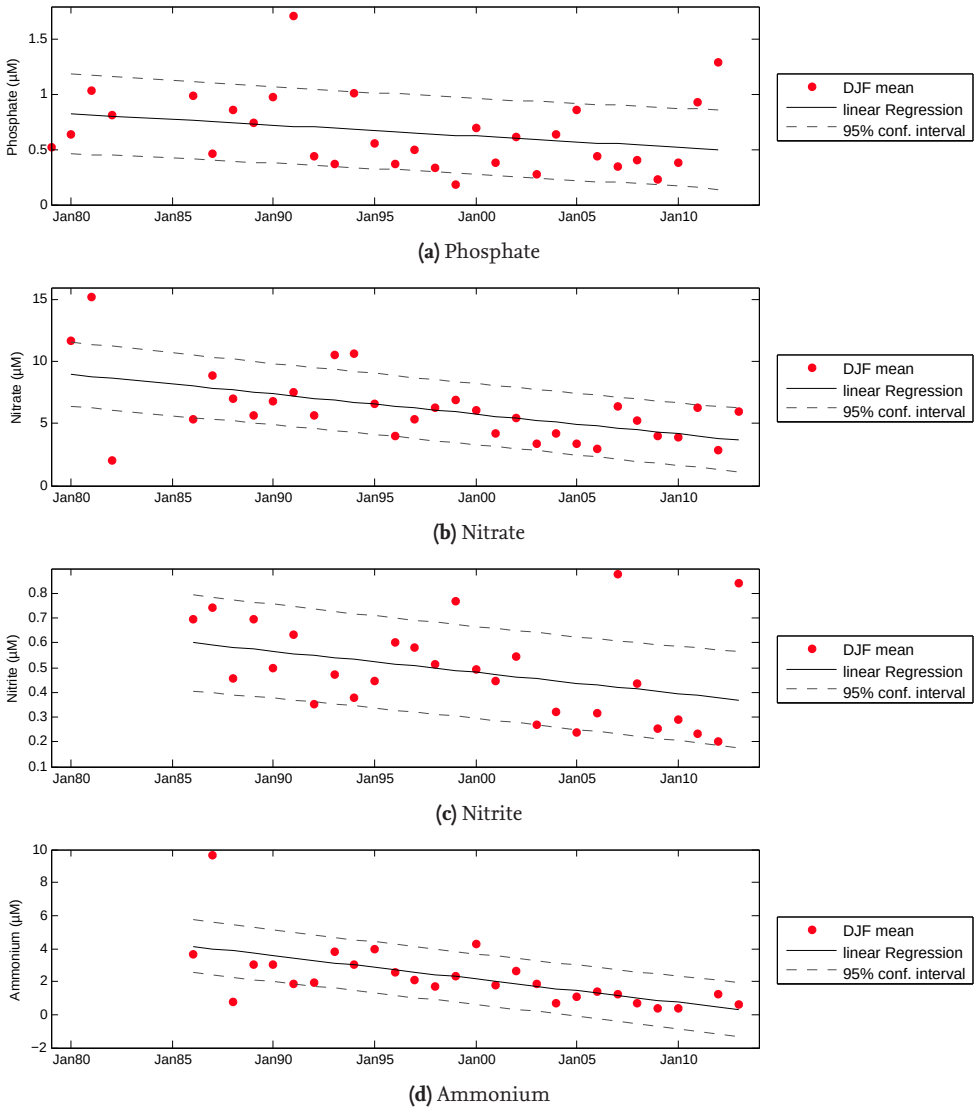

(a) Phosphate

(b) Nitrate

(c) Nitrite

(d) Ammonium

Figure 3.7.: Linear regression and 95 % confidence interval of the mean concentrations of nutrients in December, January and Febuary (DJF mean, depth=10 m)

3.1.7. Nitrite

The nitrite concentration in 10 m depth showed a similar seasonality as the nutrients described above. During the summer months April to September, the concentration was in average in the range of $0.05 - 0.01$ μM with the highest concentration of that period in June (0.12 ± 0.25 μM) and the lowest in September and October (both 0.05 ± 0.03 μM). However, during the winter months in January and February, the concentration was on average the highest during each year, with mean concentrations of 0.54 ± 0.28 μM.

Although the concentration showed large fluctuations especially during the winter months, no major breakpoints were detected and the MKT was performed using the complete time series. No homogeneous trends could be detected for all seasons, hence the months were tested individually for a longterm trend. A significant downward trend was evident in January (-0.016 μM per year), March (-0.022 μM per year) and April (-0.0025 μM per year). A negative tendency in February was present (-0.015 μM per year), but was not significant. The linear regression for the winter months DJF showed a decreasing trend of -0.0085 μM per year (fig. 3.7c).

The nitrite concentrations are dominated by an annual cycle and a minor half-year cycle, as the global power spectrum indicated. The annual cycle was present during the period 1986 to 2002 and then stopped with a short reoccurrence in 2007 to 2009 (fig. 3.8e). The biannual cycles did not occur very often, e.g. in 1989, 1998, 2000 and 2008.

3.1.8. Ammonium

Ammonium concentration in 10 m depth displayed a similar seasonal cycle as the other nutrients in the same depth with higher concentrations during the winter months December to February and lower concentrations during summer. The mean concentration of the three winter months was 2.28 ± 1.46 μM. During the summer months, the concentrations were in a mean range of 0.44 ± 0.45 μM (October) to 0.87 ± 1.73 μM (March).

For the MKT, only the time series after 1986 were considered, as there was a too long gap in which the concentrations seem to increase first before decreasing again. Again, no homogenous trend could be detected for the series including all months, so the months were tested individually. Decreasing trends were present in the months of January to April. The trends lay within a range of -0.01 μM per year (April) and -0.12 μM per year (February). In August, a significant increasing trend was detected (0.004 μM per year). If a linear trend is assumed for the year to year variation of the winter months DJF, the decrease is -0.14 μM per year (fig. 3.7d). The global wavelet spectrum is dominated by a clear annual cycle and a biannual cycle at the border of significance. As with nitrite described above, the annual cycle stopped in 2003, but did not reoccur here (fig. A.11f). Shorter cycles were present in 1986, 1993 and 2005.

The ammonium concentration in 25 m depth showed a different seasonality. In general, the mean concentration of 4.84 ± 5.07 μM is higher as in 10 m, where it is 0.90 ± 1.46 μM. Furthermore, the seasonal cycle had its yearly maxima on average in May (7.70 ± 6.30 μM) and in October (9.81 ± 10.8 μM),

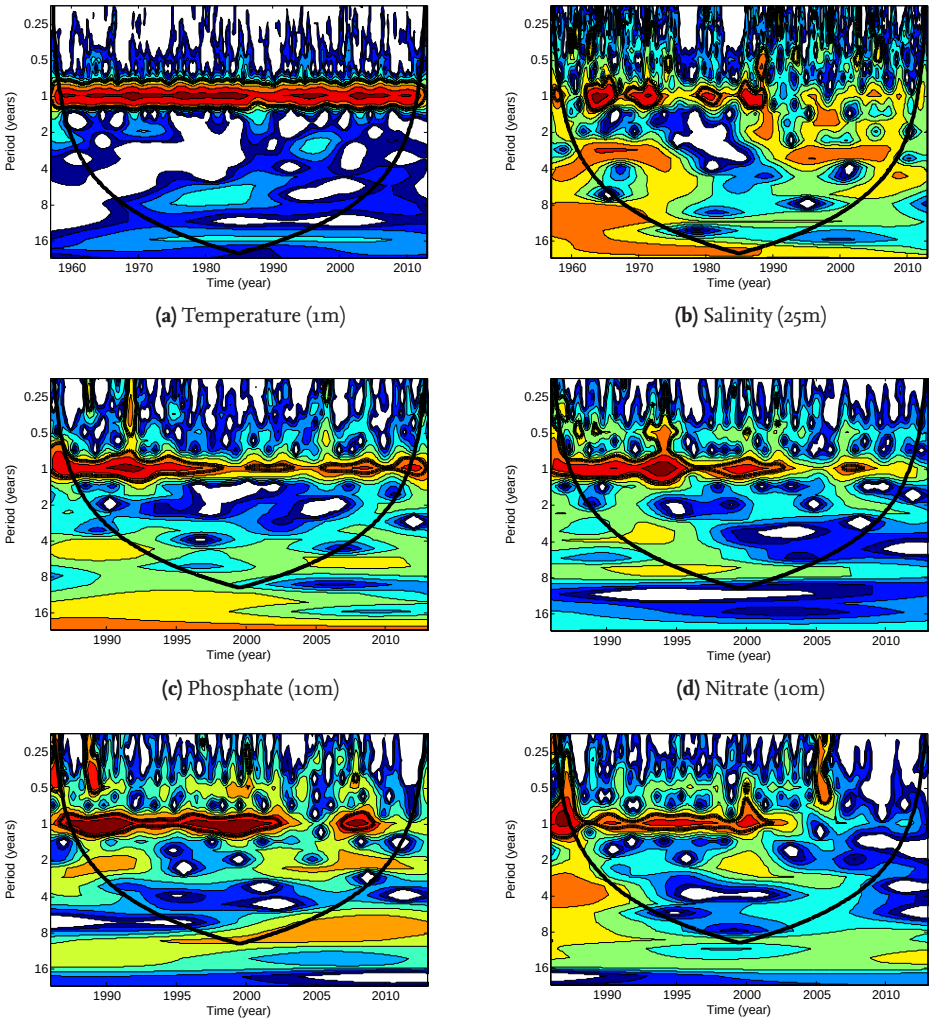

(a) Temperature (1m)

(b) Salinity (25m)

(c) Phosphate (10m)

(d) Nitrate (10m)

(e) Nitrite (10m)

(f) Ammonium (10m)

Figure 3.8.: Wavelet power spectra of selected nutrients from time series station Boknis Eck. Black lines surround significant areas at the 95 % level against red noise. In areas below the cone of influence (conic black line), edge effects might occur, these areas are not considered for further evaluation. Please note the different time spans for temperature and salinity.

and not during the winter months as it was the case in 10 m depth (fig. 3.5b).
Trends were again only evaluated for the period after 1986 and were tested individually as well as there was no homogenous trend for all seasons present. However, none of the trends was significant. The global wavelet spectrum revealed a minor biannual cycle, the annual cycle is below the border of significance. The biannual cycle is significant only in a few years such as in 1991, 1994, 1997-1999 and in 2000-2006. The annual cycle is present only around 2002 to 2005.

3.1.9. Chlorophyll a

The mean yearly distribution of the chlorophyll a concentration in the water column displayed clear seasonal variations (fig. 3.5a). Throughout the water column, the concentrations were highest in March (see below). In opposite to this spring peak, the maximal values for the second maximum in a year were more diversely distributed among the months August to December and hence the maxima could not be dated to a single month. The time series is segmented in two main parts, ranging from 1960-1975 (I) and 1988-2012 (II). These series differed considerably in mean chlorophyll a concentrations and were therefore analysed seperately (fig. 3.3b). During the first series (I), chlorophyll a concentrations were on average 5.57 ± 6.39 μg/L. In series II, the average concentration was lower with 2.85 ± 2.20 μg/L. However, the average seasonality did not change, as the highest mean concentrations in both series were detected in March and during a second maximum in fall. The lowest concentrations per year were most often found in January, which were 1.86 ± 1.82 μg/L for series I and 1.30 ± 0.8 μg/L for series II.
The two parts of the time series were separately tested for trends with the MKT. Chlorophyll a concentrations in series I did show a homogenous tendency, but no significant trend could be detected. For series II, the hypothesis of homogeneous trends had to be rejected, the months were analysed individually. Concentrations were rising significantly in Febuary with an increase of 0.06 μg/L. Tendencies for December and January were increasing as well, but not significant. Significant negative trends were detected in April (-0.11 μg/L per year), May (-0.04 μg/L per year), July (-0.04 μg/L per year) and October (-0.23 μg/L per year). In the trends of the extreme values, e.g. the 90 %-quantile, a significant trend was detected for series II. The quantile is decreasing with -0.12 μg/L per year, which is twice as high as the median decrease computed with Sen's slope.
The global wavelet spectra (see appendix A) for both series did not show a clear dominating cyclicity in chlorophyll a concentrations. In the first series, periodicities of a quarter to half a year were significant. However, the wavelet spectrum of this first series showed that these cycles were only present in few years, 1967, 1972 and 1975. The second series exhibited a significant half-year cycle, which was only present in 1993 and 1995-1997.

3.1.10. Secchi Depth

Secchi Depth displayed fluctuations throughout the whole period from 1986 to 2013 (fig. 3.3c). The mean Secchi depth was 6.8 ± 1.8 m with a mean amplitude of 2.13 m. The shallowest Secchi depth usually occurs in March (6.1 m), the deepest in January (8.2 m).

No major breakpoints were detected during the observed period. Since no heterogeneity among the seasons was detected, the MKT was performed for all seasons at one time. Although a negative median slope was present, this was not significant ($p = 0.9$). However, events with extremely deep Secchi depths decreased meaning that extreme turbidity events increased. The quantile regression of the 90 % quantile indicated a decrease of 0.08 m per year.

The global power spectrum did not reveal a dominant cycle, but periodicities of one and half a year were evident. However, the wavelet spectrum indicated that these were present only in 1986-1990 and 1996-1999.

3.2. Simulation of N_2O Concentrations

3.2.1. Comparison between Simulation and Measurements

The two different implementations in the N_2O model led to high differences in the simulated concentrations. The model without directly implemented N_2O production in the mixed layer (model 1) produced results with substantially lower residuals than the N_2O model with implemented production rates (model 2).

The simulation without implemented N_2O production (model 1) showed overall acceptable agreement with the measured concentrations and saturations calculated from measurements, but still some biases existed. The simulated concentrations (fig. 3.9a) and saturations in model 1 (fig. 3.9b) reflect the measurements within the range of their standard deviation, except for single underestimations (e.g. 2008, end of 2005) or overestimations (e.g. summer 2008, summer 2010). The mean concentration in the three different parametrisations with a range of $12.89 - 12.99$ nM were only slightly lower than the measured mean concentration 13.01 ± 3.0 nM. The simulation is in average within the range of the standard deviation of the measurements. The variability in the model reflected the seasonality of the concentrations in the measurements. Concentrations were usually highest during winter and lowest in summer.

The differences between model and measurements (residuals) reflect the model quality. The parametrisation with the lowest sum of residuals was LM86, followed by W92 and WMcG99. The absolute mean errors were 1.65 nM (W92 and WMcG99) and 1.69 nM (LM86) and thus were 13.0 % and 12.7 % of the mean measured concentration. Also the fluxes, although in average negative for all three parametrisations, differed among the three parametrisations. The highest flux density out of the water was calculated for W92 with -0.0566 nmol/s/m^2, followed by WMcG99 with -0.0516 nmol/s/m^2 and the lowest flux density was detected in LM86 with -0.0311 nmol/s/m^2. The difference of 0.0255 nmol/s/m^2 between the highest and the lowest flux density represents 45.2 % of the W92 flux (see also fig. 3.9c).

The residuals of the model were homoscedastically distributed with respect to time. With respect to the concentration, residuals were negative for low and positive for higher concentrations. They were homoscedastically distributed for measured concentrations in the range of approx. $8 - 13$ nM/L.
The model with N_2O production directly implemented (model 2) overestimated the concentrations throughout the whole simulated period. Mean simulated concentrations of 14.25 nM were higher than the measured mean concentration of 13.01 ± 3.0 nM. The same applies to the saturations, which were overestimated with 123.03 % compared to measured 115.83 %. The residuals were mainly positive and not homoscedastically distributed.

3.2.2. Parameter Estimation

Parameters for the two N_2O models were estimated with an optimisation routine. For the model with implemented production, only the rate of N_2O production after the breakdown of summer stratification (ventilation peak) was estimated. The rate was estimated to be 0.324 nM/Δt (Δt=0.5 days) with a range of -0.38 to 1.03 nM/Δt. This was only done for the parametrisation LM86, as the residuals were substantially higher than for the model without direct production (model 1).
For the model without direct N_2O production in the mixed layer, the ventilation rate was estimated for three different air-sea gas exchange parametrisations. The results including the estimated parameters and confidence intervals for the N_2O model are listed in table 3.1. The estimated ventilation rates ranged from $0.45 - 1.46$ nmol/L/Δt N_2O production, which is $0.90 - 2.92$ nmol/L per day (Δt=0.5 days). The rates increased with the different parametrisations from LM86 to W92 and WMcG99 by approximately threefold. The 95 %-confidence intervals of the estimations are in the same magnitude as the rates.

3.2.3. Seasonal Variability of the Sources and Sinks of N_2O

As the model with directly implemented N_2O production did yield considerably higher residuals, it is not included further here. Sources and sinks are presented here for the LM86 parametrisation, as this was the one with the smallest residuals.
The seasonality of N_2O concentrations displayed a clear seasonal cycle. Concentration was highest in late winter and early spring and lowest during late summer. The surface water was supersaturated with N_2O in the summer months and only occasionally undersaturated during winter months, e.g. in winter 2008/2009 and 2009/2010. In fall, coincidental with the breakdown of the summer stratification, concentration as well as saturation rises sharply for short time periods. These peaks were usually the highest concentrations respectively saturations simulated per year.
Four main processes influencing the N_2O concentration in the mixed layer were present. The processes that mainly acted as sources were N_2O diffusion into the mixed layer and enhanced N_2O production during ventilation peaks as well as upward mixing of N_2O from the subsurface layer (fig. 3.10a). The major sink was the emission to the atmosphere (fig. 3.10b), diffusion acted partly as a minor sink. In general, the input of N_2O to the mixed layer was balanced by the output.

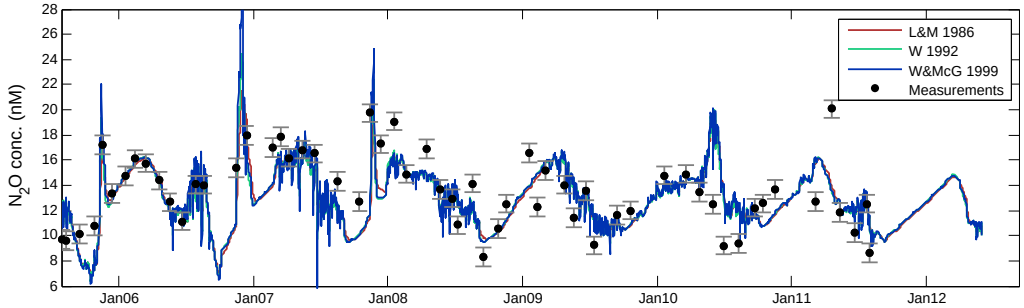

(a) N_2O concentration.

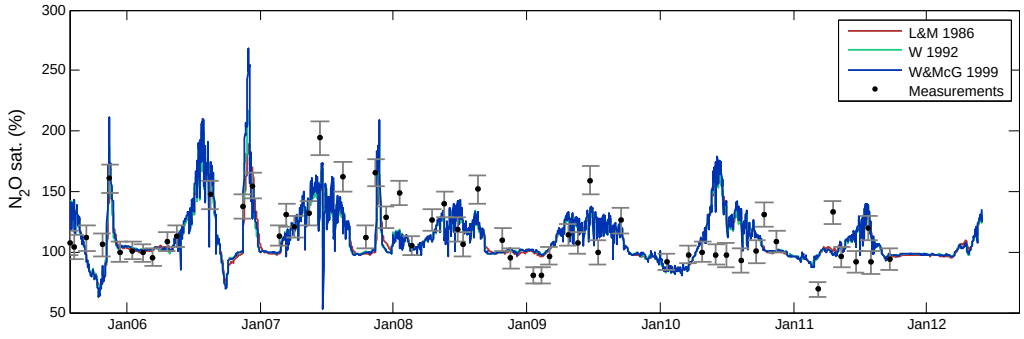

(b) N_2O saturation

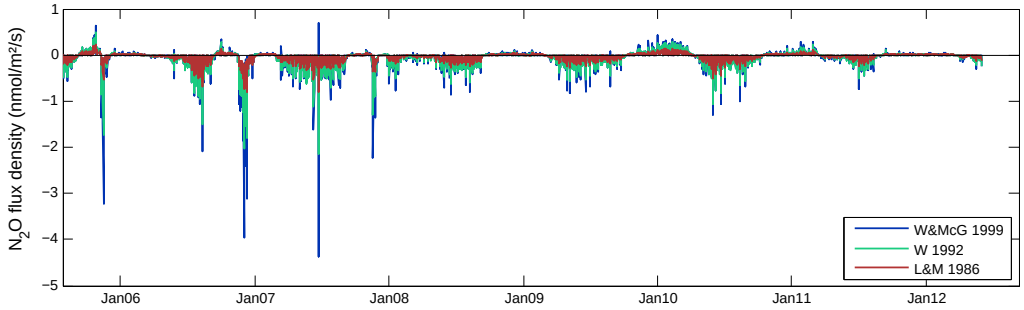

(c) N_2O flux

Figure 3.9.: Comparison of model 1 simulations (lines) and measurements (black dots) ±standard deviation. Model 1 assumed N_2O production only below the mixed layer. The three model simulations represent the three air-sea gas exchange parametrisations of LM86 (red), W92 (green) and WMcG99 (blue).Abbreviations: conc.=concentration, sat.=saturation, flux dens.=flux density.

Table 3.1.: Model results for the simulation of N_2O concentrations and parameter estimations for three different parametrisations of air-sea gas exchange for model 1 (without N_2O production) and model 2 (with N_2O production in the mixed layer). The parametrisations used were (M86, W92 and WMcG99 for model 1 and LM86 for model 2. The estimated ventilation rate refers to the N_2O production after the breakdown of fall stratification, resp. diffusion of N_2O to the mixed layer from the surface layer. Abbreviations: CI= 95% confidence interval, ME=mean error, MAE=mean absolute error, RMSE=root mean square error, conc.=concentration, sat.=saturation., Δt=0.5 days.

		Model 1 LM86	**Model 1** W92	**Model 1** WMcG99	**Model 2** LM86
Rate		Ventilation	Ventilation	Ventilation	Ventilation
Start values	$nmol/m^2/s$	1, 0.001	1, 0.001	1, 0.001	
Estimation	$nmol/m^2/s$	0.6536	1.1717	1.456	0.324
CI lower	$nmol/m^2/s$	0.3395	0.5661	0.6951	-0.3815
CI upper	$nmol/m^2/s$	0.9678	1.7772	2.217	1.03
Rate		Diff. coef.	Diff. coef.	Diff. coef.	-
Start values	m^2/s	1, 0.1	1, 0.1	1, 0.1	-
Estimation	m^2/s	0.0011	0.002	0.0017	-
CI lower	m^2/s	0.0003	0.0007	0.0005	-
CI upper	m^2/s	0.0018	0.0034	0.0028	-
ME	nM	0.735	0.718	0.708	-0.701
MAE	nM	1.66	1.65	1.68	3.4
Sum of Residuals	nM	336.51	344.83	355.08	1726.27
RMSE	nM	2.33	2.36	2.39	5.27
Mean conc.	nM	12.90 ±2.3	12.92 ±2.3	12.99±2.5	14.25±4.6
Mean sat.	%	110.96±19.0	111.14±19.6	111.81±21.7	123.02±43.2
Mean flux density	$nmol/s/m^2$	-0.03±0.1	-0.06±0.2	-0.05±0.2	-0.0755±0.2

The main input process was N_2O diffusion from the subsurface layer to the mixed layer. This diffusion input was usually highest during summer and fall and smallest in winter and spring (fig. 3.10c). In June and July, N_2O diffusion from the subsurface layer could account for more than 97 % of the total input. In July, N_2O input to the mixed layer was generally highest.
However, N_2O production during the breakdown of the stratification dominated the source processes for short periods in fall or winter. In November, the N_2O production during ventilation peaks account 100 % of the concentration input per time step. Upward mixing only played a minor role, mainly in spring and summer months. N_2O input due to flux occurred in average in single months, e.g. October, January and February, but always below 0.05 nM per Δt.
Sinks were in average highest during July. The flux to the atmosphere acted as a major sink and accounted for 100 % of the output of the mixed layer between March and September (fig. 3.10d). Throughout the year, diffusion out of the mixed layer played a minor role and occured only in September to February with contributions below 0.01 nM/Δt.

3.3. Simulation of CH_4 Concentrations

3.3.1. Comparison between Simulation and Measurements

The comparison between the measured and simulated concentrations (fig. 3.11a) resp. saturations (fig. 3.11b) showed an overall good agreement. The simulation reflects the measured concentrations and their variations except for few exceptions. During single events in fall, the concentrations were underestimated in the model. The mean concentrations calculated with the three parametrisations were in a range of 14.61 to 15.46 nM and hence lower than the mean measured concentration of 15.4 ± 2.2 nM. Still, the concentrations were within the range of the standard deviation of the measurements.
Comparable to the N_2O model, the simulated concentrations differed among the applied parametrisations for air-sea gas exchange. However, the best fit in the CH_4 model was reached with the parametrisation LM86. Here, the total sum of residuals was 2334.6 nM. The simulation that was most distant to the measurements was the simulation with the parametrisation W92 with a sum of residuals of 2970.3 nM. The mean errors were distributed accordingly among the three parametrisation with the lowest, 2.72 nM, for LM86 and the highest, 3.91 nM, for W92. The absolute errors that account only for the absolute discrepancy did not differ largely and ranged from 6.12 nM (LM86) to 6.69 nM (W92). This is approx. 40 % of the total mean measured concentration.
The fluxes differed largely among the three parametrisations, but were negative in average for all of them (fig. 3.11c). The smallest flux was calculated for the LM86 parametrisation with -0.03 nmol/s/m^2, the highest flux for W92 with -0.5 nmol/s/m^2.
The residuals were not completely homoscedastically distributed. With respect to time, the residuals were mainly positive. With respect to concentration, residuals were negative for low concentrations below 5 nM, homoscedastic between 5 and 20 nM and positive above.

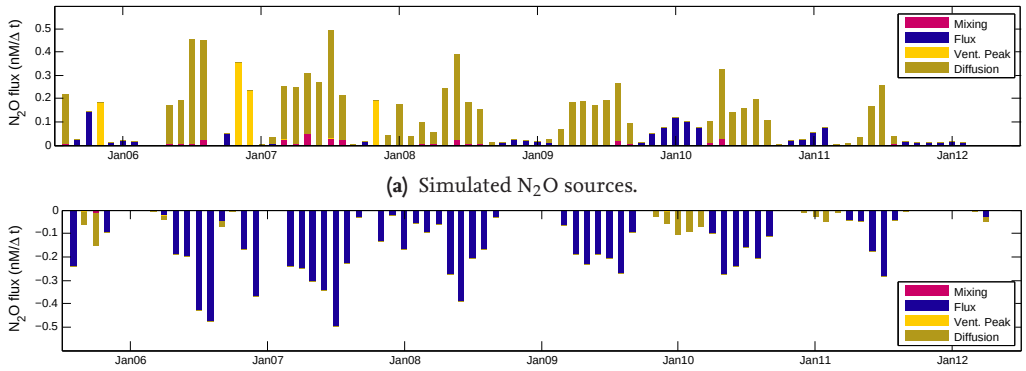

(a) Simulated N_2O sources.

(b) Simulated N_2O sinks.

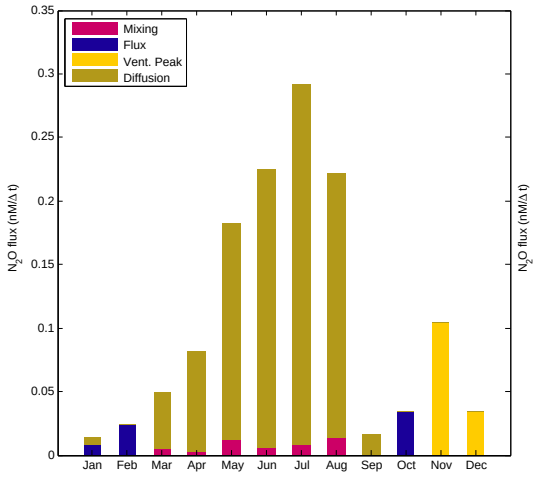

(c) Simulated N_2O sources, per month.

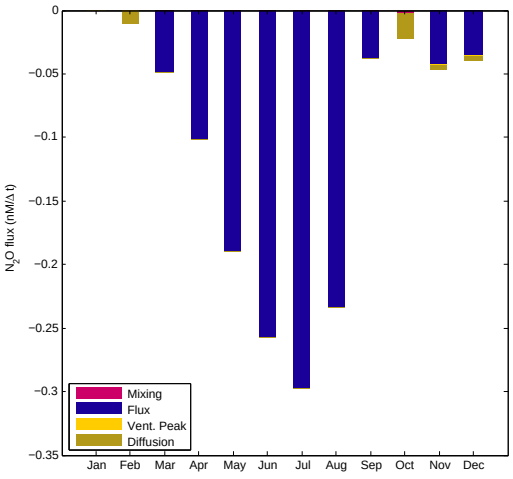

(d) Simulated N_2O sinks, per month.

Figure 3.10.: Sources (a) and sinks (b) in the N_2O model for the mixed layer. As an example, the distribution for the parametrisation W92 is shown here. The concentrations were averaged for 30-days-periods. Below are the sources (c) and sinks (d) averaged per month.

3.3.2. Parameter Estimation

In the CH_4 model, two parameters were estimated, each for the three different parametrisations of air-sea gas exchange. All results for the CH_4 model are listed in table 3.2. One of the two estimated rates was the sediment flux density of methane when the water column was completely mixed. Rates differed between the three gas exchange parametrisations and increased from LM86 to WMcG99 and W92. The lowest sediment flux density was estimated under the LM86 parametrisation with 0.0003 nmol/s/m^2, the medium one for WMcG99 with 0.0005 nmol/s/m^2 and the highest for W92 with 0.0006 nmol/s/m^2. The confidence intervals were in the same magnitudes as the flux densities and were around 50 % relative to the rate.

The second estimated rate was the chlorophyll a relationship. This reaction rate increased in the same way as the sediment flux rate for the three applied parametrisations. The lowest rate was estimated again for LM86 with 0.44 nM/Δt, increased to WMcG99 with 0.69 nM/Δt and was highest for W92 with 0.82 nM/Δt. Between LM86 and W92, the estimated rate almost doubled. Uncertainty was again high with confidence intervals of approximately 50 % of the rate.

3.3.3. Seasonal Variability of the Sources and Sinks of CH_4

Concentrations and saturations simulated by the 1D box model did not show a clear seasonality, nor did the measured concentrations. Concentrations and saturations fluctuated irregularily during the course of one year. Only in spring 2012, a pronounced peak with concentrations larger than 65 nM occured, but 4 measurements during the same time yielded concentrations only around 10 nM.

The relevance of the four processes influencing the concentration of CH_4 at the surface varies within the course of one year. Upward mixing, sediment flux and the remineralisation of organic matter (Chl. a relationship) acted as sources of CH_4 to the mixed layer (fig. 3.12a) whereas the flux to the atmosphere acted as the only sink at every time during the year (fig. 3.12b). In general, input was balanced by output of CH_4 in the surface layer.

As input processes, chlorophyll a enhanced production and sediment flux were equally important, but their magnitude varied within a year (fig 3.12d). The CH_4 production due to the chlorophyll a relationship was present throughout the year and contributed between 17.2 % (September) and 75.4 % (March). Accordingly, the absolute production due to that processes was lowest in September and highest in March. Sediment flux was present from August to March, but was highest during October. The sediment flux contributed up to 71.0 % (October) of the total input per time step. Mixing played a minor role in the months from Febuary to September with low absolute contribution. Relatively, it accounted for up to 57.7 % in June, when general input was low.

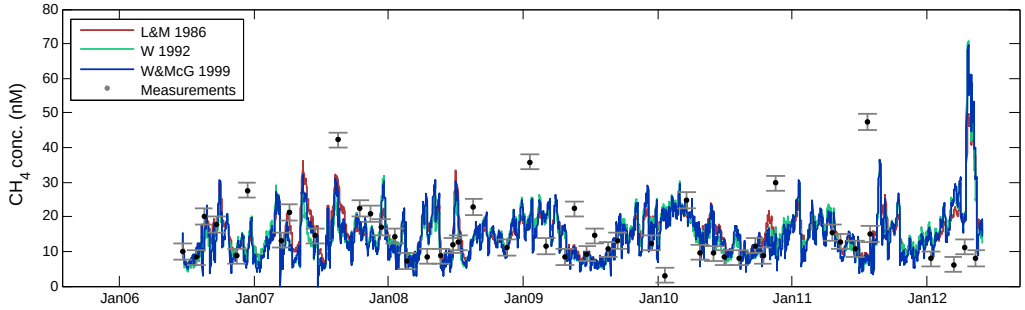

(a) CH_4 concentration.

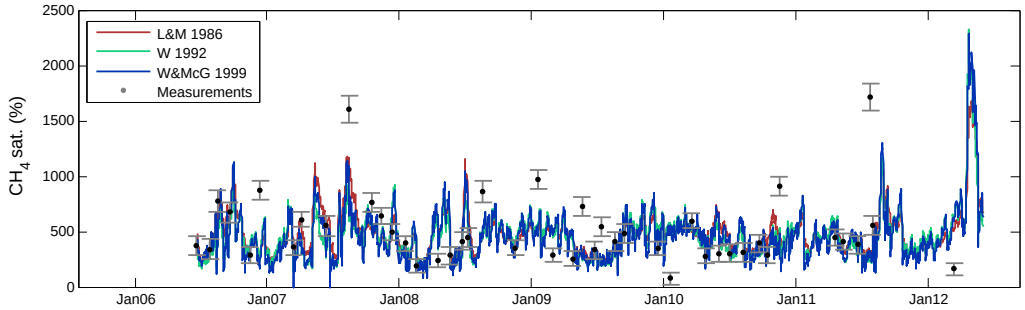

(b) CH_4 saturation.

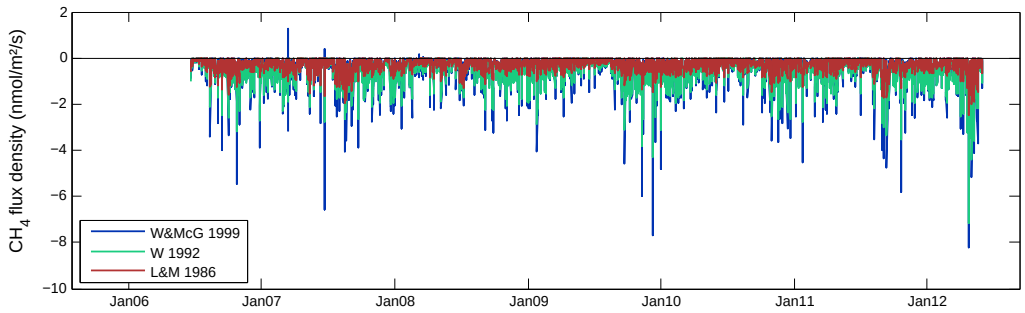

(c) CH_4 flux

Figure 3.11.: Comparison of Model simulations (lines) and measurements (black dots) ±standard deviation. The three model simulations represent the three air-sea gas exchange parametrisations of Liss & Merlivat (1986, red), Wanninkhof (1992, green) and Wanninkhof and McGillis (1999, blue). Abbreviations: conc.=concentration, sat.=saturation, flux dens.=flux density.

Table 3.2.: Model results for the simulation of CH_4 concentrations and parameter estimations for three different parametrisations of air-sea gas exchange. The parametrisations used were Liss&Merlivat 1986, Wanninkhof 1992 and Wanninkhof & McGillis 1999. Sediment= net sediment flux to the surface, Chl. A = production of CH_4 in nmol per μg chlorophyll a per liter in the bottom water. Abbreviations: , CI=95% confidence interval, RMSE=root mean square error, MAE=mean absolute error, conc.=concentration, sat.=saturation., Δt=0.5 days.

		CH_4 LM86	**CH_4 W92**	**CH_4 WMcG99**
Rate		Sediment	Sediment	Sediment
Start values	nmol/m^2/s	1, 0.0001	1, 0.0001	1, 0.0001
Estimation	nmol/m^2/s	0.0003	0.0006	0.0005
CI lower	nmol/m^2/s	0.0002	0.0003	0.0002
CI upper	nmol/m^2/s	0.0005	0.0008	0.0007
Rate		Chl. A	Chl. A	Chl. A
Start values	nmol/L/Δt	1, 0.1	1, 0.1	1, 0.1
Estimation	nmol/L/Δt	0.44	0.82	0.69
CI lower	nmol/L/Δt	0.19	0.36	0.31
CI upper	nmol/L/Δt	0.68	1.27	1.08
Mean error	nM	2.72	3.91	3.90
MAE	nM	6.12	6.69	6.67
Residuals	nM	2334.6	2970.3	2923.6
RMSE	nM	8.17	9.21	9.14
Mean conc.	nM	15.46$\pm$5.9	14.71 $\pm$6.9	14.61$\pm$7.3
Mean sat.	%	486.2808$\pm$195.4	458.49$\pm$4	457.9$\pm$234.9
Mean flux density	nmol/s/m^2	-0.30$\pm$0.3	-0.50$\pm$0.5	-0.43$\pm$0.6

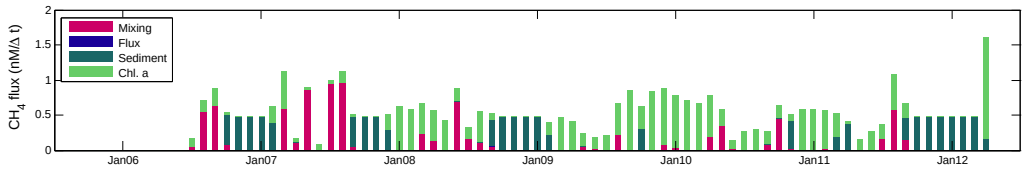

(a) Simulated CH_4 sources.

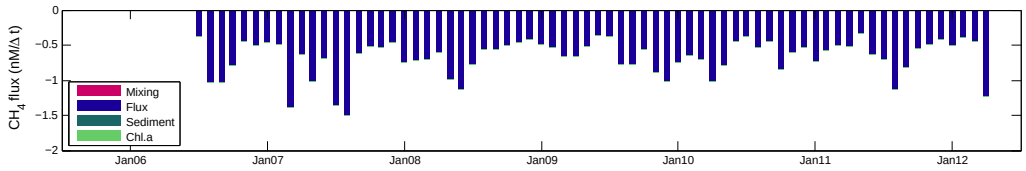

(b) Simulated CH_4 sinks.

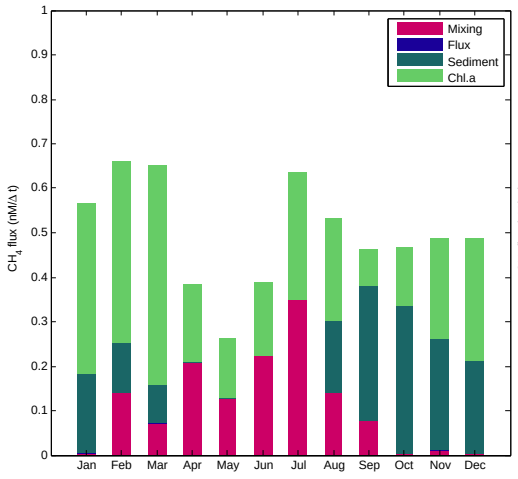

(c) Simulated CH_4 sources.

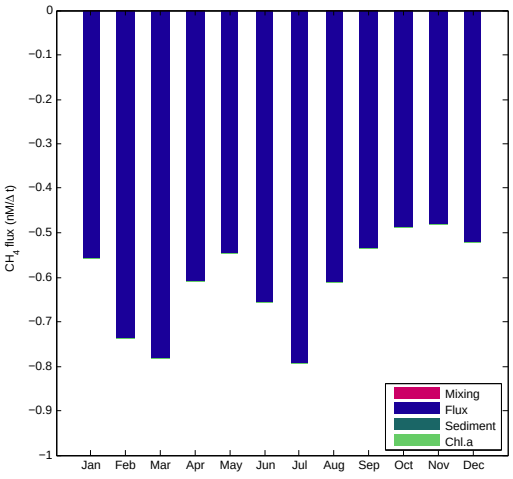

(d) Simulated CH_4 sinks.

Figure 3.12.: Sources (a) and sinks (b) in the CH_4 model for the mixed layer. As an example, the distribution for the parametrisation LM86 is shown here. The concentrations were averaged for 30-days-periods. Below are the sources (c) and sinks (d) averaged per month.

4 Discussion

4.1. Long-term Trends at Time Series Station Boknis Eck

Statistical analysis of the time series at Boknis Eck revealed that significant trends were present in all of the nine analysed parameters. The trends comprise physical, chemical as well as biological parameters and indicate that the whole system undergoes significant changes, resulting e.g. in altered living conditions for biota.

Temperature

Temperature showed trends that were in good agreement with literature. The fact that no significant trend could be detected when considering all seasons was also confirmed by the author team of BACC [2008] in an analysis of the whole Baltic Sea. They attribute the lacking significance to the large variability and the comparably short time period of 1970-2002 of their measurements. However, air temperatures showed a significant agreement with the surface temperatures of the Baltic Sea [Tinz, 1996]. For the atmosphere, trends in the range of 0.7°C [Feistel et al., 2008] to 5°C [BACC, 2008] in 100 years were reported. The increase of 1.8°C in 100 years lies within the range of these reported trends [Feistel et al., 2008]. Additionally, the linear trend matched the trend determined by the Mann-Kendall-Test for the BACC series BACC [2008], which was also the case for the surface temperature trends in this study. This indicates that temperature is increasing linearly. Siegel et al. [2006] analysed sea surface temperatures from NOAA satellites in the period 1990-2004 and found an increase of 0.8 K (= 0.533 K/decade). Although the time span is different, this is still in the range of the measured, yet nonsignificant increase at BE. Siegel et al. [2006] also found an increase in the annual temperature amplitude in the late 1990's, which is in very good agreement with the BE time series.

Most of the warming in the sea surface at BE can be attributed to the spring season, as April and May were the months with the highest temperature increase. At the same time, temperature in the bottom water did not increase as fast as at the surface, which results in an overall significant increase in the density gradient in spring. Hence, stratification starts earlier in a year, which may lead in turn to a reduced ventilation. This is disucssed in context with oxygen depletion below.

Furthermore, the temperature amplitudes per year in the second half of the time series (1986-2013) differed strongly from the ones in the first half (1957-1985). Colder and warmer years both increased

in frequency. With both extremes increasing, the quantile regression yielded no significant rise in the 90 % quantile, as not the mean but the variance changed. Carpenter and Brock [2006] proved with a numerical model for the case of eutrophication in lakes, that complex systems increase their variability prior to regime shifts. An increase in standard deviation would then indicate such a shift about a decade in advance. The year-to-year variability is increasing in the BE time series, so a further monitoring is highly recommended to check the hypothesis of an upcoming regime shift.

Salinity

No trend could be detected for salinity at BE in the median, which is in agreement with findings of the BACC author team. They report no significant changes for the salinity in the 20^{th} century at numerous monitoring stations [BACC, 2008]. However, an increase in the 10 % quantile indicated that less water containing low salinities reached the bottom, which is in agreement with the significant increase in salinity for March and April. Apparently, less fresher water from the surface reaches the bottom, which could be a further hint for a stronger stratification discussed in connection with oxygen depletion below.

During the last century, several major saltwater inflows have been detected in the Baltic Sea [BACC, 2008]. Among the 25 strongest events, seven occured during the time span 1957-2013. The strongest inflow occurred in January 1993, less strong events in 1965,1969, 1973, 1976, 1980 and in 2003 (in decreasing magnitude) [BACC, 2008]. The salinity time series at BE does not show pronounced maximal salinities for these dates. It is unlikely that the major salinity inflows did not reach BE, as the time series station is located at the Boknis Eck channel which is a direct connection to the Belt Sea. Apparently, the salinity in 25 m already reflects the salinity of the inflowing water and does not change within a major inflowing event. Probably, the salinity in different water depths would be a better indicator for these saltwater intrusions.

Furthermore, the regular annual cycle of salinity in the bottom has stopped since the late 1980ies. Such abrupt changes are known to occur also in the Baltic Sea in general, and one of the latest regime shifts was detected around 1990 [Dippner et al., 2012]. This is coincident with the stopping of the regular annual cycle. However, a mechanistic explanation is not possible based on the time series data of BE. The thermal regime could play a role for the mixing and thus the salinity distribution in the water column, but salinity changes are also driven by external factors such as wind and precipitation. Thus, the reason for this abrupt stop cannot be resolved based on the data of BE.

Nutrients and Biological parameters

The nutrient and phytoplankton cycle, the latter indicated by the chlorophyll a concentrations at the surface, showed a typical annual seasonality. Smetacek [1985] described the annual cycle of the plankton and nutrients in the Kiel Bight in five stages. These stages can be found throughout the observed time span. During winter, nutrient concentrations are generally higher than in summer, while biomass remains low. The low biomass analysed in Smetacek [1985] is comparable to the low

chlorophyll a concentration in winter in this study. During spring and triggered by weather conditions, the first phytoplankton bloom occurs [Smetacek, 1985]. In average, March was the month with the annual maximum in chlorophyll a. Simultaneously, nutrients decreased in March as well, reflecting the uptake by phytoplankton. A second bloom during fall occured, but could not be pinpointed to a single month in average. Apparently, fall blooms occurred over a broader time span. This explains why the annual cycles were not pronounced in the wavelet spectrums, as they do not show a regular annual cycle. The ammonium concentrations at 25 m water depth indicate remineralisation of organic matter after the blooms. Ammonium production occurs during decomposition of organic matter [Bange et al., 2010b], when further oxidation to nitrite or nitrate is hindered by low oxygen concent. Intensified ammonium production takes place in April and from September on, when ammonium concentrations in the bottom water rise again. This matched well the cycle of plankton at the surface and indicates a lag of about one month between dieback of the blooms and remineralisation. However, there were no significant long-term trends in the concentration of ammonium in 25 m depth. The lack of trend indicates that remineralisation stays on a constant level during the whole period, despite the decrease in nutrient concentrations.

Although the seasonal cycle varied only little with respect to the yearly course, the magnitude of the nutrient and chlorophyll concentration did change significantly during 1980-2012 (nutrients) resp. 1960-2012 (chlorophyll a). In general, the concentrations of nutrients during the winter months were significantly decreasing. This decrease has been detected in several other stations of the Baltic Sea as well. For nitrate, trends in the Bornholm and Arkona basin increased until the early 1990's and decreased since then [Feistel et al., 2008]. Conley et al. [2002] analysed total nitrogen concentrations in the Danish waters and found a decrease from 1980 to 2003. Carstensen et al. [2006] reported a decrease of the nutrient discharges from Denmark by 50 % from 1988 to 2002. In the BE time series, nitrate measurements were only available from 1986 on, but the general decrease since then was confirmed. For phosphorous discharge, Carstensen et al. [2006] detected a decrease of 80 % which he attributes mainly to the installation of wastewater treatment plants. Further studies found phosphate to increase until the 1980's and since then showing strong fluctuations without a clear trend [Feistel et al., 2008]. Phosphorous did show stronger fluctuations than nitrate in the BE series, but did also show a significant decrease since 1985.

Accompanied by this significant decrease in nutrient concentrations is a decline in chlorophyll a concentrations. This is most striking when comparing the means between the two chlorophyll series 1960-1975 and 1986-2013 where the concentration fell from 5.5 ± 6.39 to 2.9 ± 2.6 μg/L. Additionally, decreasing trends for the second period were found. As lower nutrients concentrations would lead to less production and less intense algal blooms, these findings match well. HELCOM [2009] registered a decreasing trend in Chlorphyll a concentrations since the mid 1990's for the Kattegatt and Belt Sea. Wasmund and Uhlig [2003] also found a decreasing, yet nonsignificant, trend for the chlorophyll a concentrations in the Kattegatt and Belt Sea and attributed it to the decreasing nutrient concentrations.

On the other hand, no significant trend could be detected in Secchi depth. The annual course of

Secchi depth with a minimum in March and a maximum during winter matched the findings of the chlorophyll a cycle. However, one would expect an increase in Secchi depth, as less production would increase the transparency of the water column [Tyler, 1968]. This was not the case, the extreme values with high Secchi depths did even decrease over time. The decrease of 8 cm per year in the 90 % quantile is in agreement with a linear slope found in the Swedish Baltic Sea of 5 cm per year [Sanden and Hakansson, 1996]. Due to low plankton densities during winter, high Secchi depths are expected during this period. However, the turbidity during the winter months is increasing despite a general decrease of nutrient concentrations. This may have several causes, that can only be speculated on here. It could mean that production increased during winter, as for example also temperature had an increasing trend in January at the surface.

Another striking fact is the stopping of the annual cycle for the nitrogen species nitrite, nitrate and ammonium in 10 m depth. The annual cycle that exists until around 2003 reflects the regular seasonal variation during the course of one year as described above. However, this seasonality seems to stop around 2003. The concentrations of the nitrogen species all show strong fluctuation in the years 2004 and 2005, which might also be the reason for the significantly shorter cycles present in the wavelet power spectrum for ammonium in 10 m. Chlorophyll a also shows more fluctuations in the short-term during 2004 and 2005. The reasons remain unclear. Apparently, the timing of the blooming events became irregular, which can be attributed to the nitrogen species, as phosphorous did keep its seasonal cycle.

Oxygen and Ventilation System

The oxygen concentration declined significantly with a simultaneous increase in hypoxic and anoxic events in the bottom water during the period 1957-2013. The spreading of hypoxic and even anoxic zones in marine coastal ecosystems is known to occur worldwide and is often related to eutrophication [Diaz and Rosenberg, 2008]. The Baltic Sea is affected by oxygen decline over large areas [HELCOM, 2009], which have increased since 2001. These findings match well with the oxygen decline in the BE time series.

At first sight, this decline is not in agreement with the significantly decreasing nutrient concentrations. As oxygen depletion is often related to oxygen consumption by remineralisation of organic matter [HELCOM, 2009], one would expect the oxygen concentrations to be anticorrelated with the nutrient concentration. Apparently, the decline in oxygen concentration in the bottom water of Boknis Eck had additional reasons and cannot only be related to the stimulation of phytoplankton growth by nutrient input. Already Hansen et al. [1999] found a weak correlation of oxygen with winter nutrient concentrations, using a shorter time series of BE. Conley et al. [2002] also detected a, yet nonsignificant, trend in oxygen decline in coastal regions with a simulatenous decrease of the total nitrogen load.

There are studies that relate this ongoing decline in oxygen concentrations to remobilisation processes in the sediment [Conley et al., 2002, Pitkänen et al., 2001]. This process occurs in marine systems as well and has been shown to happens in Baltic Sea sediments [Virtasalo et al., 2005]. Re-

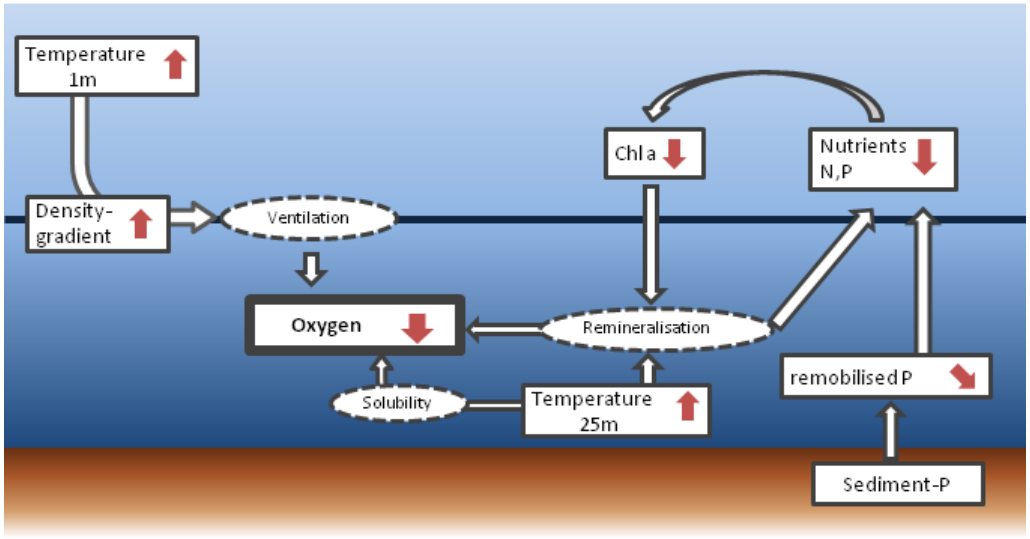

Figure 4.1.: Schematical illustration of the processes beging responsible for the decline in oxygen despite the decreaseing trends in nutrients. (1) Stronger density gradient hampers ventilation, (2) temperature increase in the bottom water decreases solubility of oxygen, (3) temperature increase in the bottom water enhances remineralisation and thus oxygen consumption.

sponsible for the sedimentary release of phosphorous are anoxic conditions, that mobilized metals by reduction, e.g. iron [Virtasalo et al., 2005]. The mobilisation of these compounds results in a mobilisation of sorbed or chemically bonded phosphorous. As a macronutrient, phosphorous enhances biological production and thus slows down the recovery from eutrophication [Conley et al., 2002]. This remobilisation can also counterbalance the decrease in nutrient input, as a case study in the Gulf of Finland revealed [Pitkänen et al., 2001]. At Boknis Eck, phosphorous concentrations were high in the bottom water throughout the time, with a distinct maximum in the months with low oxygen conditions. The elevated concentrations support the hypotheses that remobilisation from the sediment plays an important role and keeps the phosphorous active in the system. However, the concentrations of phosphorous in the bottom water showed a significant decrease from 1980-2013. If remobilisation was the only process responsible for the oxygen decline, oxygen concentrations should have decreased accordingly. This was not the case, thus phosphate remobilisation may not be the key process responsible for oxygen decline.

Several findings indicate, that the ongoing decrease of oxygen is strongly connected to physical factors, which is schematically shown in fig. 4.1. First, temperature is increasing in the bottom water during summer stratification. This increase has two effects. The first one is a purely physical effect, as the solubility of oxygen decreases with increasing temperature. However, the oxygen saturations showed a significant decrease as well. The oxygen saturation opposite to the concentration take into account changes in temperature. A decrease in the oxygen saturation means that the decrease in concentration cannot be accounted completely to the physical effect of solubility.

Rising temperature has a second effect that might be more important than the solubility effect. Rising temperatures enhance remineralisation of organic matter that is sedimented to the ground [Hoppe et al., 2012]. This means the oxygen consumption rises. A strong correlation (R=0.7, $p < 0.05$) could be detected between temperature and oxygen in 25 m depth. Apparently, the remineralisation is not limited by the input of organic matter but e.g. by temperature. As remineralisation is a process mainly maintained by microorganisms, higher temperature lead to higher turnover rates and thus more oxygen consumption. This hypothesis is further supported by the lacking trend of bottom water ammonium concentration. Despite lower nutrient input, ammonium concentrations in the bottom water did not decline, indicating that remineralisation might be enhanced by other factors and counterbalance the decrease in nutrients. Rising temperatures could explain this ongoing remineralisation.

Second, there is evidence for an alteration in the ventilation at Boknis Eck. With the temperatures rising in spring at the surface while no significant rising trend could be detected at the bottom, the density gradient within the water column significantly increases in April. With a stronger density gradient through the water column already in April and May, water exchange between surface and bottom is hampered. This is in agreement with the finding that salinity in the bottom water increases in March and April, meaning that the stratification leads to an hampered exchange between fresh surface and saline bottom water. As a consequence, the bottom water becomes less aerated during the summer. With the earlier onset of the stratification, oxygen is used up earlier. If the stratification is still stable in September or October, the oxygen concentration is lower compared to years where the onset of stratification started later that year. Indeed, there is a significant correlation between the surface temperature in May and the oxygen concentration at the bottom water in September with $R=-0.5$ ($p < 0.05$). The density gradient decreases significantly in July and October with half the magnitude as the increase in April. However, during July, the stratification is already stronger so a small decline might not improve the ventilation significantly. The density gradient in October also does not influence the oxygen decline in September. This highlights that even though there are months with increasing and decreasing trends in density gradient, the timing is important for the ventilation.

Jonasson et al. [2012] modelled the oxygen conditions in the North Sea-Baltic Sea transition zone and concluded that physical processes are of major importance for the ventilation and might be a reason for the ongoing decline in oxygen. The results of this study support the hypothesis of the major role of physical processes based on observational data. Jonasson et al. [2012] did not analyse the development of the thermocline over time with respect to stratification stability, but with respect to saltwater inflow and wind. As salinity, temperature and also wind contribute to the stratification and thus the density gradient, the results of the model can be compared to the observational data here.

Some causes for oxygen decline that were found in earlier publications were not further analysed in this study. Among them are for example the consideration of meterological factors such as precipitation or windstress. Hansen et al. [1999] found a correlation between oxygen decline and pre-

cipitation, which he attributed to the input of nutrients by run-off. However, this correlation was only valid when excluding the period 1957-1975. In this study, only direct factors in the water column are analysed as they are assumed to play the most important role. However, run-off after increased precipitation may enhance oxygen decline additionally. Furthermore, the influence of wind was not directly tested, although a decrease in windstress could also have a stabilizing effect for the stratification. Lehmann et al. [2011] analysed the climate variability in the Baltic Sea in a comparable period and found that wind stress during September to December was decreasing. This decrease would further extend the stratification period and weaken ventilation. Still, it is assumed that the examination of the density gradients would at least partly reflect changes in stratification by external driving forces such as wind.

A further reason for oxygen decline was presented by Conley et al. [2007]. They advocated for a regime shift in the benthic community to explain the decrease in oxygen concentration concurrent with a decrease in nutrients. According to them, the benthic community shifted to a community that does not incorporate fresh organic matter into the sediment anymore, therefore increasing oxygen consumption by remineralisation.

A further reason for oxygen depletion independent from nutrient input is discussed in literature, namely the stopping of advection of oxygen enriched water through the Danish straits. In 2002, with the latest major saltwater inflows occuring in 1983 and 1993, it was believed that this stagnation was responsible for the decline in oxygen concentrations. However, the major saltwater inflow in 2003 did not measurably improve the oxygen conditions in the long-term afterwards. On the other hand, inflowing saltwater from the the Kattegatt could also decrease the oxygen concentration, as it can already be depleted in oxygen [Weigelt, 1990]. This means that the role of saltwater inflow remains unclear. It is difficult to track the salt water inflows at BE, as could be seen by the lacking maximal values for salinity in the years of major saltwater inflows. This means that the advected water is apparently similar in chemical and physical parameters, so changes are difficult to detect. The role of advection of different water masses can therefore not be estimated accurately.

In summary, evidence points to a combination of several processes that lead to oxygen depletion in the bottom water despite the decrease of nutrient inputs. Increased temperature and changes in the ventilation are most likely the responsible factors. This would implicate that the oxygen depletion is a reaction to changing climatic conditions, in addition to anthropogenic eutrophication. Besides, meteorological conditions and biological shifts can enhance further oxygen depletion.

4.2. Processes influencing Trace Gas Concentrations

4.2.1. Nitrous Oxide

Model Quality

There were large differences in the model with and without directly implemented N_2O production. When N_2O production was attributed to the whole water column, concentrations were substantially overestimated. This means that the AOU relationship shown in figure 2.8 is based on a incorrect assumption. The assumption was, that the mean production is valid for the whole water column. Apparently, this is not the case, and production mainly takes place below the mixed layer. Therefore, this model version is not further included in the discussion.

The 1D box model to simulate the concentrations for nitrous oxide in the mixed layer based on upward mixing and diffusion reflected the seasonal variability of the concentrations in the observed period. Mean errors of the model with all parametrisations of air-sea gas exchange were in the range of the mean annual standard deviation of the measurements. No temporal pattern for single over- or underestimations was found. Especially coastal regions are very dynamic, which may not be accurately reflected in a 1D box model.

Quality of estimated Parameters

The estimation of the production rates for the ventilation peak and the diffusion coefficient seems to be in the right magnitude, since the model was able to reproduce the measurements within an acceptable range of uncertainty. The rate of N_2O production after the breakdown of summer stratification lies within the range of reported nitrification rates. Grundle and Juniper [2011] measured ammonium oxidation rates in a fjord near Vancouver which is also temporally stratified during the year. The measured ammonium oxidation rates were in the range of undetectable to 0.319 μM/day. Seitzinger and Kroeze [1998] reported nitrification rates in estuaries in a range from 0 to 22 μM/day in a review. The yield of N_2O by ammonium oxidation is only a small fraction, and the estimated rates were all at the lower end of these ranges.

The range of the mean N_2O production in the water column as shown in the segmented AOU relationship (fig. 2.8) is 0 to 3 nmol/L/day. This is an underestimation of the production rate in the bottom water, as the production was averaged over the water column. The results showed that production mainly takes place below the mixed layer, thus these rates cannot be compared with rates from locations with direct ammonium oxidation.

The diffusion coefficient was higher than eddy diffusion coefficients that were found in the literature. Oudot et al. [1990] found an eddy diffusion coefficient of 0.2 cm^2/s to explain N_2O transport from the deep water in the Atlantic. Here, 11 to 20 cm^2/s were needed to support the N_2O concentration in the mixed layer. It could be that this way of implementing the process of N_2O input to the

mixed layer may not be accurate, but it was the best available to reproduce the measurements.
The uncertainties in both the estimated and the externally calculated rates were comparably high. The rates may indicate the right magnitude, but can only be seen as a first rough estimate for production rates at BE. Experimentally determined turnover rates are still highly needed to quantify the processes involved in the nitrogen cycle at BE.

Comparisons of the different Parametrisations for air-sea Gas Exchange

The different parametrisations for wind dependent transfer velocities resulted in differences in the simulated concentrations, but these were small compared to the total annual variability. A reason for that could be that the mean wind speed during the observed period was 7.5 m/s. At this windspeed, the three different parametrisations did not differ substantially (fig. 2.7). For the open ocean, where higher windspeeds can be expected, the parametrisation may play a more important role than at the location of BE. Nevertheless, the parametrisation of LM86 yielded the lowest residuals and can thus be considered as the most accurate one at the location of BE.
Also flux densities to the atmosphere varied with the three different parametrisations with an increasing order of LM86, WMcG99 and W92 (fig. 3.9c). Flux densities were highest when there was the highest input to the mixed layer due to diffusion from the subsurface layer. A seasonality with highest fluxes in summer, when there was the highest input from the subsurface layer, was observed. Apparently, production was highest in summer when oxygen was low, and N_2O was consequently transported to the mixed layer. Flux densities were in agreement with previous studies. Bange et al. [1998]) calculated flux densities in the range of $4 - 37$ pmol/m^2/s (LM86) and $7 - 72$ pmol/m^2 (W92) with the same parametrisations in the Baltic Sea. In this model, the flux densities were in the given range but at the upper end of these values. A reason for that might be the huge fluxes during the ventilation peak events, that bias the mean.

Temporal Variability of Sources and Sinks of Nitrous Oxide at Boknis Eck

Saturations of N_2O showed a clear seasonal cycle during the simulated period, suggesting a temporal variation of sources and sinks. By far the most important sink of N_2O in the mixed layer was the flux to the atmosphere. N_2O loss due to diffusion could only appear when N_2O enriched water overlies water with a lower concentration. This process played only a minor role, but was present in fall and winter 2010 and 2011. In general, output of N_2O compensated the input, but temporal accumulation was likely to happen. For example, the input during January or November was higher than the flux to the atmosphere (fig. 3.10c and 3.10d), which may reflect the accumulation of N_2O to the atmosphere due to cooling of the surface. With colder water temperatures at the surface, the solubility of the gas increases and thus N_2O may temporarily be accumulated. This indicates that the temperature may have a modulating effect on N_2O fluxes.
The most important source was diffusion from the subsurface to the mixed layer. This is indirectly an indication for higher production in the subsurface during these times. As bottom water is un-

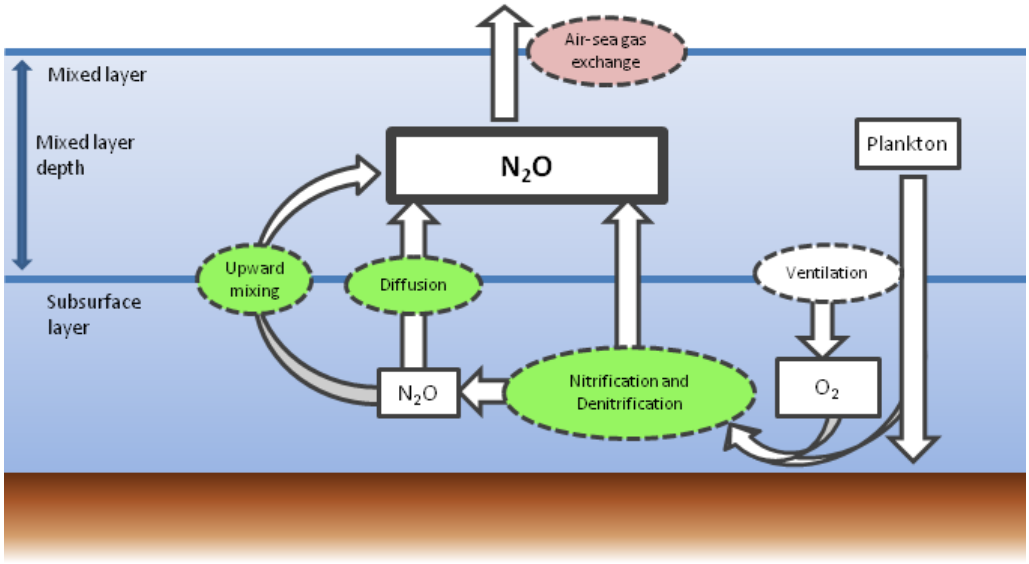

Figure 4.2.: Processes implemented in the model that influence N_2O concentrations in the mixed layer (bold border). Processes that mainly act as a source to N_2O in the mixed layer are marked in green, processes that mainly act as a sink are marked in red.

dersaturrated in oxygen during stratification (see section 3.1.2), nitrification or even denitrification occurs and might be the source for N_2O, either in the water column or in the sediment [Bange et al., 2010b]. If there is a higher production in the subsurface layer, the gradient across the mixed layer becomes stronger and more N_2O is transported to the mixed layer (eq. 2.23)

Enhanced nitrification after the breakdown of the fall stratification was implemented seperately. The temporal resolution of the measurements that fueled the model simulations was too low to capture events on such a short time scale. The timing of the ventilation peak which was set to a defined decrease in oxygen in the water column and the occurrence of enhanced NH_4^+ concentrations at the bottom during the last 30 days seemed to reflect this process well. Comparable data exists only from Schweiger et al. [2007]. In November and December 2005, she measured enhanced production of hydroxylamine and accounted it to enhanced nitrification after accumulation of organic matter originating from the fall bloom. Then, ammonium accumulates if anoxic conditions are present. Naqvi et al. [2010] measured N_2O production in a time series at BE and detected an enhanced production after the breakdown of summer stratification. These ventilation peaks occurred in 2005 to 2007 and in 2010. The model did not simulate pronounced ventilation peaks in 2008, 2009 and 2011, although the measurements suggested a small ventilation peak in 2010. Apparently, oxygen concentration did not increase fast enough to promote strongly enhanced N_2O production as implemented in the model.

This process of enhanced N_2O production after oxygen increase again cannot be found in the time series in the oxygen minimum zone off coastal Chile measured by Naqvi et al. [2010]. In this time series, N_2O peaks usually occur before oxygen concentration in the bottom water rise again. An explanation for the different timing cannot be given here, but the simulation results support the

hypothesis that at BE, the N_2O production is enhanced after the breakdown of the summer stratification. Cornejo et al. [2007] analysed N_2O concentrations, saturation and fluxes during the course of the years 2000 and 2001 in the oxygem minimum zone off the coast of Chile. They obtained a similar seasonal cycle with highest fluxes during autral winter, comparable to the highest fluxes measured in this study at BE during northern hemispheric summer. However, they, did not report any enhanced N_2O production after the breakdown of summer stratification.

In summary, the relevance of processes that serve as an input of N_2O to the mixed layer varied in time. The largest source is diffusion due to subsurface N_2O production, which is highest during summer stratification. Upward mixing may play a minor role during summer, when the mixed layer depth is increasing. Fluxes from the atmosphere to the mixed layer do occur rarly in the winter when the surface water is undersaturated. The loss of N_2O can almost completely be accounted to the flux to the atmosphere. An overview on the described processes influencing the concentrations of N_2O in the mixed layer that are implemented in the model is given in figure 4.2. The segmented AOU relationship apparently reflects only the production below the mixed layer. If the model is expanded to comprise the subsurface layer as a further box, this relationship might be a good starting point.

Missing Processes

Apart from the inaccurate rate estimations described above, the discrepancy between measurements and simulation may have occurred due to some processes that were not included in the model. The missing of one or more processes is also indicated by the distribution of the residuals against concentrations. The residuals are positive for higher concentrations and negative for lower concentrations. This means that lower concentrations are overestimated, higher concentrations are underestimated in the model. Apparently, a sink process being responsible for lower concentrations in the measurements is missing in the model, and a production process might not be represented accurately. Several possible processes might be missing: First of all, the model is a 1D box model and does not account for advection in any way. The missing advection might be the main drawback, as N_2O production in other areas could influence trace gas concentrations at Boknis Eck. This might be a reason for single measurements that could not be explained by the model. Furthermore, no flux from the sediment was included in the model. The sediment is known to act either as a source or a sink of N_2O in the Baltic Sea [Bange et al., 1998]. However, it may mainly influence the bottom water concentration, and the model accounts for upward mixing of N_2O. If the model should be expanded to the whole water column or if subsurface concentrations are not available, a simulation of the role of the sediment is needed.

4.2.2. Methane

Model Quality

The simulation of the methane concentrations in the surface layer with the 1D box model reflected the seasonality of the measurements in an overall good agreement. Most of the simulatated concentrations were in the range of the standard deviation of the measurements, but single measurements could not be reproduced. These events included under- as well as overestimations in the model. The model underestimated single concentrations spread over the whole simulated time period. They are not coincident with upwelling events calculated with the BSIOM model (pers. comment A. Lehmann). Overestimations mainly took place during spring 2012, when an exceptionally high chlorophyll a concentration led to an increase in the simulated concentrations but not in the observational data. As 4 measurements in a row indicated substantially lower concentrations than the simulation, the simulated peak seems unrealistic. Apparently, a process limiting CH_4 production or enhancing CH_4 oxidation is missing in the model. However, the concentrations resp. saturations simulated in spring 2012 were not unusual, as saturations of up to 15500% have been measured in the Baltic Sea before [Bange et al., 1998]. Nevertheless, the mean errors are still in an acceptable range, so the model reflects the basic processes well.

Quality of estimated Parameters

As in the N_2O model, the uncertainties of the estimated parameters in the CH_4 simulation were high, as indicated by 95 % confidence intervals in the same magnitude as the estimated rates. Again, the estimations are based on few observations and might be biased by other missing processes. They can only be seen as a first rough estimation and should be confirmed by experimental measurements. For the parametrisation of CH_4 production rates based on chlorophyll a concentrations, examples in literature are missing. The connection and the timing between a chlorophyll a peak at the bottom and enhanced CH_4 concentrations has been proved by Bange et al. [2010a], but turnover rates for comparison are unfortunately not available. In contrary to this chlorophyll a relationship, upper and lower bounds for flux rates in the Eckernförde Bay are available from Jackson et al. [1998]. He gave a range of $3 - 20$ μmol/m^2/d (=$0.3 - 0.23$ nmol/m^2/s), but stated that the data was insufficient to determine the flux of free methane more accurately. This flux from the sediment was comparable to the flux to the atmosphere at this location during the same time [Bussmann and Suess, 1998]. However, the flux rate from the sediment less all the processes occuring in the water column below the surface was estimated about three magnitudes smaller in this model. Although the flux to the atmosphere in this model was in the range of the flux densities given in Bussmann and Suess [1998], the flux estimated from the sediment is not comparable. However, as the resulting concentrations at the surface match the measured ones, the magnitude of the estimated parameters still seems reasonable. Furthermore, the profiles of methane concentrations indicate that methane is effectively removed within the water column, as the concentration decreases towards the surface. The estimated rate comprises methane flux from the sediment less this removal.

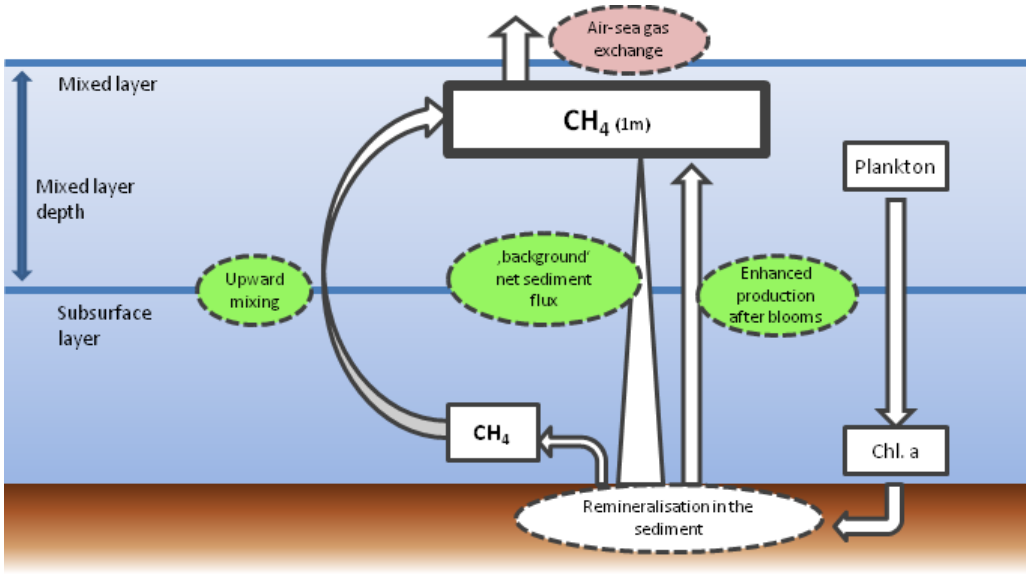

Figure 4.3.: Processes that influence the concentration of CH_4 in the surface layer at Boknis Eck according to the 1D box model. Processes that act as a source are marked in green, processes that act mainly as sinks were marked in red.

Comparisons of the different Parametrisations for air-sea Gas Exchange

The different parametrisation for the wind dependance of air-sea gas exchange resulted only in minor differences that were within the range of standard deviations of the measurements. As with the N_2O model, the main reason for this might be that the mean wind speed was in a range where the three parametrisations do not differ substantially. However, for the CH_4 model, the parametrisation LM86 revealed the least sum of residuals as well as the smallest mean errors and can thus be considered as the most accurate one at the location of BE.

The different parametrisations in air-sea gas exchange led to different magnitudes of flux densities, increasing in the order from LM86, W92 and WMcG99. Bange et al. [1994] detected flux densities in the range of 0.11 nmol/m^2/s (Febuary 1992) and 13.89 nmol/m^2/s (July 1992) in the Baltic Sea using the parametrisation LM86. All mean flux densities calculated here lie in this range. In a further study, Bange et al. [1998] calculated flux densities in the range of 358 to 2426 pmol/m^2/s (LM86) and 591 to 4252 pmol/m^2/s (W92). Given these ranges, the simulated flux densities in this study lie at the lower end. In agreement with the lower flux densities, also the saturations simulated here were at the lower end. In general, the model seems to reproduce concentrations as well as fluxed accurately in average, but may be biased for single events.

Temporal Variability of Sources and Sinks of Methane at Boknis Eck

Although the overall methane concentrations and saturations did not show a clearly pronounced seasonal cycle, the contribution to surface methane by different processes varied during the course of one year. An overview for the processes acting as sources or sinks to surface CH_4 is provided in figure 4.3. In contrast to N_2O, the sediment played the most important role for the sources of methane to the surface water. Although the sediment flux and the chlorophyll a relationship are implemented seperately, they are both processes that occur in the sediment and influence the water column concentration by exchange processes across the sediment-water interface. They are modelled seperately as the concentration profiles indicated that there is a background flux from the sediment and a further, modulated flux, which was implemented with a lag of 1 month according to Bange et al. [2010a]. The sediment played a major role when the water column was mixed and the sediment was in direct contact with the surface layer without a strong pycnocline or chemocline. As the sediment flux was implemented as such a constant 'background' input to the surface layer, the influence in this time of the year was expected. The input of CH_4 to the surface layer due to the chlorophyll a relationship did not show a clear regular seasonality during the simulated period (fig. 3.12a). This implementation was an attempt to parametrise remineralisation of organic material. During the winters 2007, 2008, 2009 and 2012, only background sediment flux and hardly any chlorophyll a related input of CH_4 to the surface layer was present. On the other hand, during winter 2010, chlorophyll a related input of CH_4 dominated. As intended, the input of CH_4 due to remineralisation closely followed the concentrations of chlorophyll a, so the missing regularity was explained by the irregularities in the chlorophyll a concentrations at the bottom. Upward mixing only played a minor role, mainly during spring and summer when the mixing layer deepens and CH_4 enriched water from the bottom was brought to the surface by mixing. The only sink of CH_4 in the whole simulated period was the flux to the atmosphere, which compensated the input of CH_4 to the surface column. However, physical processes such as temperature and wind speed seemed to have a modulating effect, as the input to the surface layer was not always directly compensated by the output. The dominant role of the sediment was also in agreement with the understanding of the methane cycling in coastal areas [Reeburgh, 2007]. Processes such as the in-situ production of methane in the water column in anoxic microenvironment apparently did not play a quantitative role at Boknis Eck.

Results are comparable to measurements carried out by Gülzow et al. [2012] in the open Baltic Sea in 2010, although their measured concentrations were in general lower with a maxima of 832 % compared to more than 1500 % in this study. They accounted the yearly maxima to the deepening of the mixed layer, when methane enriched bottom water was transferred to the mixed layer. This upward mixing also played a considerable role at BE. Per year, they found the highest flux to the atmosphere during winter, which matched the findings of this study. The concentrations and saturations fluctuated much more at BE than in the open Baltic Sea, indicating that BE is a much more dynamic system. This dynamic might at least be partly attributed to the proximity of the coast and the consequential shallow water depth. As sedimental processes are assumed to have the largest influence on methane production, a small distance between sediment and surface leaves less room for methane

removal in the water column. Thus, the signal from the sediment may be stronger pronounced at the surface at BE than at the deeper, open Baltic Sea.

Missing Processes

As the model is a simple 1D box model, there were a variety of processes that are not included in the model. These processes could be responsible for the temporary over- or underestimations in the model. The residuals for measured concentrations larger than 20 nM were all positive, indicating that the model underestimates concentrations in that range and a production process is missing. These might be advection of CH_4 from other locations or in-situ production. The occurence of methane input by seepage is possible as a process in general [Bussmann and Suess, 1998, Jackson et al., 1998, Whiticar, 2002], but unlikely to have occurred during the simulated period, as the salinity profiles did not indicate the influx of freshwater [Bussmann and Suess, 1998]. It is possible that chlorophyll a might not be a good parameter to estimate the in-situ production, but it was the best available. As alternative parameters, sediment input or input of organic material in general could serve for better parametrisations.

4.3. Nitrogen and Methane Cycling under a Scenario of continuing long-term Trends

In a further step, the relevant processes according to the 1D box model are discussed in the context of the long-term trends detected in the time series analysis.

One of the most striking trends was the significant decline in oxygen concentration in the bottom water. At the same time, hypoxic or anoxic events are increasing in frequency. As the concentration in oxygen defines the redox conditions in the water and has a strong effect on chemical reactions in the water column, the development of oxygen might be a key parameter with respect to the cycling of methane and nitrous oxide. Both trace gases are involved in reactions that are highly oxygen dependent [Bange et al., 2010b]. Thus, weakened ventilation and increased oxygen depletion are considered as the key parameters influencing the production and consumption of these trace gases.

Methane is only formed under anoxic conditions by methanogenesis [Reeburgh, 2007]. Under a scenario of increasing oxygen depletion, the conditions favour methanogenesis closer to or at the sediment surface [Schmaljohann, 1996]. At the same time, methane oxidation is likely to be lower under reducing conditions [Schmaljohann, 1996]. This may result in a direct increase of CH_4 transported to the surface and hence a higher flux to the atmosphere. With increasing temperatures at the same time, bacterial turnover rates are likely to increase [Hoppe et al., 2012]. This increase may lead to an enhanced remineralisation that could compensate the decline in organic matter input resulting from decreasing nutrient enrichment (see section 4.1).

To quantify relevant processes in the future, the model applied here should be adapted. In the CH_4 model, there is no direct implementation of an oxygen dependent process, as parametrisation of

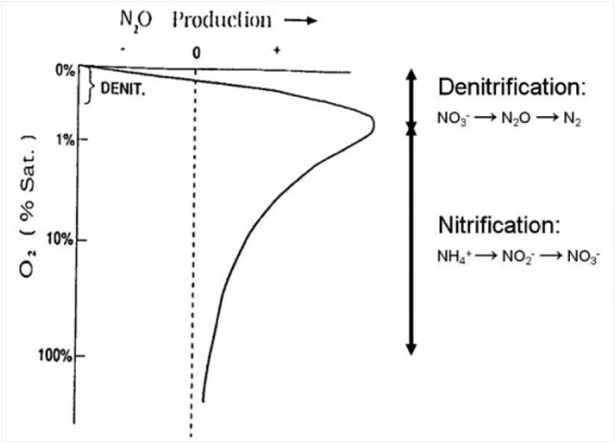

Figure 4.4.: N_2O source processes in relation to oxygen saturation [source: Bange et al., 2010b]. There is no clearly defined threshold between nitrification and denitrification with respect to oxygen saturation, both processes can occur simulatenously.

remineralisation is done by a correlation with chlorophyll a according to Bange et al. [2010a]. If the oxygen availability and not the input of organic matter is the limiting factor, then the model will produce inaccurate results. A possible way to assess the influence of oxygen concentrations would be to seperate the process of methane formation and methane consumption. Still, accurate turnover rates for these processes are essential to achieve an accurate implementation.

Concerning nitrous oxide, both nitrification and denitrification depend on oxygen concentrations. Although these processes were found to take place below the mixed layer, it could be shown that they influence the mixed layer concentrations via diffusion. An enhancement of both nitrification and denitrification therefore effects indirectly the mixed layer concentrations. The regimes of N_2O production due to nitrification and denitrification with respect to oxygen saturation are illustrated in figure 4.4. Accordingly, the decrease in oxygen saturation would lead to enhanced N_2O production. Also, remineralisation including nitrification might be enhanced by increased temperatures at the bottom that stimulate bacterial turnover. However, the mean N_2O production relative to the bottom water AOU (fig. 2.8) indicated that a certain threshold may be reached above which this relationship does not exist anymore. Then, N_2O production rates and consequently the N_2O concentrations start to decline. A reason for that might be that the sediment becomes suboxic close to the surface and forms a net sink of N_2O due to the enhancement of denitrification [Bange et al., 2010b]. N_2O might then diffuse into the sediment, representing a further sink to dissolved N_2O additional to the emission to the atmosphere. This process is likely to occur only if the bottom water is highly depleted in oxygen. The total annual N_2O emission is still likely to be rising with decreasing oxygen content, as even though there are temporary anoxic events, oxygen concentrations favouring nitrification are very likely more frequent.

A further, emission enhancing process is the warming of the sea water. As a consequence, the solubility of gases decreases for both methane [Wiesenburg and Guinasso, 1979] and nitrous oxide [Weiss and Price, 1980]. This may lead to a further increase in flux to the atmosphere of these two climate

relevant gases.

For both gases, the scenario of ongoing oxygen depletion, temperature increase and intensified stratification is likely to affect the processes acting as sources or sinks. This may lead to enhanced emissions to the atmosphere. However, to quantify the altered emission and relate them to oceanic parameters, further investigations are needed. Thus, a continuing monitoring of the trace gases as well as the parameters influencing the processes, e.g. oxygen, chlorophyll a and temperature, is crucial for a comprehensive understanding of the development of trace gas emissions at Boknis Eck.

5 Conclusion and Outlook

Both focuses of the study, the statistical analysis of the long-term trends as well as the development of the 1D box models to simulate trace gas concentrations provided insight into the past and present state of Boknis Eck.

The detection of significant long-term trends in all of the nine studied oceanographic parameters in the period of 1957 to 2013 revealed that Boknis Eck is subjected to extensive changes that comprise biological, biogeochemical and physical factors, with implications for the ecosystem. The key parameter in this context is the oxygen concentration, which declines in the bottom water. Oxygen depletion was previously often linked to nutrient input, however, the study revealed that physical factors such as temperature and intensified stratification may counteract the significant decline in eutrophication. Increased bacterial remineralisation due to temperature increase and a stronger and possibly longer lasting stratification accompanied with a weaker ventilation are likely to enhance oxygen depletion. It could be proved that the remobilisation of phosphate from the sediment contributes to oxygen depletion, but is not the major process. Most of the trends detected at Boknis Eck are similar to developments in other regions in the Baltic Sea. Thus, monitoring at the Time Series Station Boknis Eck is highly valuable to detect changes representative for large parts of the Baltic Sea.

The box models for both methane and nitrous oxide reproduced the respective measured concentrations within an acceptable range of uncertainty and provided information on the quantitative relevance of each process. Methanogenesis in the sediment with subsequent transport to the water column was the main source for surface methane. The release of methane from the sediment could be modeled as a constant background release and an enhanced release after phytoplankton blooms. Nitrous oxide was found to be produced below the mixed layer and transported there via eddy diffusion or upward mixing. Enhanced production of nitrous oxide after the breakdown of summer stratification was implemented seperately and temporarily increased the production of nitrous oxide by more than 60%. This study could show that besides the seasonal variations, emissions can also be enhanced significantly for short time periods, which is important to consider for further monitorings. By far the most important sink for both methane and nitrous oxide was the emission to the atmosphere. In a scenario of further oxygen depletion, as revealed by the statistical analyses, trace gas emissions are estimated to grow, as source processes for both gases are highly oxygen dependent.

Continuing the monthly measurements at Time Series Boknis Eck is of major importance to monitor and understand future changes in the Baltic Sea. To further substantiate the hypothesis of weakened ventilation as a reason for oxygen depletion, measurements with a higher spatial resolution

are needed. A sequence of CTD profiles (conductivity, temperature, depth) comprising several years would allow to determine the precise location and gradient of the pycnocline and therefore would enable conclusions on the altered ventilation.
Concerning the modelling of trace gases, experimentally derived flux rates would be needed to further develop the model. It could be shown that the implementation of biological processes in contrast to physical processes lacks accurate parametrisations. Accurate turnover and flux rates would help to precisely define the processes involved in the cycling of methane and nitrous oxide and improve the quantification of relevant processes.

Bibliography

B. Babenerd. Increasing oxygen deficiency in Kiel Bay (Western Baltic) - a paradigm of progressing coastal eutrophication. *Meeresforschung*, (33):121–140, 1991.

BACC. *Assessment of climate change for the Baltic Sea basin*. Springer, 2008.

H. W. Bange. Air-sea exchange of nitrous oxide and methane in the Arabian Sea: A simple model of the seasonal variability. *Indian Journal of Marine Sciences*, 33(1):77–83, 2004.

H. W. Bange, U. H. Bartell, S. Rapsomanikis, and M. O. Andreae. Methane in the Baltic and North Seas and a reassessment of the marine emissions of methane. *Global Biogeochemical Cycles*, 8(4): 465–480, 1994.

H. W. Bange, S. Dahlke, R. Ramesh, L.-A. Meyer-Reil, S. Rapsomanikis, and M. O. Andreae. Seasonal study of methane and nitrous oxide in the coastal waters of the Southern Baltic Sea. *Estuarine, Coastal and Shelf Science*, 47:807–817, 1998.

H. W. Bange, M. O. Andreae, S. Lal, C. S. Law, S. W. A. Naqvi, P. K. Patra, T. Rixen, and R. C. Upstill-Goddard. Nitrous oxide emissions from the Arabian Sea: A synthesis. *Atmos. Chem. Phys.*, 1:61–71, 2001.

H. W. Bange, K. Bergmann, H. P. Hansen, A. Kock, R. Koppe, F. Malien, and C. Ostrau. Dissolved methane during hypoxic events at the Boknis Eck time series station (Eckernförde Bay, SW Baltic Sea). *Biogeosciences*, 7:1279–1284, 2010a.

H. W. Bange, A. Freing, A. Kock, and C. Löscher. Marine pathways to nitrous oxide. In *Nitrous Oxide and Climate Change*. Earthscan, 2010b.

H. W. Bange, H. P. Hansen, F. Malien, K. Lass, A. Dale, J. Karstensen, C. Petereit, and G. Friedrichs. Boknis Eck Time Series Station (SW Baltic Sea): Measurements from 1957 to 2010. *LOICZ Inprint*, 2011(1):16–22, 2011.

D. R. Bates and P. B. Hays. Atmospheric nitrous oxide. *Planetary and Space Science*, 15(1):189–197, 1967.

U. Berger and J. Heyer. Distribution and activity of methanotrophic bacteria in a brackish water ecosystem. *Limnologica*, 8:141–144, 1999.

E. Bonsdorff, E. M. Blomqvist, J. Mattila, and A. Norkko. Coastal eutrophication: Causes, consequences and perspectives in the Archipelago areas of the Northern Baltic Sea. *Estuarine, Coastal and Shelf Science*, 44:63–72, 1997.

A. F. Bouwman, K. W. Van der Hoek, and J. G. J. Olivier. Uncertainties in the global source distribution of nitrous oxide. *Journal of Geophysical Research: Atmospheres*, 100(D2):2785–2800, 1995.

G.E.P. Box, G.M. Jenkins, and C.R. Reinsel. *Time Series Analysis*. John Wiley & Sons, 4. edition, 2008.

W. S. Broecker and T.-H. Peng. Gas exchange rates between air and sea. *Tellus*, 26(1-2):21–35, 1974.

J. Burkey. Matlab function: Seasonal Kendall trend test for data with and without serial dependance, 2012. URL `http://www.mathworks.com/matlabcentral/fileexchange/22389-seasonal-kendall-test-with-slope-for-serial- dependent-data/content/sktt.m`.

I. Bussmann and E. Suess. Groundwater seepage in Eckernförde Bay (Western Baltic Sea): Effect on methane and salinity distribution of the water column. *Continental Shelf Research*, 18(14-15):1795–1806, 1998.

I. Bussmann, P. R. Dando, S. J. Niven, and E. Suess. Groundwater seepage in the marine environment: role for mass flux and bacterial activity. *Marine Ecology Progress Series*, (178):169–177, 1999.

S. R. Carpenter and W. A. Brock. Rising variance: a leading indicator of ecological transition. *Ecology Letters*, 9(3):311–318, 2006.

J. Carstensen, D. J. Conley, J. H. Andersen, and G. Aertebjerg. Coastal eutrophication and trend reversal: A Danish case study. *Limnoloby and Oceanography*, 5(1):398–408, 2006.

R. J. Cicerone and R. S. Oremland. Biogeochemical aspects of atmospheric methane. *Global Biogeochemical Cycles*, 2(4):299–327, 1988.

J. E. Cloern. Our evolving conceptual model of the coastal eutrophication problem. *Marine Ecology Progress Series*, (210):223–253, 2001.

D. J. Conley, C. Humborg, L. Rahm, O. P. Savchuk, and F. Wulff. Hypoxia in the Baltic Sea and basin-scale changes in phosphorus biogeochemistry. *Environmental Science & Technology*, 36(24):5315–5320, 2002.

D. J. Conley, J. Carstensen, G. Aertebjerg, P. B. Christensen, J. L. Dalsgaard, T. Hansen, and A. B. Josefson. Long-term changes and impacts of hypoxia in Danish coastal waters. *Ecological applications*, 17(5):165–184, 2007.

M. Cornejo, L. Farias, and M. Gallegos. Seasonal cycle of N_2O vertical distribution and air-sea fluxes over the continental shelf waters off central chile. *Progress in Oceanography*, (75):383–395, 2007.

P. J. Crutzen. The influence of nitrogen oxides on the atmospheric ozone content. *Quarterly Journal of the Royal Meteorological Society*, 96(408):320–325, 1970.

C. de Boyer Montegut, G. Madec, A. S. Fischer, A. Lazar, and D. Iudicone. Mixed layer depth over the global ocean: An examination of profile data and a profile-based climatology. *Journal of Geophysical Research: Oceans*, 109(C12):n/a–n/a, 2004.

B. deYoung, R. Harris, J. Alheit, N. Beaugrand, N. Mantua, and L. Shannon. Detecting regime shifts in the ocean: data considerations. *Progress in Oceanography*, 60:143–164, 2004.

R. Diaz and R. Rosenberg. Spreading dead zones and consequences for marine ecosystems. *Science*, (321):926–930, 2008.

J. W. Dippner, C. M öller, and J. Hänninen. Regime shifts in North Sea and Baltic Sea: A comparison. *Journal of Marine Systems*, 105-108:115–122, 2012.

D. Dryssen. The Baltic-Kattegat-Skagerrak estuarine system. *Estuaries*, 16(3):63–72, 1993.

H. W. Ducklow, S. C. Doney, and D. K. Steinberg. Contributions of long-term research and time-series observations to marine ecology and biogeochemistry. *Annual Review of Marine Science*, 1: 279–302, 2009.

G. T. Evans. The role of local models and data sets in the joint global ocean flux study. *Deep Sea Reasearch I*, 46:1369–1389, 1999.

R. Feistel, G. Nausch, and N. Wasmund. *State and Evolution of the Baltic Sea, 1952-2005: A Detailed 50-Year Survey of Meteorology and Climate, Physics, Chemistry, Biology, and Marine Chemistry, Biology, and Marine Environment.* Wiley-Blackwell (an imprint of John Wiley & Sons Ltd), 2008.

C. Franzke. A novel method to test for significant trends in extreme values in serially dependent time series. *Geophysical Research Letters*, 40(7):1391–1395, 2013.

A. Freing, D. W. R. Wallace, and H. W. Bange. Global oceanic production of nitrous oxide. *Philosophical transactions of the Royal Society Biological Sciences*, (367):1245–1255, 2011.

H. E. Garcia and L. I. Gordon. Oxygen solubility in seawater: better fitting equations. *Limnology and Oceanography*, 37(6):1307–1312, 1992.

D. M. Glover, W. J. Jenkins, and S. C. Doney. *Modeling Methods for Marine Science.* Cambridge University Press, 2011.

K. Grasshoff, K. Kremling, and M. Ehrhardt. *Methods of Seawater Analysis.* Wiley-VCH, 3. edition, 1999.

A. Grinsted. Matlab function: Quantile regression, 2011.

J. Grotzinger, Th.H. Jordan, F. Press, and R. Siever. *Allgemeine Geologie.* Springer Spektrum, 2008.

D. A. Grundle and S. K. Juniper. Nitrification from the lower euphotic zone to the sub-oxic waters of a highly productive British Columbia fjord. *Marine Chemistry*, 126:173–181, 2011.

M. Grunwald, O. Dellwig, M. Beck, J. W. Dippner, J. A. Freund, C. Kohlmeier, B. Schnetger, and H.-J. Brumsack. Methane in the southern north-sea: sources, spatial distribution and budgets. *Estuaries, Coastal and Shelf Science*, 81:445–456, 2009.

W. Gülzow, G. Rehder, J. Schneider v. Deimling, T. Seifert, and Zs. Toth. One year of continuous measurements constraining methane emissions from the Baltic Sea to the atmosphere using a ship of opportunity. *Biogeosciences Discuss.*, (9):9897–9944, 2012.

J. Hanninen, I. Vuorinen, and P. Hjelt. Climatic factors in the Atlantic control the oceanographic and ecological changes in the Baltic Sea. *Limnology and Oceanography*, 45(3):703–710, 2000.

H. P. Hansen, H. C. Giesenhagen, and G. Behrends. Seasonal and long-term control of bottom-water oxygen deficiency in a stratified shallow-water coastal system. *ICES Journal of Marine Science*, 56:65–71, 1999.

HELCOM. Convention on the protection of the marine environment of the Baltic Sea area. *Helsinki Convention*, (115B):1–27, 1974.

HELCOM. Eutrophication in the Baltic Sea - an integrated assessment of the effects of nutrient enrichment in the Baltic Sea region. *Baltic Sea Environment Proceedings*, (115B):1–145, 2009.

R. M. Hirsch and J. R. Slack. A nonparametric trend test for seasonal data with serial dependence. *Water Resources Research*, 20(6):727–732, 1984.

H.-G. Hoppe, H. C. Giesenhagen, R. Koppe, H.-P. Hansen, and K. Gocke. Impact of change in climate and policy from 1988 to 2007 on environmental and microbial variables at the time series station Boknis Eck, Baltic Sea. *Biogeosciences Discuss.*, 9:18655–18706, 2012.

IPCC. *Climate Change 2007: Synthesis Report. Contribution of Working Groups I, II and III to the Fourth Assessment Report of the Intergovernmental Panel on Climate Change.* IPCC, 2007.

D. R. Jackson, K. L. Williams, T. F. Wever, C. T. Friedrichs, and L. D. Wright. Sonar evidence for methane ebullition in Eckernförde Bay. *Continental Shelf Research*, 18(14-15):1893–1915, 1998.

B. Jähne, G. Heinz, and W. Dietrich. Measurement of the diffusion coefficients of sparingly soluble gases in water. *Journal of Geophysical Research: Oceans*, 92(C10):10767–10776, 1987.

L. Jonasson, J. L. S. Hansen, Z. Wan, and J. She. The impacts of physical processes on oxygen variations in the North Sea-Baltic Sea transition zone. *Ocean Science*, 8:37–48, 2012.

K. Kalle. Meereskundliche chemische Untersuchungen mit Hilfe des Zeissschen Pulfrich-Photometers. V. Die Bestimmung des Gesamt-Phosphorgehaltes, des Plankton-Phosphorgehaltes (lebende Substanz) und Trübungsmessungen. *Ann. d. Hydrography*, 63:195–204, 1935.

A. B. Kara, P. A. Rochford, and H. E. Hurlburt. An optimal definition for ocean mixed layer depth. *Journal of Geophysical Research: Oceans*, 105(C7):16803–16821, 2000.

K. Karlson, R. Rosenberg, and E. Bonsdorff. Temporal and spatial large-scale effects of eutrophication and oxygen deficiency on benthic fauna in Scandinavian and Baltic waters - a review. *Oceanography and Marine Biology: an Annual Review*, 40, 2002.

R. Koenker and K. Hallock. Quantile regression. *Journal of Economic Perspectives*, (15):143–156, 2001.

J. Krey. Die Bestimmung des Chlorophyll a in Meerwasser-Schöpfproben. *Meereskundliche Arbeiten der Univeristät zu Kiel*, 65:201–209, 1939.

J. Krey, B. Babenerd, and J. Lenz. Beobachtungen zur Produktionsbiologie des Planktons in der Kieler Bucht 1957 - 1975. *Berichte aus dem Institut für Meereskunde*, 1:1–20, 1980.

A. Kulkarni and H. Von Storch. Monte Carlo experiments on the effect of serial correlation on the Mann-Kendall test of trend. *Meteorologische Zeitschrift*, 4(2):82–85, 1995.

H. U. Lass and W. Matthäus. On temporal wind variations forcing salt water inflows into the Baltic Sea. *Tellus A*, 48(5):663–671, 1996.

A. Lehmann. A three-dimensional baroclinic eddy-resolving model of the Baltic Sea. *Tellus*, 47A: 1013–1031, 1995.

A. Lehmann, K. Getzlaff, and J. Harlass. Detailed assessment of climate variability in the Baltic Sea area for the period 1958 to 2009. *Climate Research*, 46:185–196, 2011.

J. Lelieveld, P. J. Curtzen, and F. J. Dentener. Changing concentration, lifetime and climate forcing of atmospheric methane. *Tellus*, 50(2):128–150, 1998.

P. S. Liss and L. Merlivat. Air-sea gas exchange rates: Introduction and synthesis. In *The role of air-sea gas exchange in geochemical cycling*. Springer, 1986.

C. R. Löscher, A. Kock, M. Könneke, J. LaRoche, H. W. Bange, and R. A. Schmitz. Production of oceanic nitrous oxide by ammonium-oxidizing archaea. *Biogeosciences*, (9):2419–2429, 2012.

H. B. Mann. Nonparametric tests against trend. *Econometrica*, 13(3):245–259, 1945.

M. Mengis, R. Gächter, and B. Wehrli. Sources and sinks of nitrous oxide N2O in deep lakes. *Biogeochemistry*, 38:281–301, 1997.

S. W. A. Naqvi, H. W. Bange, S. W. Gibb, C. Goyet, A. D. Hatton, and R. C. Upstill-Goddard. Biogeochemical ocean-atmosphere transfers in the Arabian Sea. *Progress in Oceanography*, 65:116–144, 2005.

S. W. A. Naqvi, H. W. Bange, L. Farias, P. M. S. Monteiro, M. I. Scranton, and J. Zhang. Marine hypoxia/anoxia as a source of CH_4 and N_2O. *Biogeosciences*, (7):2159–2190, 2010.

C. D. Nevison, R. F. Weiss, and D. J. Erickson. Global oceanic emissions of nitrous oxide. *Journal of Geophysical Research: Oceans*, 100(C8):15809–15820, 1995.

C. Oudot, C. Andrie, and Y. Montel. Nitrous oxide production in the tropical atlantic ocean. *Deep Sea Research Part A. Oceanographic Research Papers*, 37(2):183–202, 1990.

H. Pitkänen, J. Lehtoranta, and A. Räike. Internal nutrient fluxes counteract decreases in external load: The case of the Estuarial Eastern Gulf of Finland, Baltic Sea. *Ambio*, 30(4):194–301, 2001.

A. R. Ravishankara, J. S. Daniel, and R. W. Portmann. Nitrous oxide (N2O): the dominant ozone-depleting substance emitted in the 21st century. *Science*, 326:123–125, 2009.

W. S. Reeburgh. Oceanic methane biogeochemistry. *Chemical reviews*, 107(2):486–513, 2007.

G. Rheinheimer and D. Nehring. *Meereskunde der Ostsee*. Springer, 2. edition, 1995.

W. Roedel. *Physik unserer Umwelt: die Atmosphähre*. Wiley-VCH, 3. edition, 2000.

U. Rönner. Distribution, production and consumption of nitrous oxide in the Baltic Sea. *Geochimica et Cosmochimica Acta*, 47(12):2179–2188, 1983.

R. Rosenberg. Negative oxygen trends in Swedish coastal bottom waters. *Marine Pollution Bulletin*, 21 (7):335–339, 1990.

P. Sanden and B. Hakansson. Long-term trends in Secchi depth in the Baltic Sea. *Limnology and Oceanography*, 41:346–351, 1996.

R. Schlittgen and B. H. J. Streitberg. *Zeitreihenanalyse*. Oldenburg Wissenschaftsverlag, 2001.

R. Schmaljohann. Methane dynamics in the sediment and water column of Kiel harbour (Baltic Sea). *Marine Ecology Progress Series*, (131):263–273, 1996.

T. Schreiber and A. Schmitz. Improved surrogate data for nonlinearity tests. *Physical Review Letters*, 77(4):635–638, 1996.

B. Schweiger, H. P. Hansen, and H. W. Bange. A time series of hydroxylamine (NH_2OH) in the Southwestern Baltic Sea. *Geophysical Research Letters*, 34(24), 2007.

S. P. Seitzinger and C. Kroeze. Global distribution of nitrous oxide production and N inputs in freshwater and coastal marine ecosystems. *Global Biogeochemical Cycles*, 12(1):93–113, 1998.

P. K. Sen. Estimates of the regression coefficient based on Kendall's Tau. *Journal of the American Statistical Association*, 63(324):1379–1389, 1968.

H. Siegel, M Gerth, and Tschersich G. Sea surface temperature development of the Baltic Sea in the period 1990-2004. *Oceanologica*, 48:119–131, 2006.

V. Smetacek. The annual cycle of Kiel Bight plankton: A long-term analysis. *Estuaries*, 8(2):145–157, 1985.

O. Thiessen, M. Schmidt, F. Theilen, M. Schmitt, and G. Klein. Methane formation and distribution of acoustic turbidity in organic-rich surface sediments in Arkona basin, Baltic Sea. *Continental Shelf Research*, 26:2469–2483, 2006.

B. Tinz. On the relation between annual maximum extend of ice cover in the Baltic Sea and sea level pressure as well as air temperature field. *Geophysica*, 32:319–341, 1996.

C. Torrence and A. Compo, G.P. Matlab function: Wavelet analysis, 2004. URL `http://paos.colorado.edu/research/wavelets/`".

C. Torrence and G. P. Compo. A practical guide to wavelet analysis. *Bulletin of the American Meteorological Society*, 79(1):61–78, 1998.

M.H. Trauth. *Matlab recipes for Earth Sciences*. Springer, 3. edition, 2010.

J. E. Tyler. The Secchi disc. *Limnology and Oceanography*, 13(1):1–6, 1968.

UNESCO. Background papers and supporting data on the international equation of state of seawater 1980. *Unesco technical papers in marine science*, 1981.

J. J. Virtasalo, T. Kohonen, I. Vuorinen, and T. Huttula. Sea bottom anoxia in the Archipelago sea, Northern Baltic Seaimplications for phosphorus remineralization at the sediment surface. *Baltic Sea Environment Proceedings*, 224(1-4):103–122, 2005.

W.C. Wang, Y.L. Yung, A.A. Lacis, T. Mo, and J.E. Hansen. Greenhouse effects due to man-made pertubations of trace gases. *Science*, 194(4266):685–690, 1976.

R. Wanninkhof. Relationship between wind speed and gas exchange over the ocean. *Journal of Geophysical Research*, 97(C5):7373–7382, 1992.

R. Wanninkhof and W. R. McGillis. A cubic relationship between air-sea CO2 exchange and wind speed. *Geophysical Research Letters*, 26(13):1889–1892, 1999.

N. Wasmund and S. Uhlig. Phytoplankton trends in the Baltic Sea. *Journal of Marine Science*, 60: 177–186, 2003.

M. Weigelt. Oxygen conditions in the deep water of Kiel Bay and the impact of inflowing salt-rich water from the Kattegatt. *Meeresforschung*, (33):1–22, 1990.

M. Weigelt. Short- and long-term changes in the benthic communitiey of the deeper parts of Kiel Bay (Western Baltic) due to oxygen depletion and eutrophication. *Meeresforschung*, (33):197–224, 1991.

R. F. Weiss and B. A. Price. Nitrous oxide solubility in water and seawater. *Marine Chemistry*, 8(4): 347–359, 1980.

W. A. Welschmeyer. Fluorometric analysis of chlorophyll a in the presence of chlorophyll b and pheopigments. *Limnology and Oceanography*, 39(8):1985–1992, 1994.

M. Whiticar. Diagenetic relationships of methanogenesis, nutrients, acoustic turbidity, pockmarks and freshwater seepages in Eckernförde Bay. *Marine Geology*, 182:29–53, 2002.

D. A. Wiesenburg and N. L. Guinasso. Equilibrium solubilities of methane, carbon monoxide, and hydrogen in water and sea water. *Journal of Chemical & Engineering Data*, 24(4):356–360, 1979.

K. H. Wiltshire and C.-D. Dürselen. Revision and quality analyses of the Helgoland Reede long-term phytoplankton data archive. *Helgoland Marine Research*, 58(4):252–268, 2004.

W. A. Woodward and H. L. Gray. Global warming and the problem of testing for trend in time series data. *Journal of Climate*, 63:953–964, 1993.

K. Yu, Z. Lu, and J. Stander. Quantile regression: applications and current research areas. *Journal of the Royal Statistical Society: Series D (The Statistician)*, 52(3):331–350, 2003.

S. Yue and C. Y. Wang. Applicability of prewhitening to eliminate the influence of serial correlation on the Mann-Kendall test. *Water Resources Research*, 38:1–7, 2002.

Appendices

A Time Series Analysis

A.1. Time Series

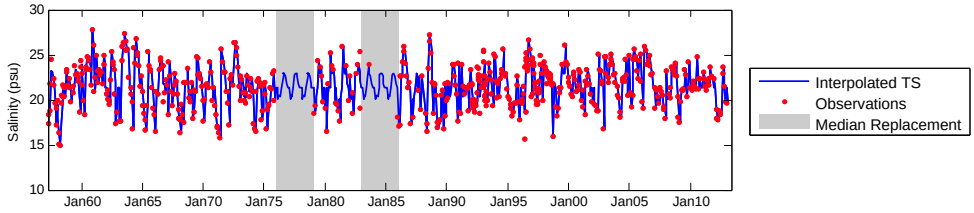

Figure A.1.: Boknis Eck time series of salinity at 25 m depth.

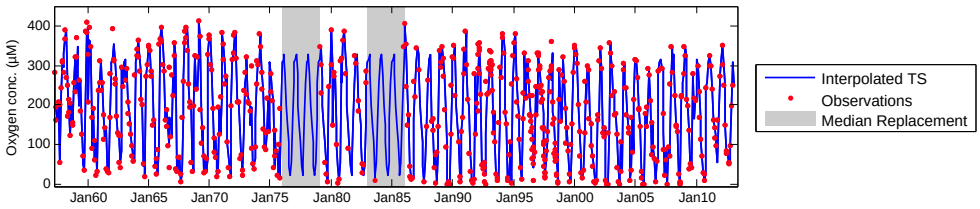

Figure A.2.: Boknis Eck time series of oxygen concentration at 25 m depth.

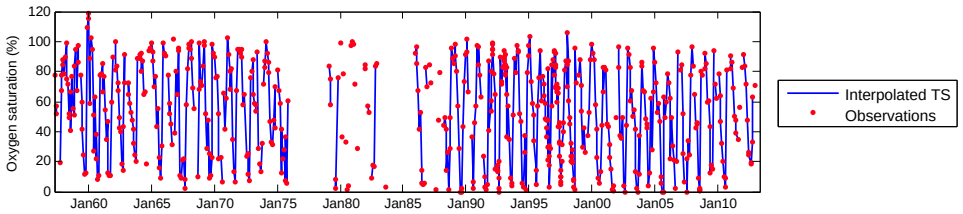

Figure A.3.: Boknis Eck time series of oxygen saturation at 25 m depth.

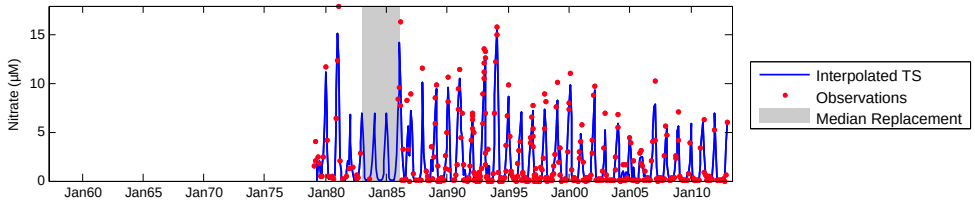

Figure A.4.: Boknis Eck time series of nitrate at 10 m depth.

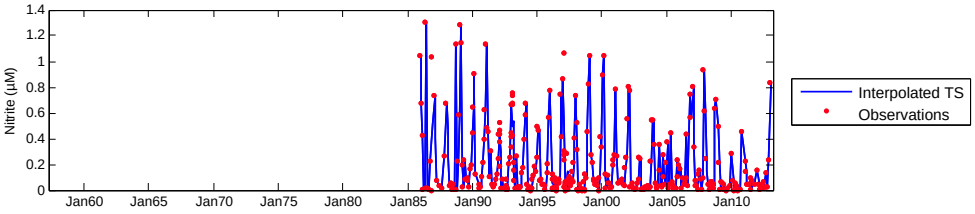

Figure A.5.: Boknis Eck time series of nitrite concentration at 10 m depth.

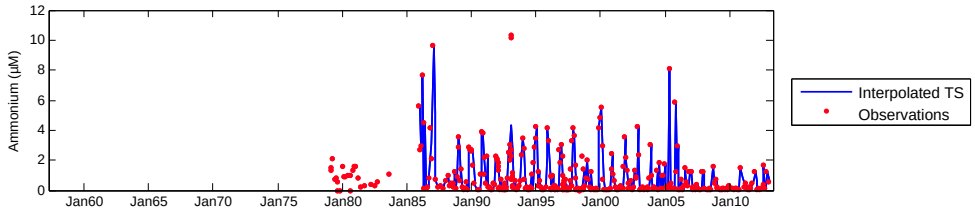

Figure A.6.: Boknis Eck time series of ammonium concentration at 10 m depth.

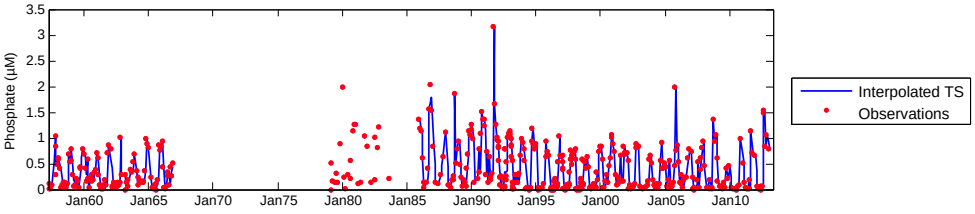

Figure A.7.: Boknis Eck time series of phosphate concentration at 10 m depth.

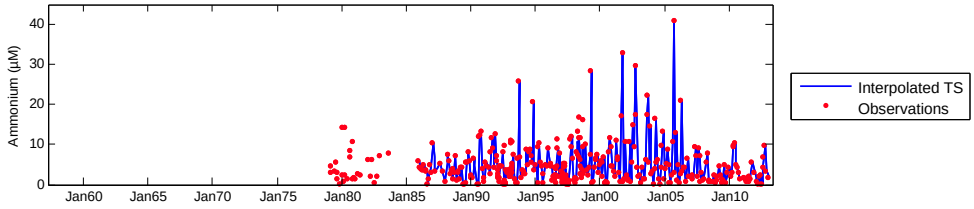

Figure A.8.: Boknis Eck time series of ammonium concentration at 25 m depth.

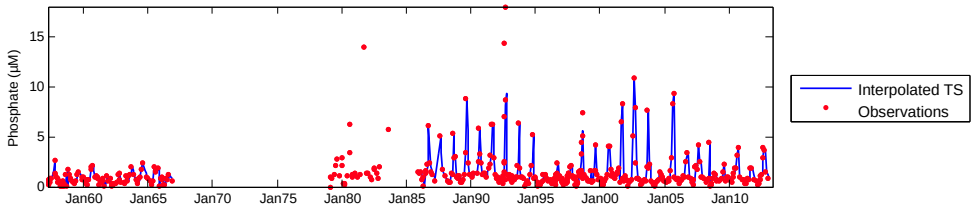

Figure A.9.: Boknis Eck time series of phosphate concentration at 25 m depth.

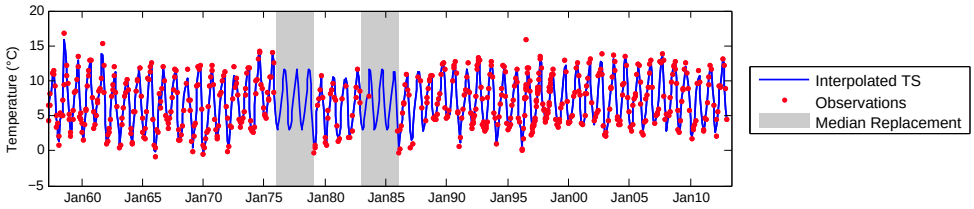

Figure A.10.: Boknis Eck time series of temperature at 25 m depth.

A.2. Wavelet Power Spectra

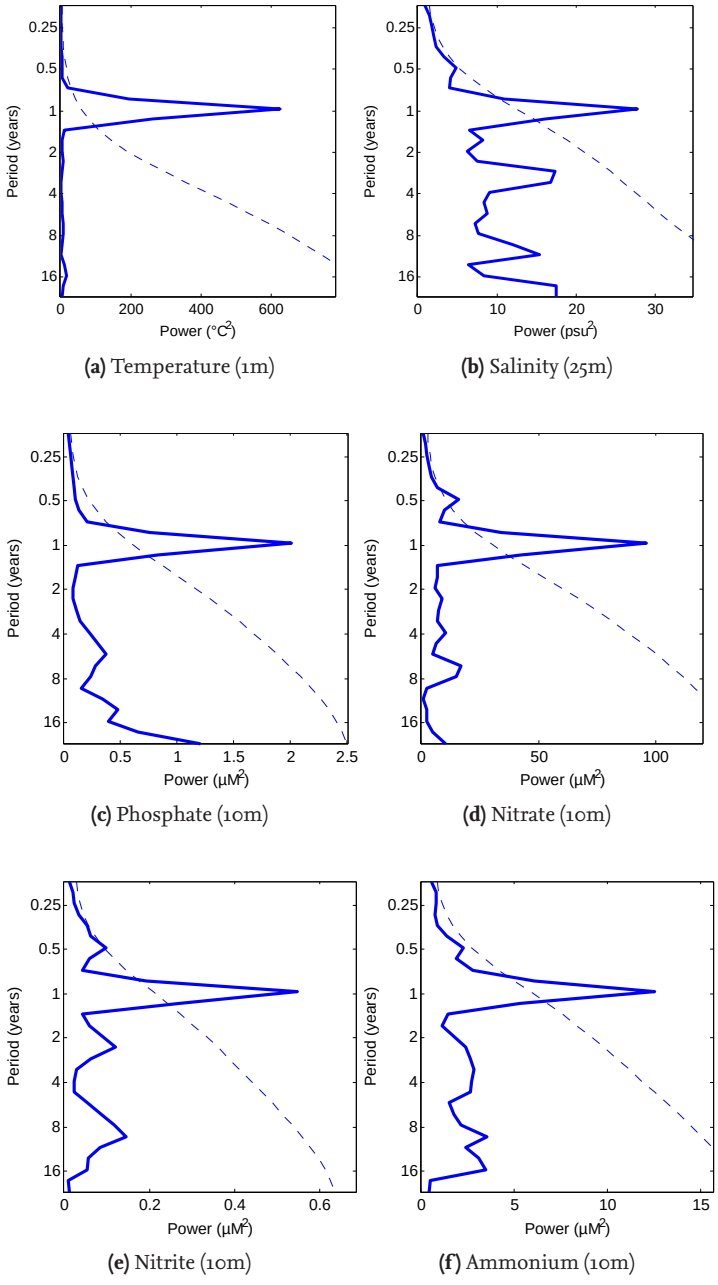

(a) Temperature (1m) **(b)** Salinity (25m)

(c) Phosphate (10m) **(d)** Nitrate (10m)

(e) Nitrite (10m) **(f)** Ammonium (10m)

Figure A.11.: Global power spectra of Wavelet analysis shown in the main part. Dashed line indicates 95 % significance.

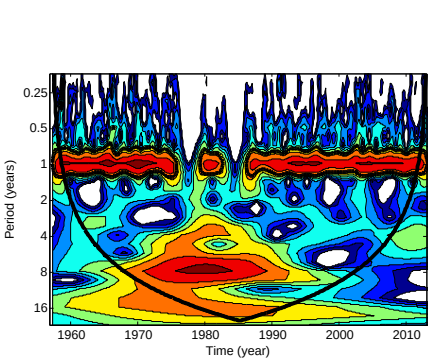

(a) WPS Temperature (25m)

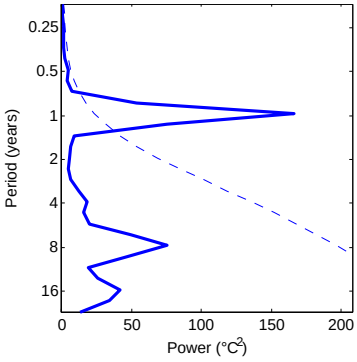

(b) GPS Temperature (25m)

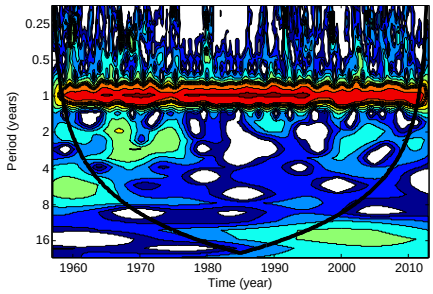

(c) WPS Oxygen conc. (25m)

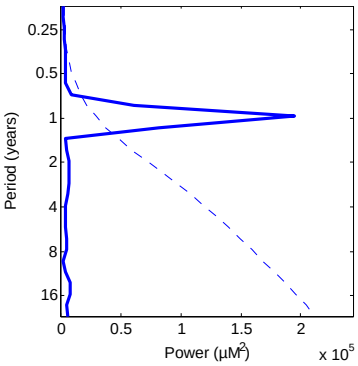

(d) GPS Oxygen conc. (25m)

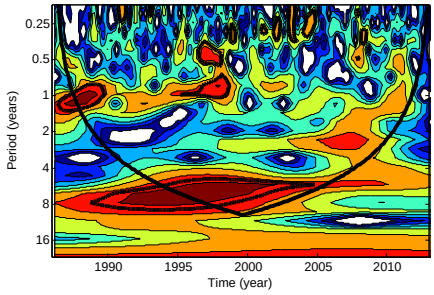

(e) WPS Secchi Depth

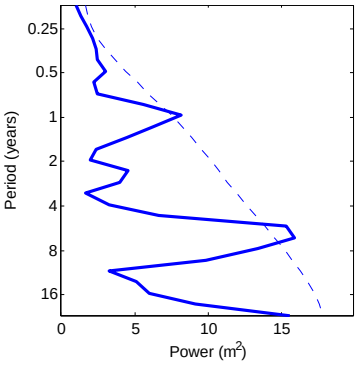

(f) WPS Secchi Depth

Figure A.12.: Wavelet power spectra (WPS) and global power spectra (GPS) of Wavelet analysis. Dashed line in GPS indicates 95 % significance, black lines in WPS indicate 95 % significance, both against red noise.

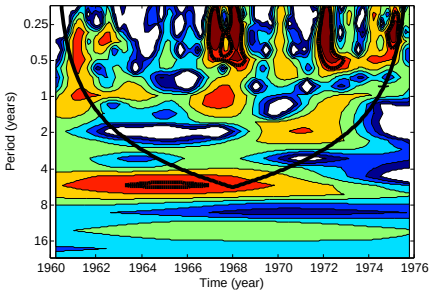

(a) WPS chlorophyll a I (10m)

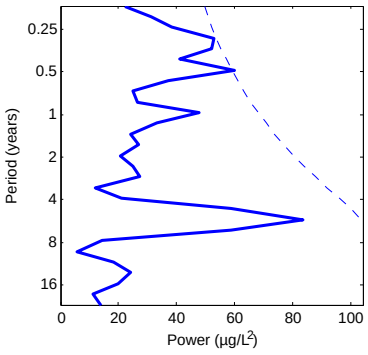

(b) GPS chlorophyll a I (10m)

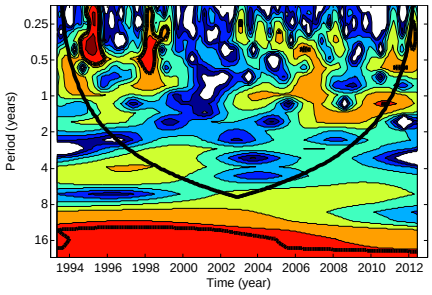

(c) WPS chlorophyll a II (10m)

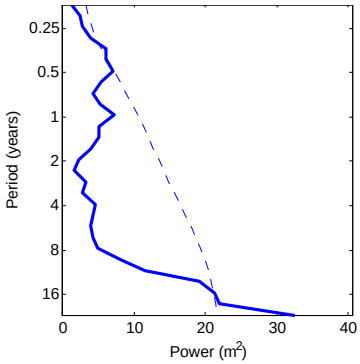

(d) GPS chlorophyll a II (10m)

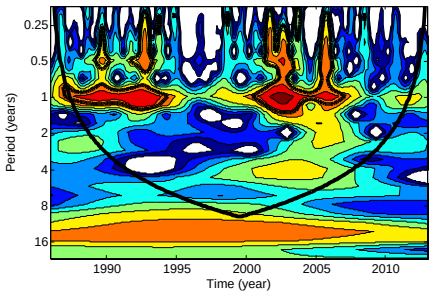

(e) WPS Phosphate conc. (25m)

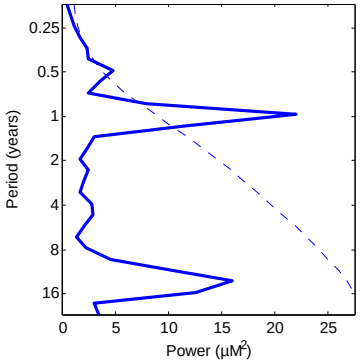

(f) WPS Phosphate conc. (10m)

Figure A.13.: Wavelet power spectra (WPS) and global power spectra (GPS) of Wavelet analysis. Dashed line in GPS indicates 95 % significance, black lines in WPS indicate 95 % significance, both against red noise.

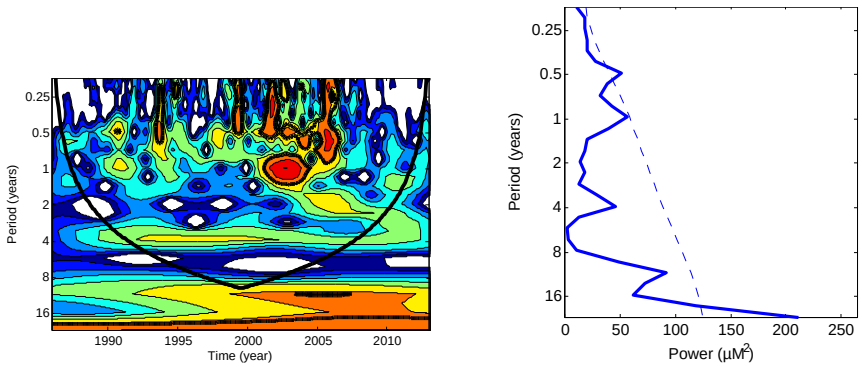

(a) WPS Ammonium (25m)

(b) GPS Ammonium (25m)

Figure A.14.: Wavelet power spectra (WPS) and global power spectra (GPS) of Wavelet analysis. Dashed line in GPS indicates 95 % significance, black lines in WPS indicate 95 % significance, both against red noise.

A.3. Test Statistics

Table A.1.: Test statistics for the monthly Mann-Kendall-Test on oxygen saturation. Only significant results are shown. C.I.=confidence interval on Sen's slope. Tau b=Kendall's Tau for time series including ties.

	Tau b	p-value	Sen's slope	C.I. 5 %	C.I. 95 %
January	-0.226	0.03199	-0.26160	-0.51662	-0.01980
April	-0.262	0.00538	-0.32668	-0.56178	-0.14646
May	-0.241	0.01638	-0.31665	-0.58901	-0.06367
July	-0.322	0.00051	-0.47285	-0.71218	-0.23360
September	-0.316	0.00052	-0.22392	-0.39066	-0.09583

Table A.2.: Discriptive Statistics, Mann-Kendall-statistics (MKT) and quantile regression results of BE time series. *indicates significance in quantile regression. Tau b=Kendall's Tau for time series including 12 seasons and ties.

Parameter	**Temperature**	**Temperautre**	**Salinity**	**Oxygen**	**Secchi depth**	**Chlorophyll a I**	**Chlorophyll a II**
Unit	°C	°C	psu	μM	m	μg/L	μg/L
Depth	1 m	25 m	25 m	25 m	-	10 m	10 m
Start date	30.04.1957	30.04.1957	30.04.1957	30.04.1957	11.02.1986	31.03.1960	19.04.1988
End date	06.02.2013	06.02.2013	06.02.2013	06.02.2013	06.02.2013	02.12.1975	26.06.2012
Mean	9.74	7.02	21.55	183.52	6.77	5.47	2.86
Std.	6.00	3.64	2.35	116.95	1.76	6.39	2.06
Perc. gaps	17.91	18.69	19.22	19.35	8.75	5.05	15.28
Mean filled	9.57	7.00	21.53	186.59	6.71	5.46	2.68
Std. filled	5.90	3.37	2.17	112.77	1.71	6.31	2.10
Autocorr. lag1 filled	0.82	0.97	0.56	0.73	0.36	0.01	0.29
MKT							
homogeneity	no	yes	yes	no	yes	yes	no
Tau b seasonal	0.146	0.190	0.013	-0.215	0.06	0.105	-0.156
p-value	6.8234E-4	4.43E-10	0.6656	1.8969E-12	0.1511	0.0633	0.0006
p-value adjusted	3.8E-8	0.273	0.9428	0.2384	0.9393	0.4081	0.4704
Sen's slope	0.0176	0.0242	0.0016	-0.9104	-0.0167	0.0714	-0.0383
Quantile regression							
90 % quantile data	0.0024	n.d.	-6.1304E-4	-0.0523	-0.0063*	-0.0111*	-0.0067*
p.t. 95 %	0.0027	n.d.	0.0022	0.0642	0.0026	0.0075	0.0043
p.t. 5%	-0.0029	n.d.	-0.0022	-0.0625	-0.0028	-0.0076	-0.0044
10 % quantile data	0.0014	n.d.	0.0021*	-0.0655*	-0.0012	-7.6931E-4	-0.0015
p.t. 95 %	0.0028	n.d.	0.0017	0.0506	0.00544	0.0426	0.0164
p.t. 5 %	-0.0031	n.d.	-0.0016	-0.0525	-0.0058	-0.0403	-0.0177

Table A.3.: Discriptive Statistics, Mann-Kendall-statistics (MKT) and linear regression results of BE time series. *indicates significance. Percent of gaps (Perc. gaps) for whole time series and if a shorter one is used, the number of gaps is given in brackets. n.d.=no data

Parameter	**Phosphate**	**Phosphate**	**Nitrate**	**Nitrite**	**Ammonium**	**Ammonium**
Unit	μM	μM	μM	μM	μM	μM
Depth	10 m	25 m	10 m	10 m	10 m	25 m
Start date	30.04.1957	30.04.1957	12.03.1979	07.01.1986	12.03.1979	12.03.1979
End date	06.02.2013	06.02.2013	06.02.2013	06.02.2013	06.02.2013	06.02.2013
Mean	0.3891	1.846	2.0961	0.1971	0.799	4.8385
Std.	0.4233	3.4011	3.4286	0.2668	1.4834	5.1499
Perc. gaps	32.8105 (7.4812)	34.25	48.1046 (18.6475)	7.7307	9.7257	10.9726
Mean filled	0.4455	1.5533	2.1265	0.2141	0.946	4.9692
Std. filled	0.4522	1.7213	3.2026	0.2681	1.4272	5.1007
Autocorr. lag1 filled	0.6205	0.5438	0.6394	0.5129	0.4925	0.252
MKT (DJM)	since 1986					
Tau b	-0.1282	n.d.	-0.3935	-0.3735	-0.5157	n.d.
p-value	0.359	n.d.	0.002	0.0057	1.75E-04	n.d.
Sen's slope	-0.0067	n.d.	-0.1402	-0.0129	-0.1177	n.d.
Lineare Regression (DJM)						
slope	-0.095	n.d.	-0.16	-0.0085	-0.14	n.d.
Pearson's R	-0.7236	n.d.	-0.5436	-0.3651	-0.5941	n.d.

Table A.4.: Test statistics for Mann-Kendall-Test performed monthly. Only significant results are shown. Slopes are given in Unit per month. Adjusted p-value refers to the correction for autocorrelation. C.I.=confidence interval on Sen's slope.

	Tau b	p-value	Sen's slope	C.I. 5 %	C.I. 95 %
Temperature 1m (°C)					
January	0.206	0.048100	0.03	0	0.05
April	0.354	0.000099	0.07	0.03	0.10
May	0.290	0.002500	0.06	0.02	0.09
Temperature 25m (°C)					
January	0.232	0.02569	0.03	0.00	0.06
February	0.199	0.04448	0.03	0.00	0.06
March	0.220	0.01621	0.03	0.01	0.06
April	0.307	0.00073	0.04	0.02	0.06
June	0.227	0.02580	0.03	0.00	0.05
September	0.253	0.00469	0.04	0.01	0.06
Oxygen 25m (μM)					
January	-0.266	0.01143	-1.45	-2.42	-0.33
March	-0.286	0.00168	-1.18	-1.96	-0.46
April	-0.314	0.00075	-1.63	-2.46	-0.69
May	-0.274	0.00594	-1.20	-2.35	-0.37
July	-0.340	0.00015	-1.51	-2.22	-0.79
August	-0.203	0.03037	-0.71	-1.32	-0.08
September	-0.353	0.00008	-0.76	-1.31	-0.36
Salinity (psu)					
March	0.189	0.03862	0.04	0.00	0.07
April	0.232	0.01145	0.06	0.01	0.10
Chlorophyll a I 10m (μg/L)					
February	-0.497	0.01759	-0.30	-0.70	-0.06
Chlorophyll a II 10m (μg/L)					
February	0.295	0.02135	0.06	0	0.22
April	-0.380	0.00205	-0.11	-0.19	-0.03
May	-0.327	0.01834	-0.04	-0.09	-0.01
July	-0.286	0.01723	-0.04	-0.12	-0.01
October	-0.301	0.03109	-0.12	-0.23	-0.01
Secchi Depth (m)					
January	-0.322	0.04157	-0.10	-0.23	0
February	-0.277	0.03752	-0.11	-0.23	0
March	-0.266	0.02465	-0.13	-0.22	-0.01
Density gradient (kg/m^4)					
April	0.320	0.00049	0.00204	0.00094	0.00322
July	-0.190	0.04335	-0.00132	-0.00251	-0.00002
October	-0.210	0.03818	-0.00132	-0.00255	-0.00007

Table A.5.: Test statistics for Mann-Kendall-Test performed monthly. Only significant results are shown. Slopes are given in Unit per month. C.I.=confidence interval on Sen's slope.

	Tau b	p-value	Sen's slope	C.I. lower	C.I. upper
Nitrate 10m (μM)					
January	-0.325	0.01846	-0.18	-0.27	-0.03
February	-0.386	0.00190	-0.25	-0.43	-0.10
March	-0.327	0.00446	-0.11	-0.33	-0.01
April	-0.565	0.00000	-0.03	-0.06	-0.01
December	-0.305	0.03541	-0.11	-0.22	0.00
Nitrite 10m (μM)					
January	-0.291	0.04991	-0.02	-0.03	0.00
March	-0.263	0.02708	-0.02	-0.03	0.00
April	-0.284	0.02403	0.00	0.00	0.00
October	-0.364	0.01427	0.00	-0.01	0.00
Phosphate 10m (μM)					
January	-0.442	0.00287	-0.02	-0.04	-0.01
February	-0.535	0.00002	-0.03	-0.04	-0.02
March	-0.258	0.03008	-0.02	-0.04	0.00
September	-0.251	0.02421	-0.01	-0.02	0.00
December	-0.399	0.00730	-0.03	-0.05	-0.01
Phosphate 25m (μM)					
January	-0.266	0.07385	-0.01	-0.03	0.00
February	-0.443	0.00047	-0.02	-0.03	-0.01
March	-0.424	0.00045	-0.03	-0.05	-0.01
April	-0.249	0.04185	-0.01	-0.03	0.00
June	0.288	0.03431	0.02	0.00	0.04
September	-0.247	0.03000	-0.12	-0.25	-0.01
Ammonium 10m (μM)					
January	-0.312	0.03500	-0.090	-0.158	-0.006
February	-0.487	0.00015	-0.119	-0.183	-0.069
March	-0.372	0.00155	-0.018	-0.034	-0.005
April	-0.375	0.00229	-0.015	-0.030	-0.004
August	0.254	0.03931	0.004	0.000	0.009
Ammonium 10m (μM)					
no significant results					

B Model Input Data

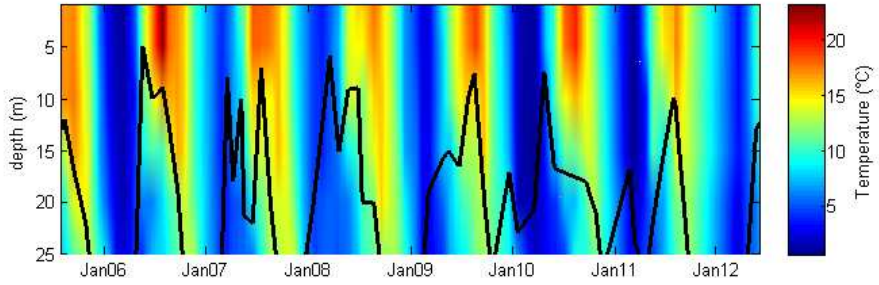

Figure B.1.: Temperature depth profiles during model simulation. Mixed layer depth is indicated by black line. Spatially interpolated between 6 standard depths (1, 5, 10, 15, 20 and 25 m), temporarily interpolated between monthly measurements.

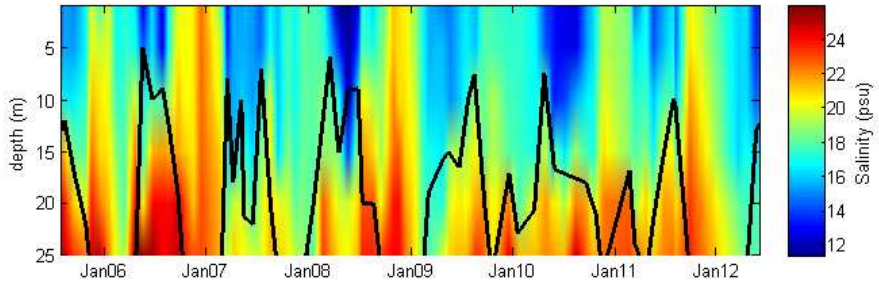

Figure B.2.: Salinity depth profiles during model simulation. Mixed layer depth is indicated by black line. Spatially interpolated between 6 standard depths (1, 5, 10, 15, 20 and 25 m), temporarily interpolated between monthly measurements.

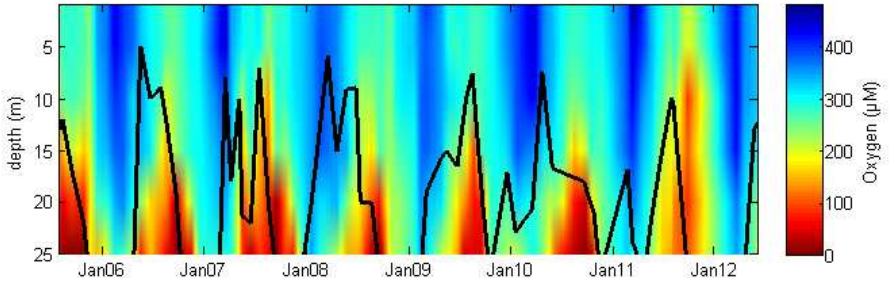

Figure B.3.: Oxygen concentration depth profiles during model simulation. Mixed layer depth is indicated by black line. Spatially interpolated between 6 standard depths (1, 5, 10, 15, 20 and 25 m), temporarily interpolated between monthly measurements.

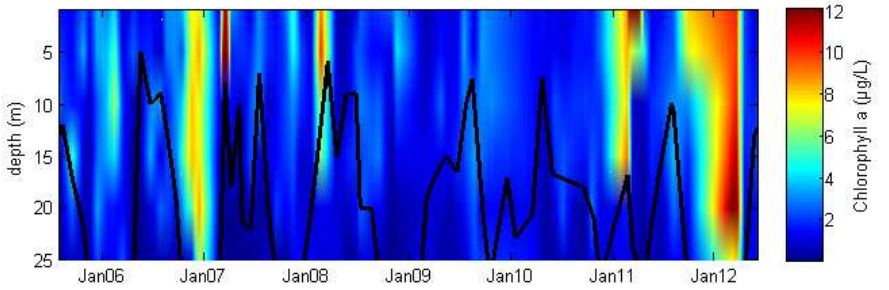

Figure B.4.: Chlorophyll a concentration depth profiles during model simulation. Mixed layer depth is indicated by black line. Spatially interpolated between 6 standard depths (1, 5, 10, 15, 20 and 25 m), temporarily interpolated between monthly measurements.

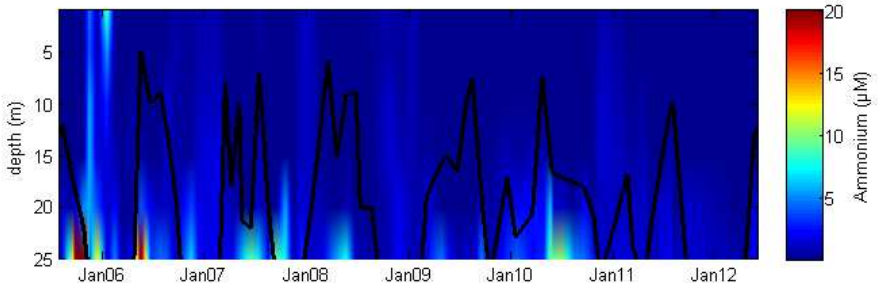

Figure B.5.: Ammonium concentration depth profiles during model simulation. Mixed layer depth is indicated by black line. Spatially interpolated between 6 standard depths (1, 5, 10, 15, 20 and 25 m), temporarily interpolated between monthly measurements.

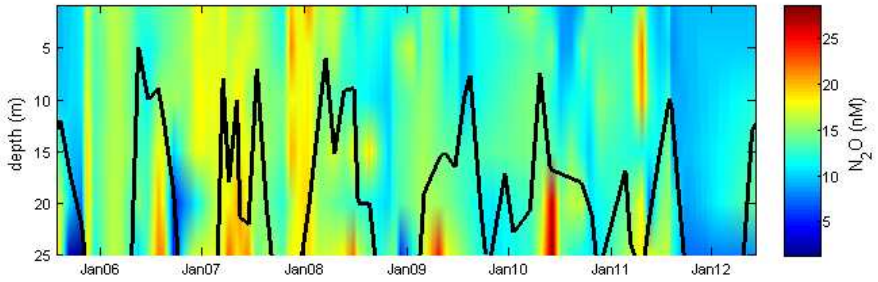

Figure B.6.: N_2O concentration depth profiles during model simulation. Mixed layer depth is indicated by black line. Spatially interpolated between 6 standard depths (1, 5, 10, 15, 20 and 25 m), temporarily interpolated between monthly measurements. In the 1D box model, only the concentrations below the mixed layer were used as input for subsurface concentration.

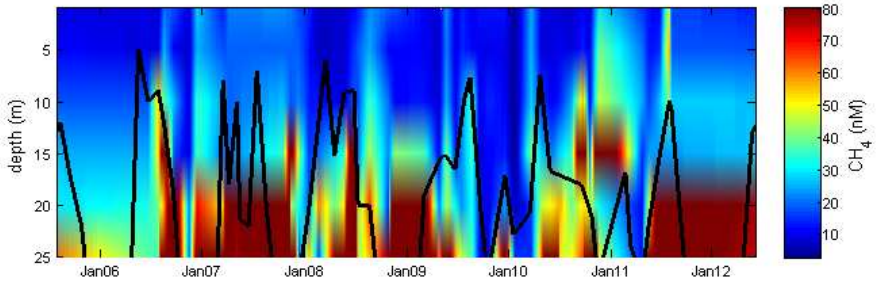

Figure B.7.: CH_4 concentration depth profiles during model simulation. Mixed layer depth is indicated by black line. Spatially interpolated between 6 standard depths (1, 5, 10, 15, 20 and 25 m), temporarily interpolated between monthly measurements. In the 1D box model, only the concentrations below the mixed layer were used as input for subsurface concentration.

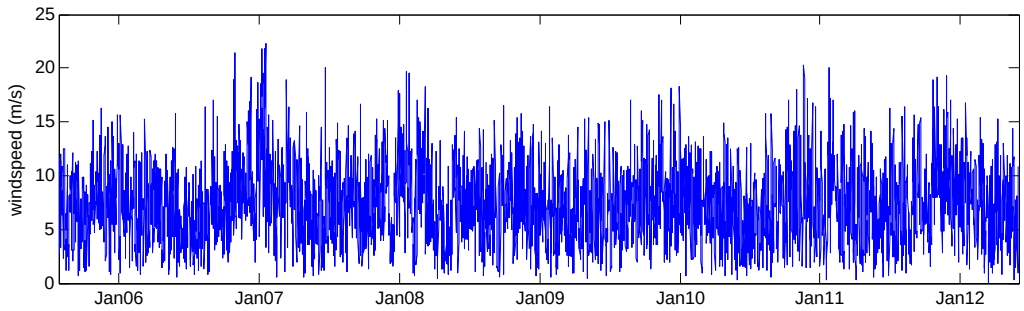

Figure B.8.: Wind data obtained from DWD normalised to 10m height.

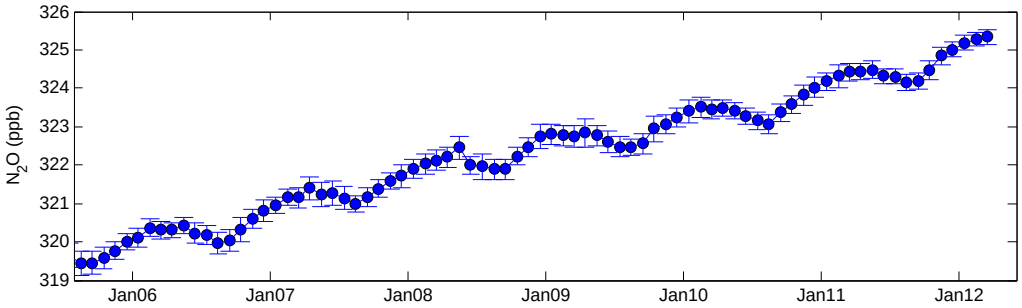

Figure B.9.: Dry air mole fraction data, measured at Mace Head (Ireland), as used for the 1D box model for N_2O. Errorbars indicate standard deviation in measurements.

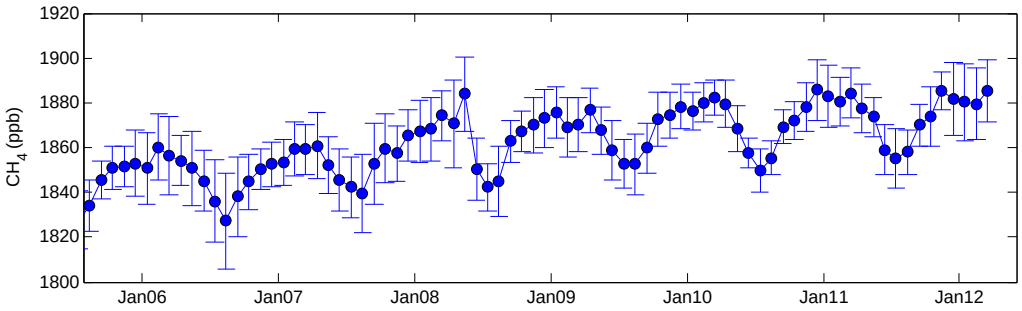

Figure B.10.: Dry air mole fraction data, measured at Mace Head (Ireland), as used for the 1D box model for CH_4. Errorbars indicate standard deviation in measurements.